TARGET TRACKING AND SENSOR PLACEMENT FOR DOPPLER–ONLY MEASUREMENTS

A THESIS SUBMITTED TO
THE GRADUATE SCHOOL OF NATURAL AND APPLIED SCIENCES
OF
MIDDLE EAST TECHNICAL UNIVERSITY

BY

SÜLEYMAN AYAZGÖK

IN PARTIAL FULFILLMENT OF THE REQUIREMENTS
FOR
THE DEGREE OF MASTER OF SCIENCE
IN
ELECTRICAL AND ELECTRONICS ENGINEERING

SEPTEMBER 2015

Approval of the thesis:

TARGET TRACKING AND SENSOR PLACEMENT FOR DOPPLER–ONLY MEASUREMENTS

submitted by **SÜLEYMAN AYAZGÖK** in partial fulfillment of the requirements for the degree of **Master of Science in Electrical and Electronics Engineering Department, Middle East Technical University** by,

Prof. Dr. Gülbin Dural Ünver _____
Dean, Graduate School of **Natural and Applied Sciences**

Prof. Dr. Gönül Turhan Sayan _____
Head of Department, **Electrical and Electronics Eng**.

Assoc. Prof. Dr. Umut Orguner _____
Supervisor, **Electrical and Electronics Eng. Dept., METU**

Examining Committee Members:

Prof. Dr. Mübeccel Demirekler _____
Electrical and Electronics Eng. Dept., METU

Assoc. Prof. Dr. Umut Orguner _____
Electrical and Electronics Eng. Dept., METU

Prof. Dr. Çağatay Candan _____
Electrical and Electronics Eng. Dept., METU

Assoc. Prof. Dr. Afşar Saranlı _____
Electrical and Electronics Eng. Dept., METU

Assoc. Prof. Dr. M. Burak Güldoğan _____
Electrical and Electronics Eng. Dept., Turgut Özal Uni.

Date: 09.09.2015

I hereby declare that all information in this document has been obtained and presented in accordance with academic rules and ethical conduct. I also declare that, as required by these rules and conduct, I have fully cited and referenced all material and results that are not original to this work.

Name, Last Name: Süleyman Ayazgök

Signature :

ABSTRACT

TARGET TRACKING AND SENSOR PLACEMENT FOR DOPPLER–ONLY MEASUREMENTS

Ayazgök, Süleyman

M.S., Department of Electrical and Electronics Engineering

Supervisor : Assoc. Prof. Dr. Umut Orguner

September 2015, 104 pages

This thesis investigates the problems of target tracking and optimal sensor placement with Doppler-only measurements. First, a single point track initialization algorithm proposed in the literature is investigated for Doppler-only tracking. The initialization algorithm is based on separable least squares method and involves a grid-based optimization. Second, particle filters are considered for Doppler-only tracking and they are compared to an extended Kalman filter (EKF). It is shown that a classical bootstrap particle filter, rather surprisingly, is inferior to the EKF in a Doppler-only tracking scenario. The reasons for this strange behavior are discussed. Then, classical sequential Monte Carlo tools are investigated to improve the behavior of the bootstrap particle filter. In this regard, two new particle filters, namely, a sequential importance resampling particle filter with optimal proposal distribution and a Rao-Blackwellized particle filter are derived and implemented. The results show that, although there are occasional improvements in the particle filter performance for some specific parameter selections, the improvement mechanisms employed are not sufficiently effective to make the particle filters beat EKF.

Finally the problem of optimal sensor placement is considered for Doppler-only tracking. A 1D target motion is considered on a road/line segment and the optimization criterion for sensor placement is selected to be the total position Cramer Rao Lower Bound (CRLB) over the road/line segment. The results obtained using numerical optimization tools are utilized to propose a simple sub-optimal sensor placement strategy with explicit formulae for the sensor positions. The proposed strategy is shown to have very close cost values to the optimal strategy.

Keywords: Doppler-only, target tracking, track initialization, particle filter, EKF, sensor placement

ÖZ

SADECE DOPPLER ÖLÇÜMLERİYLE HEDEF İZLEME VE SENSÖR YERLEŞTİRİMİ

Ayazgök, Süleyman

Yüksek Lisans, Elektrik ve Elektronik Mühendisliği Bölümü

Tez Yöneticisi: Doç. Dr. Umut Orguner

Eylül 2015, 104 sayfa

Bu tez çalışması sadece Doppler ölçümlerinin kullanıldığı durumlar için hedef izleme ve sensör yerleştirimi problemleriyle ilgilenmektedir. Öncelikle sadece Doppler ölçümleriyle hedef izleme için literatürde önerilen tek noktalık bir iz başlatma algoritması incelenmiştir. Bu algoritma ayrık en küçük kareler yöntemini kullanmakta ve ızgara tabanlı bir eniyileme yöntemi içermektedir.

Sadece Doppler ölçümleriyle hedef izleme için parçacık filtreleri düşünülmüş ve bu süzgeçler genişletilmiş Kalman filtresiyle (GKF) karşılaştırılmıştır. İlk önce klasik kendini yükselten parçacık filtresinin sadece Doppler ölçümlerinin alındığı bir hedef izleme problemi için şaşırtıcı bir biçimde GKF'den kötü çalıştığı gösterilmiştir. Bu garip davranışın nedenleri üzerinde tartışılmıştır. Sonra klasik sıralı Monte Carlo yöntemleriyle kendini yükselten parçacık süzgecinin bu davranışının iyileştirilmesi düşünülmüştür. Bu bağlamda iki yeni parçacık filtresi olan, eniyi öneri dağılımını kullanan sıralı önemlilik yeniden örnekleme parçacık filtresi ve Rao-Blackwell parçacık filtresi türetilmiş ve gerçeklenmiştir. Sonuçlarda her ne kadar özel bazı parametre seçimleri için parçacık filtresi performanslarında bazı iyileşmeler görülse

de burada kullanılan iyileştirme mekanizmalarının, parçacık filtrelerini GKF'den iyi yapmak için yeterli etkiye sahip olmadığı görülmüştür.

Son olarak sadece Doppler ölçümleriyle hedef izleme için eniyi sensör yerleştirme problemi düşünülmüştür. Burada bir boyutta bir yol/doğru parçası üzerinde hareket eden bir hedef düşünülmüş, sensör yerleştirme eniyileştirme kriteri olarak da yol/doğru parçası üzerindeki toplam pozisyon Cramer-Rao alt sınırı seçilmiştir. Sayısal eniyileme yöntemleri kullanılarak elde edilen sonuçlar, sensör pozisyonları için açık formülleri olan basit eniyi-altı bir sensör yerleştirme stratejisi önermek için kullanılmıştır. Önerilen stratejinin eniyi sonuca çok yakın maliyetler elde ettiği gösterilmiştir.

Anahtar Kelimeler: Doppler, hedef izleme, iz başlatma, parçacık filtresi, GKF, sensör yerleştirme

To My Family

ACKNOWLEDGMENTS

I would like to express my sincere gratitude to my supervisor Assoc. Prof. Dr. Umut Orguner for his advice, criticism, support and encouragements throughout the course of this work.

I would also like to thank my colleagues for their support during the course of this work.

Finally, the writing of this thesis would not have been possible without the continual support of my family and friends, to whom I am indebted.

TABLE OF CONTENTS

LIST OF TABLES

TABLES

LIST OF FIGURES

FIGURES

CHAPTER 1

INTRODUCTION

During the 19th century and at the beginning of the 20th century, researchers observed the spectrum of lights coming from the stars, galaxies and nebulas and it was observed that the color of these lights shifts to red. This observation was named as red shift. With the help of these observations, it was found that this shift was caused by the movement of the stars and it was the Doppler effect. The Doppler effect can be described briefly as: When an object transmits or reflects waves, which can be sound or electromagnetic waves/lights, the wave frequency is observed at a higher frequency than the transmission frequency if the object moves towards the observer, and at a lower frequency if the object moves away from the observer. The color of the stars shifts to red which is a lower frequency component of the spectrum. This was evidence that stars are moving away from earth, so it was considered as evidence for the expanding universe and the Big Bang theory. From this point of view, Doppler shift played an important role in understanding the universe.

Doppler shift was again investigated in space research during the cold war. Doppler shift in radio waves from satellites were utilized to track satellites, [1]. This research was continued with acoustic band ocean applications, radar applications, and target tracking in passive sensor networks. These studies, especially in the tracking applications, are focused on two main areas, namely the estimator design and the optimum sensor placement. The estimator design which is also called as tracker in tracking applications, includes the initialization problem for the tracker. Literature

surveys for these two areas of study are given in Section 1.1. The aim of this thesis and the thesis outline are given in Section 1.2.

1.1. Literature Survey about Doppler Only Tracking

1.1.1. Literature Survey about Track Initiation & Tracking with Doppler-Only Measurements

An application example of Doppler-only tracking in space research was introduced in 1970, by Salinger and Brandstatter [2], where the Doppler frequency shift of the signal transmitted by or reflected from a space vehicle was measured by multiple receivers on the earth to track the space vehicle trajectory. In [2], the dot product expression of the Doppler frequency shift was used. The dot product expression is linear with respect to the velocity, but it is nonlinear with respect to the position. Due to this, sequential estimation of the velocity and the position was proposed. This estimation procedure needs an initial guess of the position. Based on this sequential estimation procedure, two different approaches were proposed to estimate the trajectory. One of them is the global estimation with polynomials. In this method, the velocity vector is expressed as a linear combination of a set of orthonormal polynomials. For this purpose shifted Chebyshev polynomials were used. When the dynamics of the target is unknown, i.e., when the velocity cannot be expressed as a linear combination of polynomials, the second approach was proposed based on a Kalman Filter application.

Schultheiss and Weinstein gave the derivation of Fisher Information Matrix and the variance bound for velocity and position estimation with coherent Doppler measurements as well as separate frequency measurements in [3]. For simplicity only the velocity is taken as an unknown. Here, three different signal models, namely, Gaussian shaped spectrum noise, narrowband noise and pure sinusoidal signals are investigated. Also two different measurement schemes, coherent and separate frequency measurements, are considered. In the coherent measurement scheme, measurements are Fourier transforms of the received signals. Measurements such as amplitude, phase and frequency components are also used in the estimation. The

separate frequency method measures only the frequency at each sensor and the differences between them are used as measurements.

Webster introduced an exact trajectory solution from Doppler shift measurements in [4]. Single sensor and single target model are used in this solution. The sensor makes three consecutive Doppler shift measurements and calculates the ratio of these measurements. The complete derivation for constant target velocity in 2-D is given in [4]. Measurement noise was not taken into consideration in this solution.

Chan and Towers proposed a localization and tracking algorithm with Doppler shifted frequency measurements in [5]. They addressed the need of five sensors or five measurements to estimate the target state. The state in their algorithm consists of position and velocity in two dimensions and the transmitted frequency. Since the measurement function of Doppler is nonlinear in terms of these states, estimation can only be made either iteratively or with grid-search. Here, Chan and Towers proposed an algorithm which needs only a three dimensional search instead of five, which would be required for brute force grid search.

Chan and Towers proposed another estimation scheme for localization with Doppler shifted frequency measurements in [6]. In the method, Doppler measurement function is expressed as a linear transformation of the target velocity and the transmitter frequency using a matrix-valued nonlinear function of the target position with respect to sensor position. The proposed algorithm uses grid-search over target position. At each possible target position, target velocity is estimated linearly. The position which produces minimum cost is chosen. This algorithm for localization was used directly or indirectly in many Doppler-only measurement based tracking and localization applications such as the MIMO radar example given in [7].

Chan and Towers also proposed a sequential version of their algorithm given in [6] for localization with passive Doppler-only measurements in [8] especially for underwater applications. Here, for sequential localization, each sensor is used independently to estimate intermediate parameters such as the magnitude of target velocity, range, the time for the closest point of the target. A grid-search algorithm for nonlinear least square estimation given in [5] is used to estimate the intermediate

parameters. Levenberg-Marquard nonlinear optimization algorithm is used to estimate the target position and velocity from the intermediate parameters.

Chan proposed another initialization algorithm in [9]. The proposed algorithm uses the frequency derivative together with frequency measurements in the same way as in [5]. By using the derivative of frequency and the intermediate parameters, the grid search dimension can be reduced to one. At least three measurements in time are needed to initialize the algorithm. Grid search is done for the unknown transmitter frequency to estimate the target range with the help of Doppler shift and derivative measurement. The target position and velocity are estimated from the target range by using Levenberg-Marquard nonlinear optimization algorithm.

In [10], Fucheng et al. presents a variant of Extended Kalman Filter (EKF) which can be used in nonlinear estimation applications such as passive localization based on time of arrival, direction of arrival, and Doppler frequency shift. The difference of EKF from a KF is that it uses the Jacobian matrix of nonlinear functions instead of linear state transfer functions or measurement matrix in the Kalman gain and state covariance matrix calculations. The proposed modification in [10] over EKF is that after the normal EKF routine, the Jacobian matrix was recalculated with the improved state estimate and the measurement update process was repeated with this new Jacobian matrix. An improvement of this algorithm over EKF was given with an example of Doppler-only tracking.

Kusy et al. proposed an initiator algorithm and a tracking filter for Doppler based tracking in [11]. Doppler measurement model is used in the case of one transmitter and multiple receivers. Gaussian Newton algorithm was used to find the optimum solution for the initial state. Because of the possibility that the solution can be a local optimum, the author stated that more refinement is needed for the initiator. EKF was preferred to be used with this proposed track initiation algorithm. Since it is known that EKF has poor performance while the target is maneuvering, a maneuver detection algorithm and a correction method for the target state during the maneuver (with the proposed initiation algorithm) were proposed.

Ristic and Farina gave an application of Particle Filter (PF) for Doppler-Only tracking in [12]. They gave mathematical derivations of Cramer-Rao Lower Bound (CRLB) for Doppler-only tracking to evaluate the PF performance with respect to the lower bound of the estimation error. It was stated that the proposed particle filter has poor performance over the lower bound at the early stages of the tracking but it can achieve the lower bound after an initial delay. Here, the proposed filter was called as progressive correction particle filter (PC-PF) and it was developed to overcome the sample impoverishment problem that is quite common in PF implementations. In order to perform this, the weight distributions of the particles were modified progressively by a fraction of the measurement likelihood function. Even if the initial state uncertainty was high, the tracker overcomes the sample impoverishment and it converges to the true target position. It was also stated that the initialization of the filter is still an open issue for further research.

A dual filter approach for Doppler-only tracking was proposed by Battistelli et al. in [13]. In this article, observability analysis of Doppler measurement was also made and it was stated that the range, the speed and the absolute value of the relative heading (angle between range vector and velocity vector of target) are observable, but the azimuth angle of the range vector in 2-D case is unobservable. The first phase of the proposed dual stage filter is the recursive estimation of the observable state with an Unscented Kalman Filter (UKF). This filter works at each sensor individually. At the sensor network center, the second stage of the dual filter is run such that another UKF is used to estimate the overall state in the Cartesian coordinates by using the estimates of the observable states from each sensor. For the initialization of the filters, a multiple hypothesis approach was proposed.

Ristic and Farina implemented Bernoulli PF for Doppler-only tracking in multi-static case in [14]. In this article, the aim was to detect and track the target jointly by using the Doppler frequency shifts which are measured by multiple receivers which accompany a fixed single transmitter. It was stated that when false alarms exist and the detection probability of the target is less than one, optimal Bayes Filter for the detection and tracking of a target is the Bernoulli filter [15]. Bernoulli PF propagates the target state distribution and probability of existence of the target through the

prediction and estimation updates. Due to the nonlinear transformations of the random variables in prediction and estimation stages, the exact distributions cannot be calculated and therefore a PF was used to approximate the distributions. Ristic and Farina also proposed a method for the selection of active receivers in [16] to improve the information gathered from the sensors and to discard measurements from the sensors which are aligned with the target and the transmitter in the bi-static case. It was stated that receiver selection improves the track's settling durations and steady-state error performance.

Xiao et al. gave an analysis of observability and performance for bi/multi-static Doppler-only Radar in [17]. In this article, this analysis was made for a multi transmitter and one receiver case for simplicity. It was stated that this scenario can be extended to a multi transmitter and multi receiver case as well. For the single receiver case, observability analysis was made with the help of the Jacobian matrix of the Doppler measurements. In this approach, observability is checked by the rank of Fisher Information Matrix (FIM). For complete observability, FIM should be full rank. For performance analysis, the lower bounds for the position and velocity estimation were also derived. It was stated that CRLB became lower with less measurement error variance, high number of transmitters, long integration time and short transmitter wavelength. Simulation results were given by placing the transmitter and receivers at the vertices of a polygon. Besides the CRLB, GDOP (geometric dilution of precision) analysis and results were given. GDOP is proportional to the square-root of the sum of the lower bounds for each axis. This analysis showed that when the target location is closer to the sensors, the estimates can have lower error variance.

Liang et al. showed the usage of Bernoulli PF in the case of multi-target tracking with multi-static Doppler-Only measurements in [18]. The single target case for Bernoulli Filter implementation was discussed earlier in [14]. In this article, four different data fusion schemes are considered to merge information gathered from multiple receivers. The first one was the measurement fusion which uses all measurements in a one track-filter. The second one is the parallel update scheme which uses an N-track-filter with N measurements and merges the estimated states.

The third was a sequential update scheme which uses the estimates of one filter as an input to the next filter. The final fusion scheme was random update which chooses one random measurement to estimate the state. Because of the data association requirements in a cluttered environment, measurement fusion was not preferred. Simulation results with multi-Bernoulli filter for the remaining three fusion schemes were given and it was stated that the parallel update was the worst. For performance criteria, optimal sub-pattern assignment (OSPA) was used. Sequential and random update schemes have nearly the same performance for single target and multiple target cases. Because of the fact that instantaneous peaks in OSPA occurred in the random update scheme, sequential update was proposed for tracking multiple targets with multi-static Doppler-only measurements. In addition to the Bernoulli filter implementation, some comments are made for sensor placement in the multi-static case. It was stated that the maximization of the determinant of CRLB can be used for optimal sensor placement.

Lindgren et al. presented a method based on parametrized motion models for the localization of an acoustic source in a network of Doppler shift sensors in [19]. Two different motion models, namely linear and circular, and associated Doppler shift measurement functions were introduced. In these measurement functions the retardation effect in acoustic propagation was taken into consideration. For these motion models, a nonlinear least square estimator based on Gaussian Newton variable projection technique was described and an algorithm for obtaining an initial estimate was proposed. Successful experimental results were presented for the estimator and the motion models.

Guldogan et al. introduced the GM-PHD (Gaussian mixture-probability hypothesis density) filter usage for multi-target tracking with multi-static Doppler-Only measurements in [20]. The approach in [20], i.e., the PHD filter, is a practical Bayesian tracking algorithm which avoids the computationally costly data association process. Experimental results of the application of this filter for Doppler-only measurements in the acoustic band were given in [20] and it was stated that GM-PHD is successful to detect and track targets using multi-static Doppler-only measurements. In addition to this study, the sequential Monte Carlo implementation

of the PHD (SMC-PHD) for multi target tracking using Doppler-only measurements is proposed together with GM-PHD in [21]. Here, two implementations of the PHD filter were compared and it was stated that both PHD filter implementations are successful to track multiple targets but GM-PHD is more effective, efficient and easy to implement than the SMC-PHD filter.

1.1.2. Literature Survey about Sensor Placement

In addition to tracker design, sensor placement also plays an important role in the tracking performance. Optimum sensor placement for different kinds of sensors was studied by many researchers. Especially for range and bearing sensors, there are quite many research results to refer to, but there have been only a limited number of studies conducted on the optimum sensor placement problem for Doppler-only sensors. Moreover, many studies consider only localization, i.e., finding the position of the target only for a single time instant. As a result these studies all assume that the target or the object is static at all times or for a short frame of time. Nevertheless, the optimality criteria used for bearing and range measurements can give us an insight for the case of Doppler-only target tracking problem.

Moreno et al. gave the optimal sensor placement results for bearings-only measurements in 3-D scenarios in [22]. They showed the optimality criteria which can be used for any sensor placement problem. It was stated that there are three main criteria to be used in optimal sensor placement which are A-optimality, D-optimality and E-optimality. A-optimality aims to minimize the average variance of the estimate by minimizing the trace of the CRLB (Cramer-Rao Lower Bound) matrix which can be calculated by taking the inverse of the FIM (Fisher Information Matrix). D-optimality is achieved by maximizing the determinant of FIM and results in the minimum volume uncertainty ellipsoid for the estimate. Finally, E-optimality minimizes the length of the largest axis of the uncertainty ellipsoid for the estimate by minimizing the largest eigenvalue of the CRLB matrix. These criteria have some pros and cons with respect to each other. For range and bearing sensors, optimality comparisons are also made in [23]. Both Sim et al. [23] and Moreno et al. [21] chose A-optimality as the performance criterion.

In Abel's study [24], the problem of optimal sensor placement for passive source localization was investigated and a closed-form solution was found. The same solution as Carter's study [25] was reached for the optimum sensor placement on a line segment. The proposed solution was placing half of the sensors at one tip of the line segment and the other half at the other tip of the line segment. The theorem used to reach these results assumes that the received signal at the sensors is the time-delayed and amplitude changed version of the transmitted signal from one source.

Two dimensional solution for the optimum sensor placement was studied in [26] by Zhang. An optimality criterion was built on the error covariance matrix of the individual sensors. The cost function is chosen as the determinant of the combined error covariance matrix which is proportional to the harmonic mean (i.e., the inverse of the summation of the inverses) of the individual sensor error covariance matrices. With this cost function, the optimality is achieved by changing the orientation of the sensors with respect to the expected target location. This method is only valid under the condition that the covariance matrix is determined only by the orientation of the sensor with respect to the target such as in the case of range and bearing sensors. With this assumption, it was stated that the proposed sensor placement procedure yields minimum area of the uncertainty around the target for the 2-D case.

Levanon investigates the case when the sensors are at the corners of a polygon and the target is at the center while using the lowest possible GDOP as the cost function for range measurements, [27]. GDOP is unitless and as mentioned earlier in the previous subsection, it is calculated as the square root of the summation of the diagonal elements of the CRLB matrix, and it is normalized with the measurement variance. From this point of view, it is a normalized and square rooted version of A-optimality criterion used in [1]. It was stated that the normalized version of the GDOP can be used for bearing-only measurements. For bearing-only measurements, target position for the lowest GDOP is the center as in the case of range measurements when the number of sensors equals to three and when the sensors are located at the corners of the polygon. In the case that the number of the sensors is greater than three, minimum GDOP is not reached at the center but somewhere

inside the polygon. It was also stated that the lowest GDOP for bearing-only measurements is lower than that would be obtained for the range measurements.

Martinez et al. studied optimal sensor placement and motion coordination for target tracking in [28]. In this study it was aimed to find optimal sensor placement for range sensors for dynamic target conditions. They restricted the placement such that all sensors are located on the concave bound of a region inside of which the target can move. As the cost criteria, maximum determinant of FIM, i.e., D-optimality was used. For a circle region, the proposed optimum sensor placement is equally spaced placement on the circle boundary. It was also stated that using the D-optimality can result in some sensors being placed at the same point for diagonal sensor error covariance matrices, (i.e., when the sensor measurement noises are independent).

Another study for bearing-only measurements and time-of arrival based optimum sensor placement was presented in [29] and [30] respectively. In these papers, sensor measurement variances are assumed to be equal and noises are independent. Also the target is static, i.e., they have a localization problem. D-optimality was used as the performance criterion.

Soysal et al. presented the information analysis in passive radar networks for target tracking in [31]. A-optimality was used as performance criteria. Measurements include not only range but also range dot, namely Doppler measurement. Total range and Doppler uncertainty were given for passive sensors which have one transmitter located at the center of the circle and multiple receivers on that circle. This scheme was repeated for the case where the transmitter is located outside of the circle. In addition to uncertainty levels, normalized coverage area was also calculated. Normalized coverage area determines the coverage performance for circle placement. Simulation results were presented dependent on the number of the sensors and the circle radii.

Nguyen and Doğançay gave the optimum placement for moving sensors used for the localization of a static target [32]. Moving sensors was located on a circle at the center of which the target is located. Doppler frequency shift of the target echoes are measured by the sensors. D-optimality was used as the cost criterion. Determinant of

the FIM was written as a function of the angular speed, measurement noise variance values and the angle between velocity vector of the sensors and the distance vector between the sensors and the target. When the maximum angular speed of the sensors is used in the determinant equation, sensor angles are left as parameters to be searched for maximum determinant. Grid search algorithm was proposed for this search. Localization with consecutive measurements was simulated with active radars on UAVs (Unmanned Air Vehicles). From the results of the simulations, it was stated that, with the proposed optimality criterion, the movements of the UAVs are obtained in such a way that tangential velocities of the sensors are maximized.

1.2. Thesis Outline

As seen in the literature survey above, track initiation algorithm for a tracking filter, the tracking filter design and sensor placement issues are very important and open research areas for Doppler-only sensors.

The initiation of a tracking filter for Doppler-only tracking plays a great role for successful tracking. Although some initiation algorithms are given in the literature, they mostly suffer from the latency in the initialization. A single-point initialization procedure which produces an initial estimate with a single measurement from several sensors is a strong candidate to lower the latency as much as possible. Such a single-point method for Doppler-only measurements was given for a single transmitter and multiple receivers in [6] by using separable least squares estimation with a grid-search algorithm. In the first part of this thesis, this track initiation method is going to be adopted for multiple transmitter-receiver pairs and a performance analysis with respect to grid spacing is given.

Secondly, tracking filter design is still an open research area for the multi-sensor Doppler-only tracking. Since the Doppler-only measurements have a nonlinear relationship with the position in the Cartesian coordinates, the well-defined optimum tracking filters used for linear systems, i.e., Kalman Filter, cannot be used in tracking. For this nonlinear case, the nonlinear variants of the Kalman Filter such as EKF and UKF or sequential Monte Carlo methods such as Particle Filter can be good

candidates for tracking. In the second part of this thesis, first, EKF and the standard bootstrap particle filter will be compared for Doppler-only tracking. Surprisingly, it will be shown that the particle filter obtains much worse results than EKF. The reasons for this are going to be discussed. In order to see if the particle filter performance can be improved using standard sequential Monte Carlo tools, two other particle filters are going to be derived and implemented for Doppler-only tracking. These particle filters will be Sequential Importance Resampling (SIR) particle filter with optimal proposal distribution and a Rao-Blackwellized particle filter. In the SIR particle filter, the optimal proposal distribution will be obtained by using an EKF update. In the Rao-Blackwellized Particle Filter the nonlinear position states are going to be estimated using a particle filter whereas linear velocity states will be estimated with Kalman filters. The performances of the filters are going to be compared with the bootstrap particle filter and EKF on an example using different measurement noise variances.

Finally, although the optimum sensor placement problem is studied in detail for range and bearing measurements, optimum sensor placement for the Doppler-only case, especially for the tracking applications, is still an open area of research. It is known that sensor placement is a critical design parameter for any multi-sensor tracking application. To gain insight for 2-D and 3-D sensor placement cases, in the third part of this thesis, an optimum solution for sensor placement for tracking a target with a 1-D constant velocity motion is studied in detail. The solution for the optimum sensor placement for this 1-D case is obtained and its relations with the target and measurement parameters are studied.

The organization of the thesis is given as follows. A track initiation algorithm and its implementation details are given in Chapter 2. To evaluate the performance of the initiation algorithm, its implementation with an EKF is discussed. The successful results with EKF and comments on the required grid spacing for the grid-search are also given at the end of Chapter 2. In Chapter 3, alternative particle filters to bootstrap particle filter are derived and implemented. The results are compared with the bootstrap particle filter and EKF. A sensor placement problem for Doppler-only tracking is investigated and an optimum solution is obtained for 1-D case in Chapter

4. The parameters of the optimum solution are related to the problem parameters and closed form formulae are found for the sensor positions. Finally, in Chapter 5, overall comments, remarks and conclusions are given.

CHAPTER 2

A SINGLE-POINT TRACK INITIATION ALGORITHM FOR DOPPLER-ONLY TRACKING

In this chapter, a single-point track initiation algorithm to be used with a Doppler-only tracking filter will be discussed. As seen in the literature survey in Chapter 1, different localization algorithms were proposed for Doppler-only measurements, [5, 6, 8, 9]. Besides these localization algorithms which can be used as track initiators for a tracking filter, some initiation algorithms also exist in the literature, [11, 13]. The main disadvantage of these algorithms is that they are rather slow to calculate the initial estimate. A single-point initialization algorithm, which produces initial estimates using only a single measurement from several sensors, is a strong candidate for fast track initialization. In this thesis study, such a track initiation algorithm was designed at the beginning of the thesis study. However after more literature survey, it was seen that such an initiation algorithm had already been proposed in the literature. This single point initiation method for Doppler-only measurements was given for a single transmitter and multiple receivers in [6] and it uses separable least squares estimation with a grid-search algorithm. In this chapter, this method is adopted for multiple transmitter-receiver pairs and a performance analysis is made with respect to the grid spacing parameter used in the grid-search. For the grid-search, grid spacing is the main parameter which defines the performance and the computational cost. In this chapter, the effects of the grid spacing over the performance and the

possible ways to choose it are also discussed in addition to the derivation and the implementation of the method.

The organization of the chapter is given as follows. First, the measurement and the target models are given in Section 2.1. In Section 2.2 the details of the initiation algorithm, which estimates the initial target state using separable least square estimation with a grid-search, are given. The performance of the single-point track initiation algorithm is shown using an EKF. In order to construct a baseline for the performance of the EKF, CRLB values are also shown. The equations for the EKF and the CRLB are given in Section 2.3. Finally, simulation results for the track initiation algorithm and EKF for a multi-sensor Doppler-only tracking scenario are illustrated along with CRLB values in Section 2.4. In Section 2.4, RMS error values for the track initiation algorithm with respect to the grid spacing parameter are also given along with some comments on the selection of the grid spacing parameter.

2.1. Target Motion and Measurement Model

Transmitted or reflected wave from moving objects encounter a frequency shift at the observer side and this is called as Doppler shift. At the observer side wave frequency is higher if the object moves towards the observer, lower if the object moves away from the observer. Doppler sensors basically measure the received signal frequency at the observer side. Received signal can be reflected or transmitted from the target. In the case of reflection there are two cases which are named as passive and active measurements. In the passive case, source of the reflected signal is actually used for another purpose and it is also located at a different place than receivers. On the other hand, in the active case, the transmission source is intentionally used with these receivers. The transmitter waveform is unknown in most scenarios for the passive case. In the active case, the transmitted signal frequency is known by the receiver side and the difference between the transmitted and the received signal frequency can be measured at the receiver side. For the passive case, transmitter frequency is unknown and only the differences of the measured frequencies between different Doppler sensors are used, and this is called as a differential Doppler measurement.

Doppler sensors can also be categorized into two like other sensor types with respect to receiver and transmitter locations such as bi-static and monostatic. In the case that the transmitter and receiver are located at different places, the Doppler measurements are said to be bi-static measurements. Otherwise they are called monostatic measurements. Monostatic and bi-static measurements are illustrated in Figure 1 and Figure 2 respectively. For the passive bi-static case, the signal source can be TV or FM radio transmission in an urban area. In the active bi-static case, the source is usually a dedicated transmitter. Multiple receivers and/or transmitters can be used for measurements. In this case, the measurements are called to be multi-static measurements. In the multi-static case, if one transmitter is used as shown in Figure 3, all interactions of the receivers with this transmitter can be utilized. Moreover, if multiple transmitters are used, dedicated transmitter-receiver (mostly located at the same place) interactions can result in measurements as seen in Figure 4. On the other hand, in some applications measurements can be derived from the interaction of each receiver with all transmitters as seen in Figure 5.

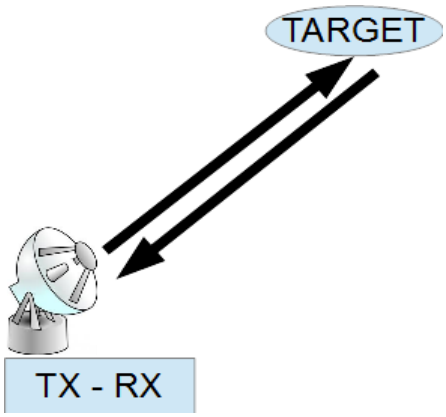

Figure 1 Monostatic measurement.

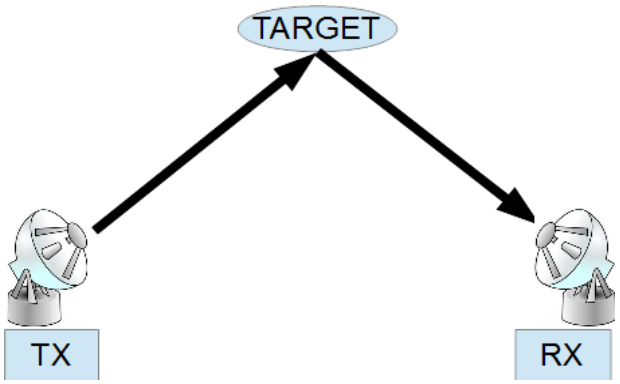

Figure 2 Bi-static measurements.

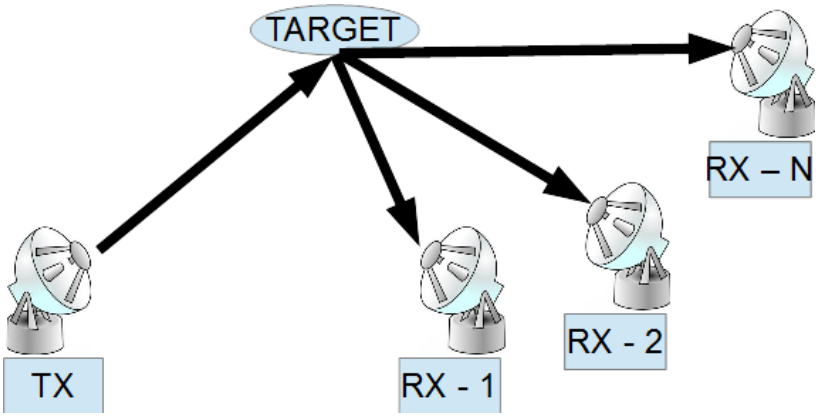

Figure 3 Multi-Static measurements with one transmitter.

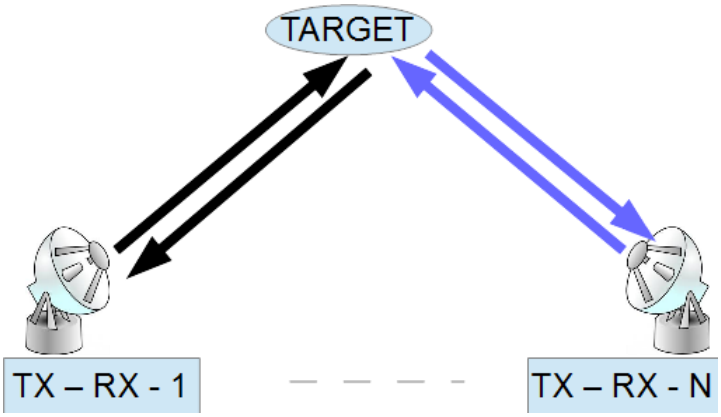

Figure 4 Multi-Static measurements with independent multiple transmitters.

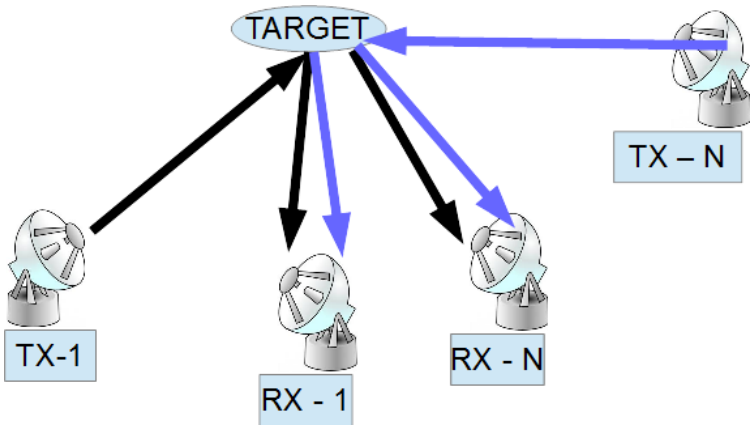

Figure 5 Multi-Static measurements with multiple Tx-Rx pairs.

For Doppler sensors, the waveform choices can be different for different applications. Some possibilities are a single tone pulse, phase or frequency modulated pulse, frequency modulated continuous wave, phase modulated continuous wave or random bandlimited noise signals. Receiver processors and the accuracy of the Doppler measurements will be different for different signal (waveform) types and these signal-level issues are out of the scope for this thesis study. In the current work, when we consider a Doppler sensor, it is assumed to measure Doppler shift with a known measurement noise variance.

The received signal frequency models for monostatic and bi-static cases are given in (2.1-2) and (2.1-6) respectively and the measurement geometries are shown in Figure 6 and Figure 7. Here,

- f_{tx} represents transmitter frequency,
- f_{rx} represents received frequency,
- f_d represents Doppler shift frequency,
- λ represents wavelength,
- v_{tx-t}, v_{t-tx}, v_{rx-t} and v_{t-rx} represent the radial velocity of the target/transmitter/receiver with respect to transmitter/receiver/target position,
- $|\vec{v}_{tx}|$, $|\vec{v}_{rx}|$ and $|\vec{v}_t|$ represent transmitter, receiver and target speeds (magnitude of velocity vector),

- α_1, α_2, α_3 and α_4 represent the angle between the velocity vector and the range vector for receiver-target pair and transmitter-target pairs respectively.
- c represents the wave speed and it is equal to the speed of light in electromagnetic wave applications, and the speed of sound in acoustic applications.

$$f_{rx} = f_{tx} + f_d \quad \text{2.1-1}$$

$$f_d = \frac{2(v_{tx-t} + v_{t-tx})}{\lambda} \quad \text{2.1-2}$$

where

$$v_{tx-t} = |\vec{v}_{tx}| \cos \alpha_1 \quad \text{2.1-3}$$

$$v_{t-tx} = |\vec{v}_t| \cos \alpha_2 \quad \text{2.1-4}$$

$$\lambda = \frac{c}{f_{tx}} \quad \text{2.1-5}$$

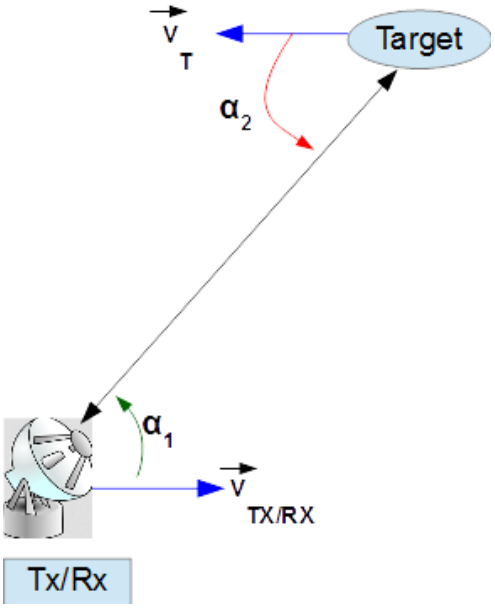

Figure 6 Monostatic measurement parameters

$$f_d = \frac{(v_{tx-t} + v_{t-tx}) + (v_{rx-t} + v_{t-rx})}{\lambda} \quad 2.1\text{-}6$$

where

$$v_{tx-t} = |\vec{v}_{tx}| \cos \alpha_1 \quad 2.1\text{-}7$$

$$v_{t-tx} = |\vec{v}_t| \cos \alpha_2 \quad 2.1\text{-}8$$

$$v_{rx-t} = |\vec{v}_{rx}| \cos \alpha_3 \quad 2.1\text{-}9$$

$$v_{t-rx} = |\vec{v}_t| \cos \alpha_4 \quad 2.1\text{-}10$$

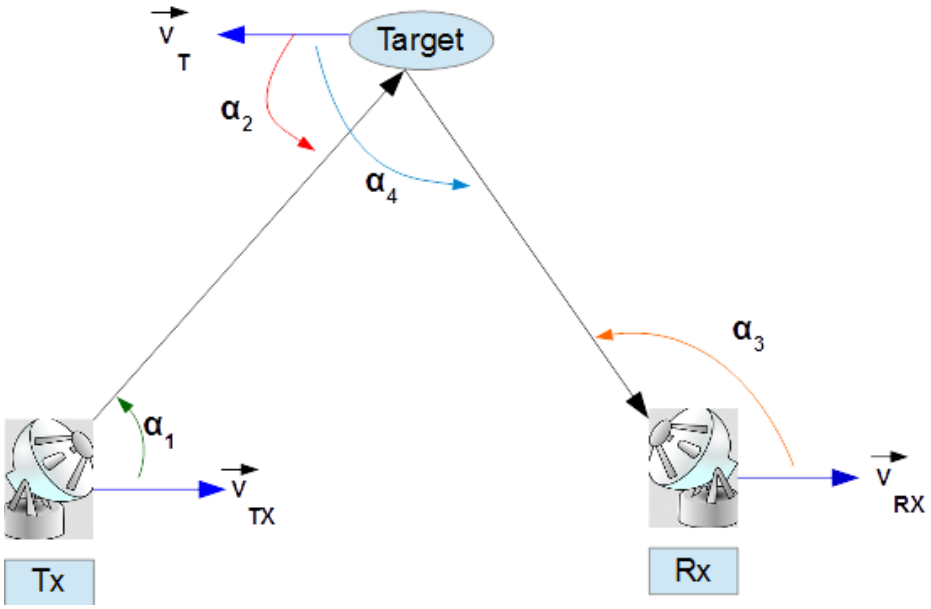

Figure 7 Bi-static measurement parameters

Without loss of generality, from this point on, active monostatic case will be considered. As seen in (2.1-2) and (2.1-6), the bi-static case formulation can be derived easily from the monostatic case.

In (2.1-2), the radial velocity is used to calculate the Doppler shift. The radial velocity can be expressed in terms of the inner product of the velocities of the transmitter and the target and the range vector between the target and the sensors in the monostatic case. When we define the radial velocity as such an inner product, this means that the Doppler shift is the projection of the target velocity vector onto range vector between the target and the sensor. Hence, (2.1-2) can be rewritten as in

(2.1-11). Here, $\vec{r}_{\mathrm{tx-t}}$ and $\vec{r}_{\mathrm{t-tx}}$represent the range vectors from the transmitter to the target and from the target to the transmitter respectively. The terms $\overrightarrow{\mathrm{v_t}}$ and $\overrightarrow{\mathrm{v_{tx}}}$ represent velocity vector of the transmitter and the target respectively. p_t and p_{tx} represent the target and transmitter position vectors respectively. $\|\vec{a}\|$ denotes the magnitude of the vector of $\vec{a}$.

$$f_d = \frac{2}{\lambda}\frac{\vec{r}_{\mathrm{tx-t}}.\vec{v}_{tx} + \vec{r}_{\mathrm{t-tx}}.\vec{v}_t}{\|\overrightarrow{r_{tx-t}}\|} \quad \text{2.1-11}$$

where

$$\vec{r}_{\mathrm{tx-t}} = p_t - p_{tx} \quad , \quad \text{2.1-12}$$

$$\vec{r}_{\mathrm{t-tx}} = p_{tx} - p_t. \quad \text{2.1-13}$$

For simplicity, the transmitter is assumed to be stationary, so $\vec{v}_{tx}$ is zero and (2.1-11) turns into (2.1-14).

$$f_d = \frac{2}{\lambda}\frac{\vec{r}_{\mathrm{t-tx}}.\vec{v}_t}{\|\vec{r}_{\mathrm{t-tx}}\|}. \quad \text{2.1-14}$$

For obtaining a more concise representation, the column vectors $\vec{r}_{\mathrm{t-tx}}$ and $\vec{v}_t$ are expanded in (2.1-15). Here, p_s and p_t are column vectors representing the position of the target and the sensor. v is the column vector representing the target velocity.

$$f_d = \frac{2}{\lambda}\frac{[p_s - p_t]^T[v]}{\|[p_s - p_t]\|} \quad \text{2.1-15}$$

where

$$p_s = [x_s\ y_s]^T, \quad \text{2.1-16}$$

$$p_t = [x_t\ \ y_t]^T \quad \text{2.1-17}$$

$$v = [v_x\ v_y]^T. \quad \text{2.1-18}$$

For the N sensor case, the Doppler measurement vector can be written as in (2.1-19).

$$F = \frac{2}{\lambda}\begin{bmatrix} \frac{[p_{s1} - p_t]^T}{\|[p_{s1} - p_t]\|} \\ \vdots \\ \frac{[p_{sN} - p_t]^T}{\|[p_{sN} - p_t]\|} \end{bmatrix}[v] \qquad 2.1\text{-}19$$

As seen in (2.1-19), the first matrix in the multiplication is a function of only the target position and not the target velocity. From this point of view, the noisy Doppler measurement model for N active sensors can be formulated as in (2.1-20).

$$y = \frac{2}{\lambda}H(p_t)[v] + e \qquad 2.1\text{-}20$$

where

$$H(p_t) = \begin{bmatrix} \frac{[p_{s1} - p_t]^T}{\|[p_{s1} - p_t]\|} \\ \vdots \\ \frac{[p_{s1} - p_t]^T}{\|[p_{sN} - p_t]\|} \end{bmatrix} \qquad 2.1\text{-}21$$

Here, e represents the measurement noise which is a white Gaussian random vector. Since the position of the sensors are known, $H(p_t, p_{s1}, .. p_{sN})$ is rewritten as $H(p_t)$. Although we derived the measurement model only for the case of N-active sensors, multi-static case for multiple transmitters and multiple receivers can be straightforwardly derived as a linear transformation of the target velocity vector with the matrix nonlinear function of the target, receiver, and the transmitter positions as in (2.1-20).

Until now, only the measurement model was given. Now the target model used in the tracking filter is given in (2.1-23). For the target motion, linear Gaussian nearly constant velocity model is used. Here X_k is the target state where x_k, y_k and $v_{x,k}, v_{y,k}$ are x-y positions and x-y velocities of the target respectively, A_k is state transition matrix, B_k is the noise gain matrix, and $w_k \sim N(w; 0; \sigma_{proc}^2 I)$ is the zero

mean white Gaussian process noise. σ_{proc}^2 is the process noise variance and Q_k is the process noise covariance matrix. ΔT is the sampling interval for the measurement process and the target motion.

$$X_k = [x_k, y_k, v_{x,k}, v_{y,k}]^T \quad \text{2.1-22}$$

$$= A_{k-1}X_{k-1} + B_{k-1}w_{k-1} \quad \text{2.1-23}$$

where

$$A_k = \begin{bmatrix} 1 & 0 & \Delta T & 0 \\ 0 & 1 & 0 & \Delta T \\ 0 & 0 & 1 & 0 \\ 0 & 0 & 0 & 1 \end{bmatrix}, \quad \text{2.1-24}$$

$$B_k = \begin{bmatrix} 0.5\Delta T^2 & 0 \\ 0 & 0.5\Delta T^2 \\ \Delta T & 0 \\ 0 & \Delta T \end{bmatrix}, \quad \text{2.1-25}$$

$$w_k \sim N(w_k; 0; \sigma_{proc}^2 I). \quad \text{2.1-26}$$

2.2. Single-Point Track Initiation Algorithm

In tracking applications, an initial state should be given to a tracking filter a priori. For instance, in most radar applications, a target acquisition radar or the tracking radar itself collects coarse target state information and this knowledge is given to the tracking radar to initialize target tracks. Although this initial state of the target does not have high accuracy, the designed filter loop eliminates the initial errors in a recursive manner during tracking and reaches a steady-state. If the initial state error is too large, especially for nonlinear measurements, the tracking filters either reach steady-state very slowly or they diverge. Therefore the initial target state determination plays a great role to start tracks properly and also to lower the tracking errors and settling time.

Initial state determination problem can be defined as an estimation problem for the position and the velocity of the target in Cartesian coordinates with the measurement model given in (2.1-20). As seen in (2.1-20), measurement function is nonlinear with respect to the target kinematic variables and this prevents the usage of well-established linear estimators. As seen in (2.1-21), Doppler measurement is linearly

dependent on the target velocity given the position variables. Unfortunately there is a nonlinear relationship with respect to the range vector between the target and the sensors which is caused by the division with the magnitude of the range vector. When commonly used least square approach is preferred, this problem can be classified as the separable least square estimation problem, [33]. Separable least square estimation attempts to minimize the error between the measurements and the estimated measurements with respect to linearly dependent parameters analytically while the nonlinearly dependent parameters are optimized numerically. In our case, the linearly dependent parameter is the velocity of the target and nonlinearly dependent parameter is the position of target.

Various researches based on separable least square estimation exist in the literature [1,5,6,8,9,11]. In [6], the problem is passive localization of a moving transmitter with several receivers. The transmitter frequency is assumed to be unknown at the receiver side. Since the measurements are linearly dependent on the transmitter frequency, the transmitter frequency is also included in the linearly dependent state like the velocity values. In this subsection, the separable least square estimation with grid-search method which is used in [6] is adapted to multi-static multiple transmitter-receiver pairs. In our scheme, the transmitter frequencies are assumed known for each transmitter-receiver pair, therefore the linear state consists of only the target velocity.

The separable least square estimation procedure we use can be described using the following steps:

i. Choose a candidate position p_t from an area of interest, and calculate $H(p_t)$ matrix in (2.1-20).
ii. Linearly estimate the velocity using the least squares method.
iii. Calculate the least squares cost function for this estimate and go back to step i for a new position candidate.

This procedure is repeated for all points on a grid over the area of interest. After completion, the grid point that gives the minimum cost is taken to be the estimated

position. The estimated velocity at this position is taken to be the least square solution in step-ii which is used as the initial velocity estimate.

The solution for the linear least square estimation problem solved in step-ii is given in (2.2-1), [33]. For simplicity, the argument p_t of $H(p_t)$ is omitted below.

$$\hat{v} = \frac{\lambda}{2}(H^T H)^{-1} H^T y \qquad 2.2\text{-}1$$

The square-error calculated in step-iii is given in (2.2-2).

$$C(p_t) = \left\| y - \frac{2}{\lambda} H\hat{v} \right\|^2 = \left\| y - H(H^T H)^{-1} H^T y \right\|^2 \qquad 2.2\text{-}2$$

$$= [y - H(H^T H)^{-1} H^T y]^T [y - H(H^T H)^{-1} H^T y] \qquad 2.2\text{-}3$$

By using the idempotent property ($I^2 = I$) of the matrix $H(H^T H)^{-1} H^T$, the cost function can be simplified as in (2.2-4).

$$C(p_t) = \left[y - H(H^T H)^{-1} H^T y \right]^T \left[y - H(H^T H)^{-1} H^T y \right] \qquad 2.2\text{-}4$$

$$= y^T y - 2y^T H(H^T H)^{-1} H^T y + y^T H(H^T H)^{-1} H^T H(H^T H)^{-1} H^T y \qquad 2.2\text{-}5$$

$$= y^T y - 2y^T H(H^T H)^{-1} H^T y + y^T H(H^T H)^{-1} H^T y \qquad 2.2\text{-}6$$

$$= y^T y - y^T H(H^T H)^{-1} H^T y \qquad 2.2\text{-}7$$

Since we consider the minimization of the cost function $C(p_t)$ over the positions, we can discard the first term in (2.2-7) since it is a constant. The modified cost functions to be used in the grid-based optimization are given in (2.2-8) and (2.2-9).

$$C'(p_t) = -y^T H(H^T H)^{-1} H^T y = -\frac{2}{\lambda} y^T H\hat{v} \qquad 2.2\text{-}8$$

$$C''(p_t) = -y^T H\hat{v} \qquad 2.2\text{-}9$$

2.3. EKF and CRLB Formulation

To evaluate the performance of the track initiation algorithm given in the previous section, it will be used with an Extended Kalman Filter. Kalman filter is the most common tracking filter used in the literature. For the linear Gaussian system case, Kalman filter is optimal. However, because of the nonlinearity in the measurement function given in (2.1-20), the Extended Kalman filter has to be used. For EKF

implementation, the target motion model given in (2.1-22) is used. A single step of EKF is composed of two steps, prediction and estimation updates like the Kalman filter as given below.

Prediction Update

$$\widehat{X}_{k|k-1} = A_{k-1}\widehat{X}_{k-1|k-1} \quad \text{2.3-1}$$

$$P_{k|k-1} = A_{k-1}P_{k-1|k-1}A_{k-1}^{T} + Q_{k-1} \quad \text{2.3-2}$$

Measurement Update

$$\widehat{X}_{k|k} = \widehat{X}_{k|k-1} + K_k\left(y_k - \widehat{y}_{k|k-1}\right) \quad \text{2.3-3}$$

$$P_{k|k} = P_{k|k-1} - K_k S_{k|k-1} K_k^{T} \quad \text{2.3-4}$$

where

$$\widehat{y}_{k|k-1} = \frac{2}{\lambda} F\left(\widehat{X}_{k|k-1}, p_{s1} \ldots p_{sN}\right), \quad \text{2.3-5}$$

$$S_{k|k-1} = J_k P_{k|k-1} J_k^{T} + R \quad \text{2.3-6}$$

$$K_k = P_{k|k-1} J_k^{T} S_{k|k-1}^{-1} \quad \text{2.3-7}$$

$$R = \sigma_{meas}^{2} I \quad \text{2.3-8}$$

2.3-1) to (2.3-8). $\widehat{X}_{k|k}$ and $\widehat{X}_{k|k-1}$ represent the estimated and predicted states respectively. $P_{k-1|k-1}$ and $P_{k|k-1}$ represent the covariance matrix for the estimated and predicted states respectively. The definitions for A_{k-1}, B_{k-1} and Q_{k-1} are given in (2.1-24) to (2.1-26). In the measurement update $F(.)$ represents the measurement function given in (2.1-20). K_k is the Kalman gain and $S_{k|k-1}$ is the innovation covariance. J_k is the Jacobian of the measurement function and its details are given in (2.3-9) to (2.3-16), [12, 20].

$$J_k = \begin{bmatrix} j_k^1 \\ \vdots \\ j_k^N \end{bmatrix}, \quad 2.3\text{-}9$$

$$j_k^i = \left[\frac{\partial F_k^i}{\partial x} \frac{\partial F_k^i}{\partial y} \frac{\partial F_k^i}{\partial v_x} \frac{\partial F_k^i}{\partial v_y}\right], \quad 2.3\text{-}10$$

where

$$\frac{\partial F_k^i}{\partial v_x} = -\frac{2}{\lambda}\frac{(x_k - x^i)}{d_k^i}, \quad 2.3\text{-}11$$

$$\frac{\partial F_k^i}{\partial v_y} = -\frac{2}{\lambda}\frac{(y_k - y^i)}{d_k^i}, \quad 2.3\text{-}12$$

$$\frac{\partial F_k^i}{\partial x} = -\frac{2}{\lambda}\left(\frac{v_{x,k}.\, d_k^i - (x_k - x^i).\, \dot{d_k^i}}{(d_k^i)^2}\right), \quad 2.3\text{-}13$$

$$\frac{\partial F_k^i}{\partial y} = -\frac{2}{\lambda}\left(\frac{v_{y,k}.\, d_k^i - (y_k - y^i).\, \dot{d_k^i}}{(d_k^i)^2}\right), \quad 2.3\text{-}14$$

$$d_k^i = \sqrt{(x_k - x^i)^2 + (y_k - y^i)^2}, \quad 2.3\text{-}15$$

$$\dot{d_k^i} = \frac{v_{x,k}(x_k - x^i) + v_{y,k}(y_k - y^i)}{d_k^i}. \quad 2.3\text{-}16$$

CRLB is a common figure of merit to compare the estimators with, [33]. CRLB is the inverse of the Fisher information matrix which can be calculated by taking the derivatives of the measurement likelihood functions. CRLB for recursive estimation is given below [12].

$$CRLB_k = FIM_k^{-1} \quad 2.3\text{-}17$$

where

$$FIM_k = (A_{k-1} FIM_{k-1}^{-1} A_{k-1}^T)^{-1} + J_k{}^T R^{-1} J_k. \quad 2.3\text{-}18$$

Here, FIM and $CRLB$ represent the Fisher information and the Cramer-Rao Lower Bound matrices respectively. A_k represents the target state transition matrix. R represents the measurement noise covariance matrix and J_k represents the Jacobian matrix given in (2.3-9).

Lower bounds for the RMS position errors, $LB_{Pos,k}$, and the RMS velocity errors, $LB_{Vel,k}$, can be calculated from the CRLB matrices as follows.

$$LB_{Pos,k} = \sqrt{diag(CRLB_k, 1) + diag(CRLB_k, 2)} \quad \text{2.3-19}$$

$$LB_{Vel,k} = \sqrt{diag(CRLB_k, 3) + diag(CRLB_k, 4)} \quad \text{2.3-20}$$

Here, $diag(A, i)$ denotes the ith diagonal element of the matrix A.

2.4. Simulation results for initiator algorithm

In this section EKF filter with the given initiator is simulated with five active Doppler sensors in a target tracking scenario. In [17], the sensors are placed on a circle and it was stated that as the number of the sensors increases, the error variances decrease significantly. However, the change in the error variance becomes minor if more than four sensors are used. Also in [6], it was stated that the initiator algorithm with five or six sensors does not produce ghost solutions. From these perspectives, it is preferred to use five sensors with four of them located on the vertices of square and one of them placed at origin. CRLB results show that the placement of one sensor at the origin or any point inside the area restricted by the sensors lowers the average error variance bound over the region of interest.

The simulations are repeated for different initial positions and different moving directions of the target. Some starting points are chosen in the square surrounded by the sensor locations and the remaining initial positions are located outside this region. The simulated starting positions and target moving directions are shown in Figure 8. The sensors are named as S1, S2,…, S5 and the targets are named as T1, T2,…, T7. Target moving directions are illustrated with line segments which start from the starting points. The lengths of the line segments represent the target speeds.

As the speed of each simulated target is different, the lengths of the line segments are not equal to each other. Exact values for the target states are given in Table 1.

Table 1 Target Initial States

Initial Point	Velocity(X,Y) m/s	Position(X,Y) m
T1	5 , 20 m/s	-500, -1000 m
T2	0, -10 m/s	-1250, 0 m
T3	-20, 5 m/s	750, 1000 m
T4	20, 0 m/s	1500, 0 m
T5	-20, -5 m/s	1500, 2500 m
T6	5, 20 m/s	-2500, -1000 m
T7	0, -10 m/s	-2500, 1000 m

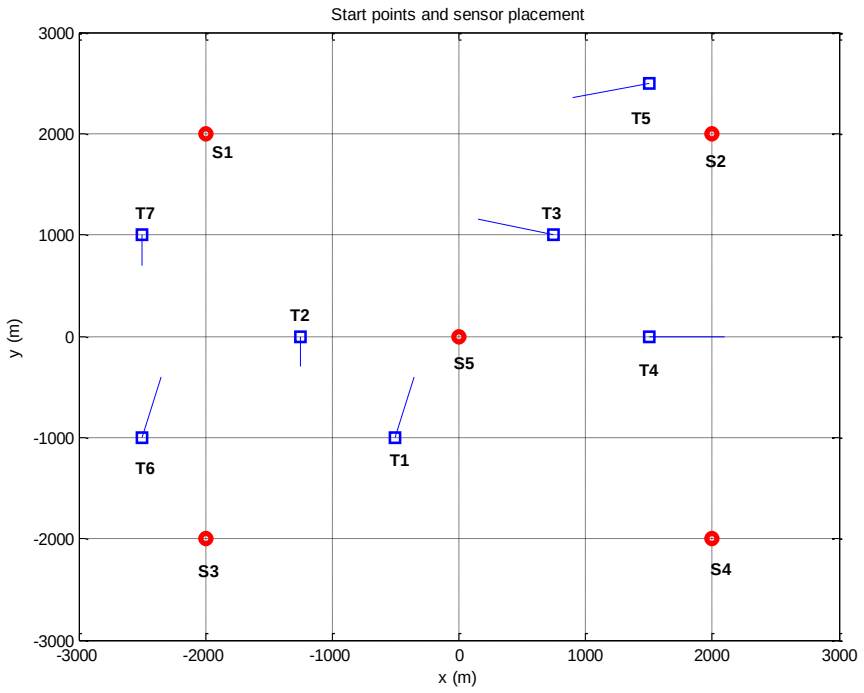

Figure 8 Sensor positions, initial target positions and moving directions.

Simulations are conducted over a time period of 100 seconds. The measurements are taken every 1 second. Target motion is modeled using a nearly constant velocity

model as given in (2.1-23) with the process noise variance value of $\sigma_{proc}^2 = 0.01\ (m/s^2)^2$. Measurement noise variance is chosen as $\sigma_{meas}^2 = 6.25\ Hz^2$, [16]. The transmission frequency is 9 GHz which is standard for the classical X-band radar applications. So the wavelength value $\lambda = 0.033$ meters is used. The results of the initialization algorithm are used to initialize the state of the filters. The calculated CRLB for the initial positions is used as the initial state covariance matrix. In the initialization algorithm, the grid-search area is restricted between -3000 meters and 3000 meters in both axes. A uniform grid spacing of 20 meters is used. The estimated and true target trajectories are given in Figure 9 to Figure 15.

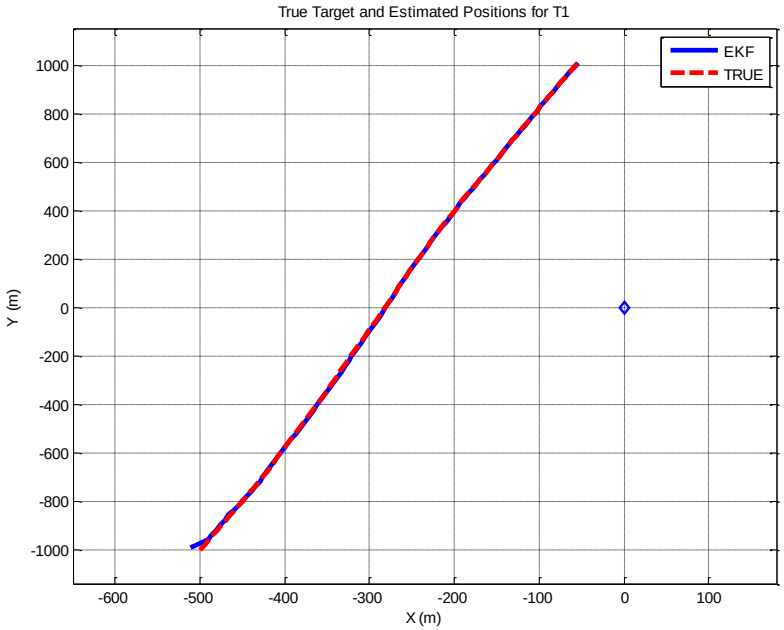

a)

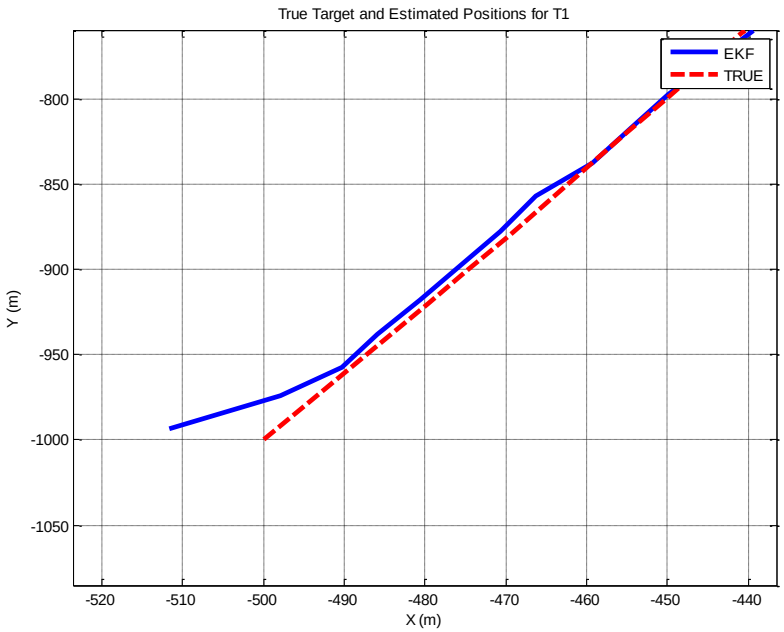

b)

Figure 9 True target positions and EKF position estimates for T1, a) whole trajectory, b) trajectory zoomed around the initial position.

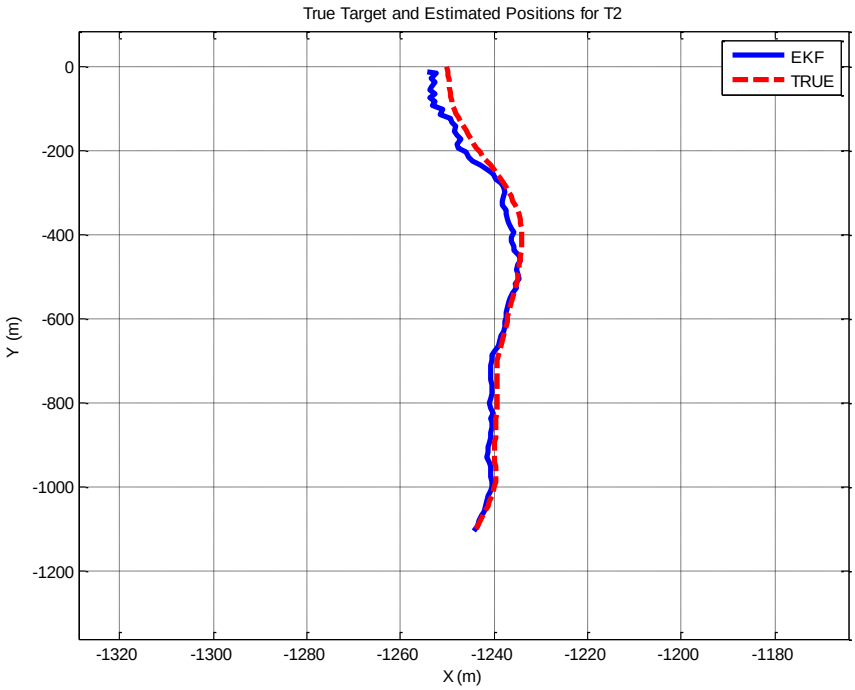

Figure 10 True target positions and EKF position estimates for T2.

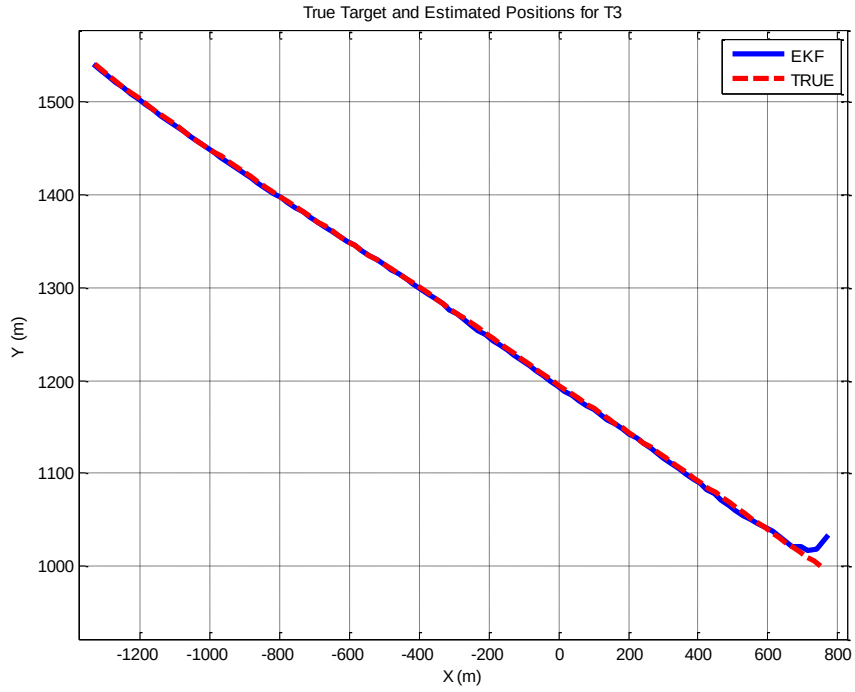

Figure 11 True target positions and EKF position estimates for T3.

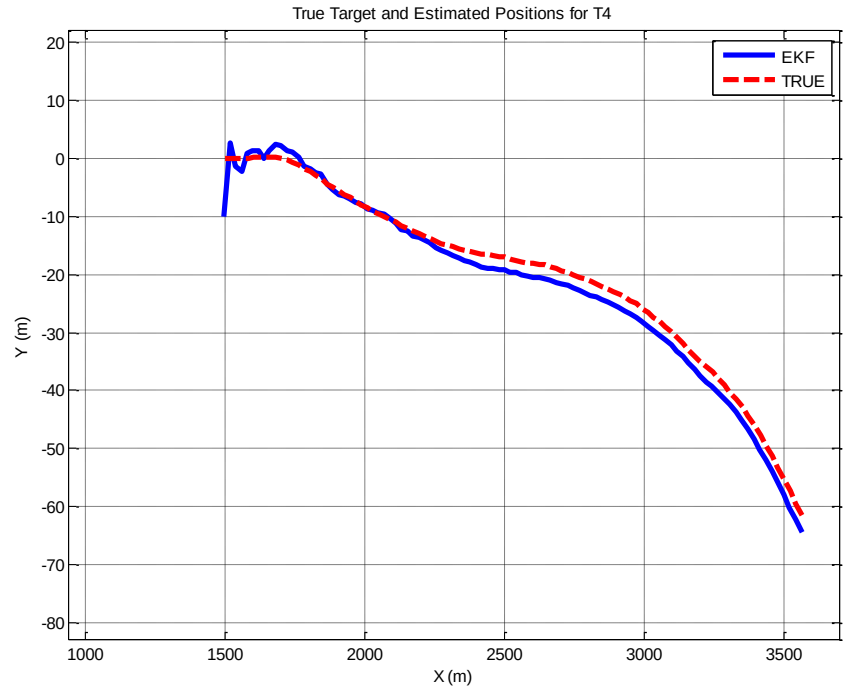

Figure 12 True target positions and EKF position estimates for T4.

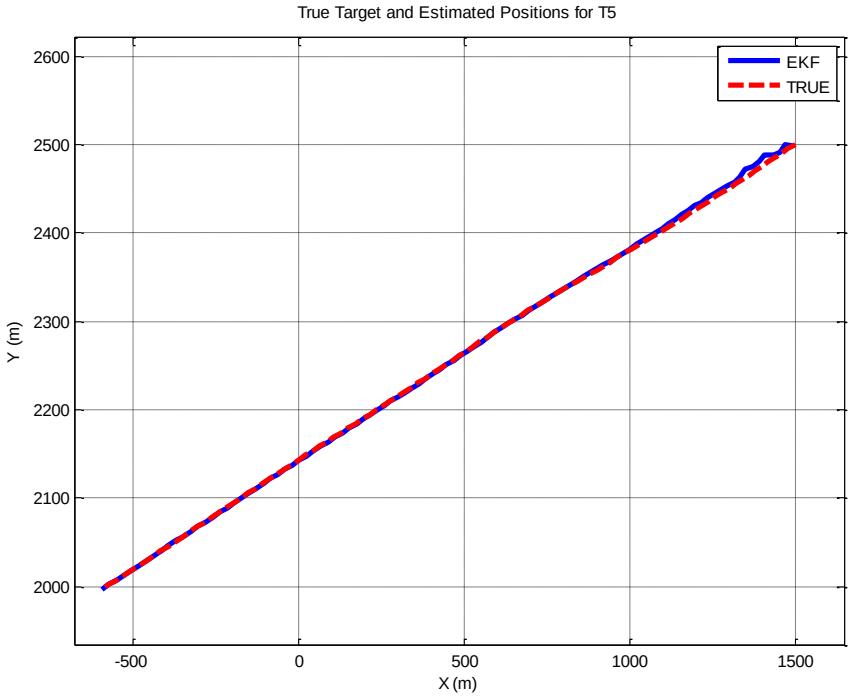

Figure 13 True target positions and EKF position estimates for T5.

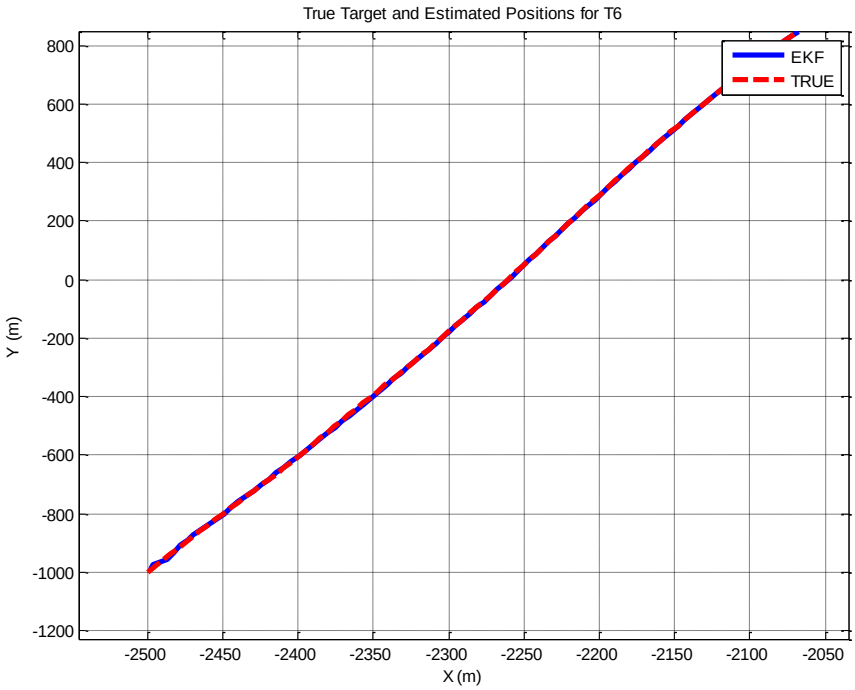

Figure 14 True target positions and EKF position estimates for T6.

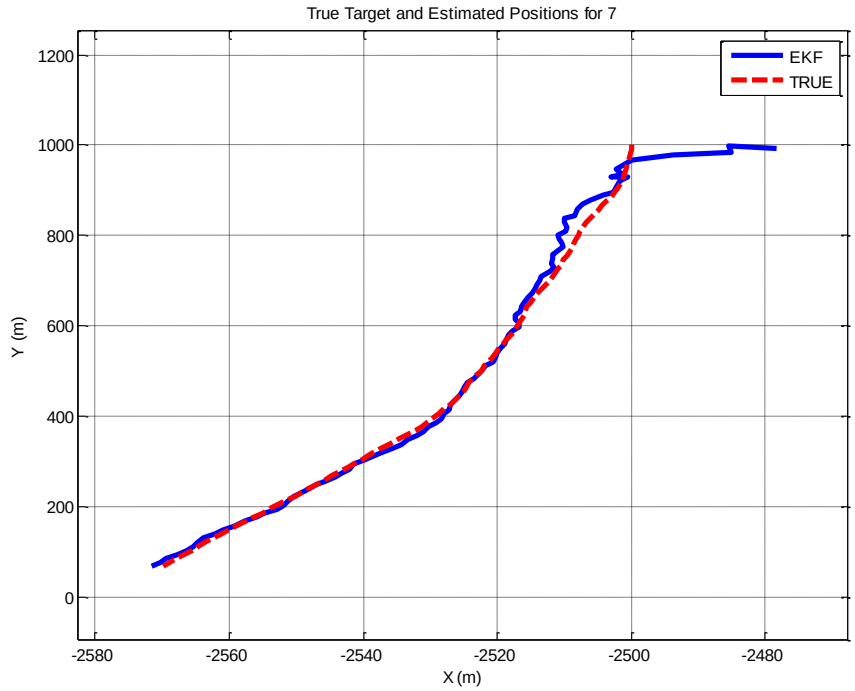

Figure 15 True target positions and EKF position estimates for T7.

As seen in the figures, EKF with the initialization algorithm provides promising results. To compare the error performance to the lower bounds, the RMS and CRLB values for the position and the velocity errors are shown in Figure 16 to Figure 29. For RMS error calculations, Monte-Carlo simulations consisting of 100 runs are conducted. CRLB expressions given in (2.3-17) and (2.3-18) are valid when the variance of the target process noise is zero. So, in these simulations, target process noise is assumed to be zero.

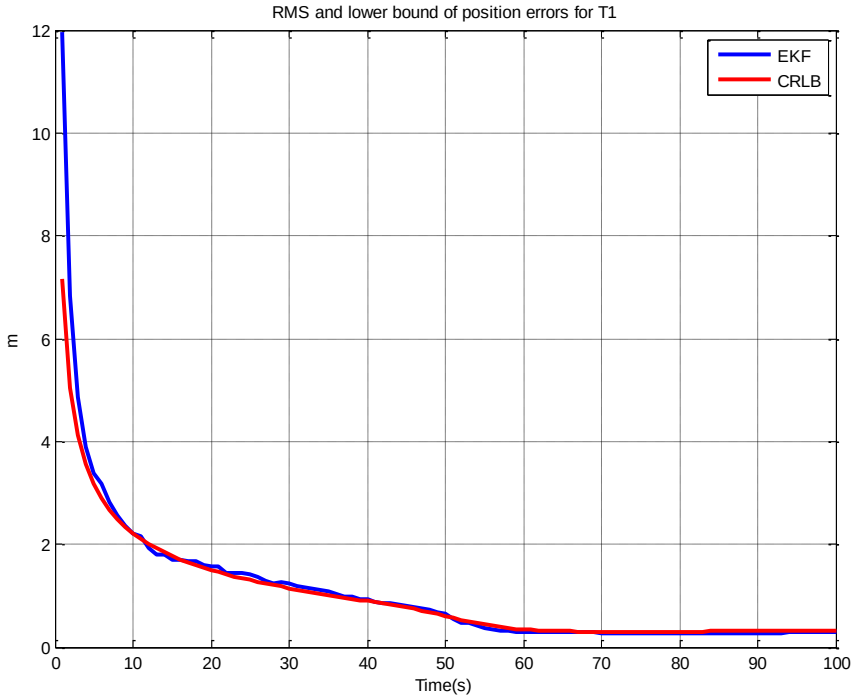

Figure 16 RMS and CRLB values for the position errors for T1.

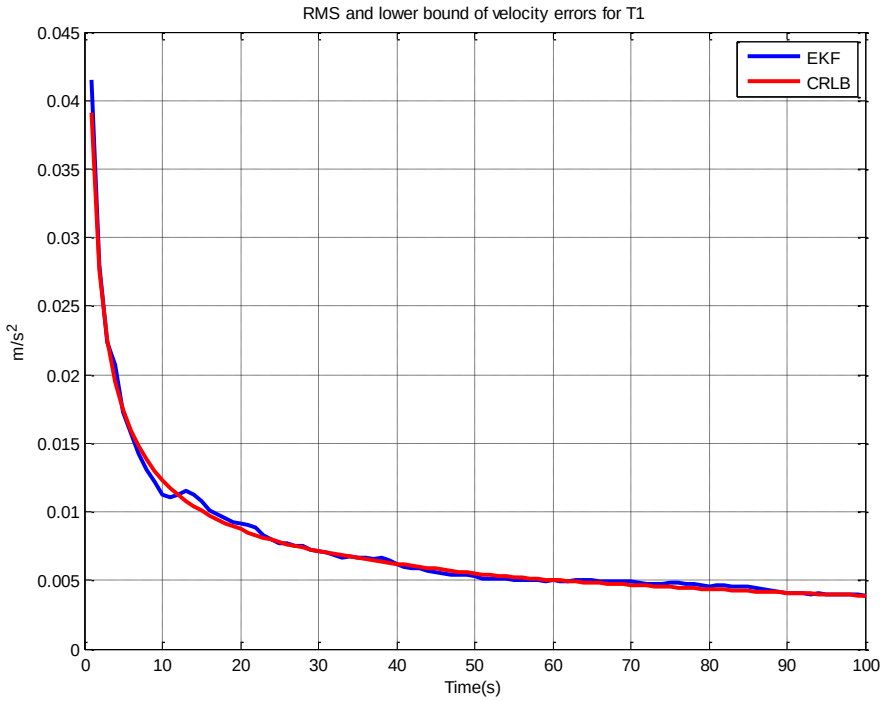

Figure 17 RMS and CRLB values for the velocity errors for T1.

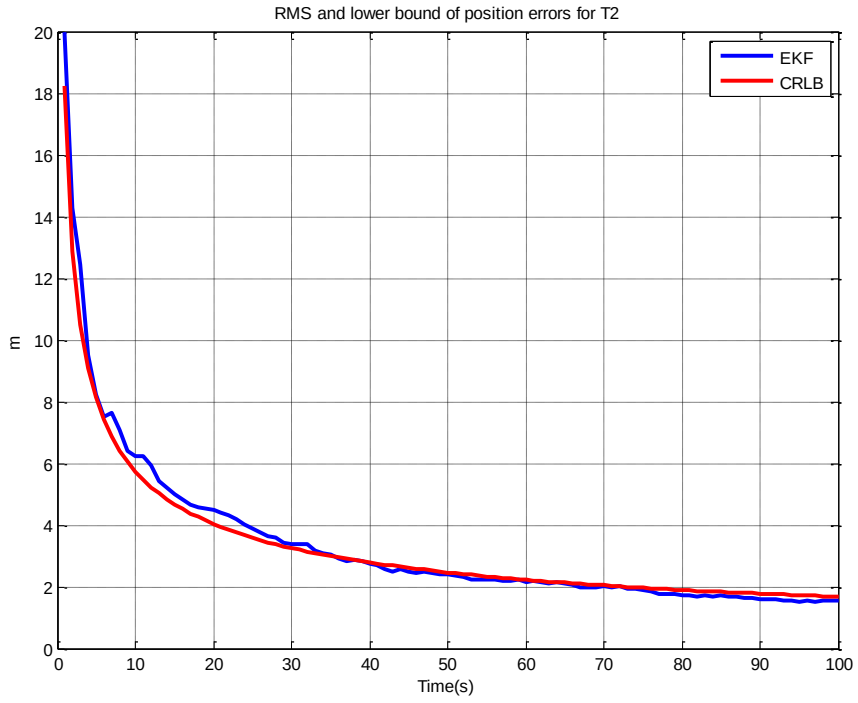

Figure 18 RMS and CRLB values for the position errors for T2.

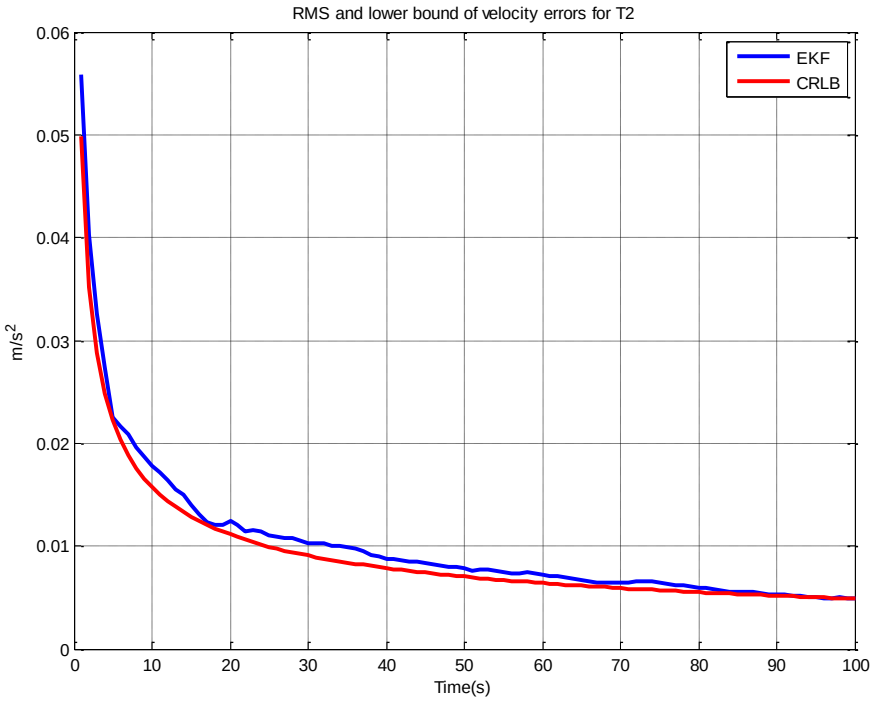

Figure 19 RMS and CRLB values for the velocity errors for T2.

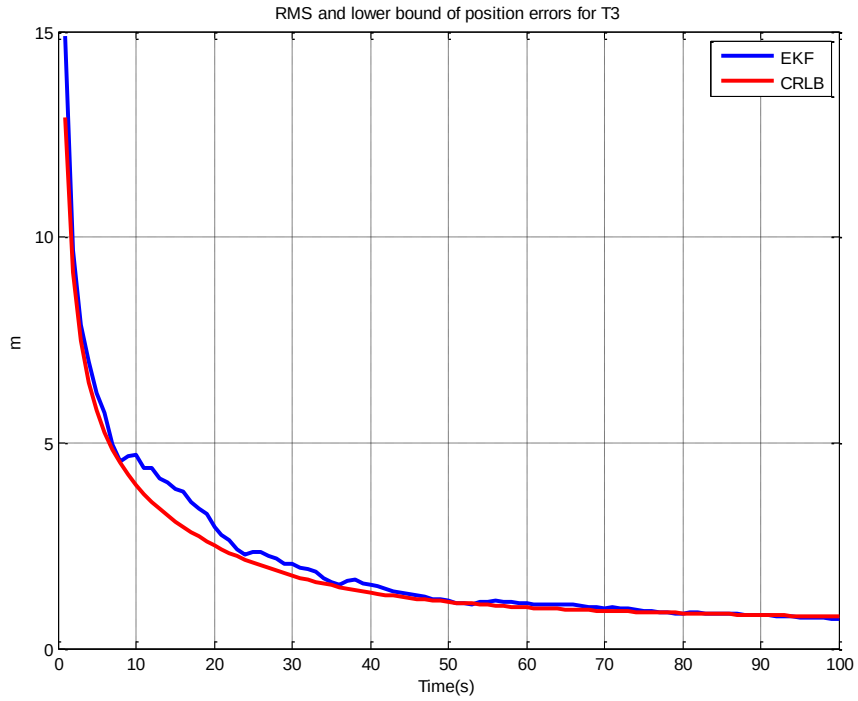

Figure 20 RMS and CRLB values for the position errors for T3.

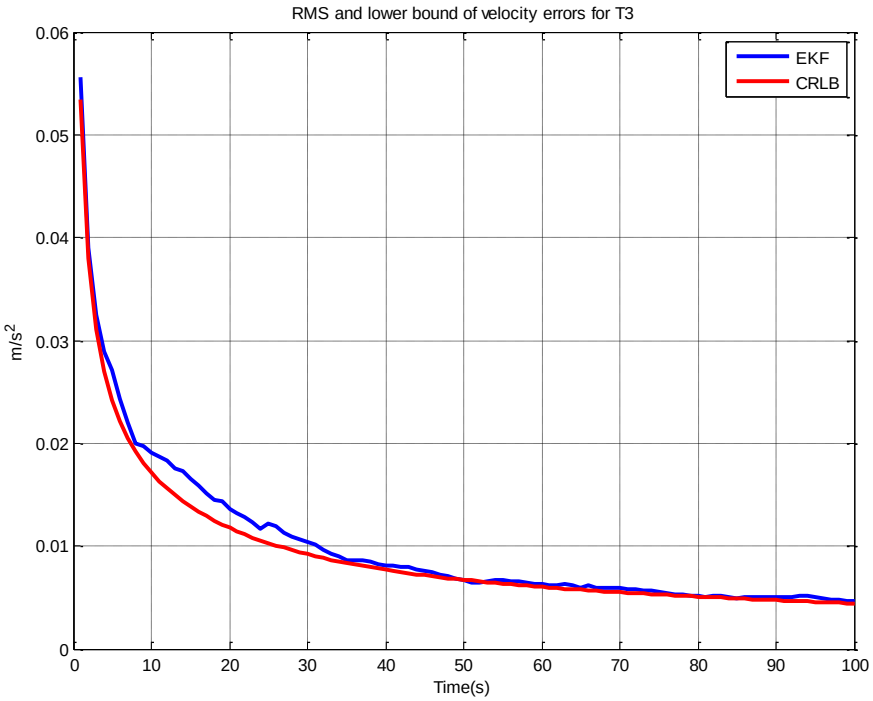

Figure 21 RMS and CRLB values for the velocity errors for T3.

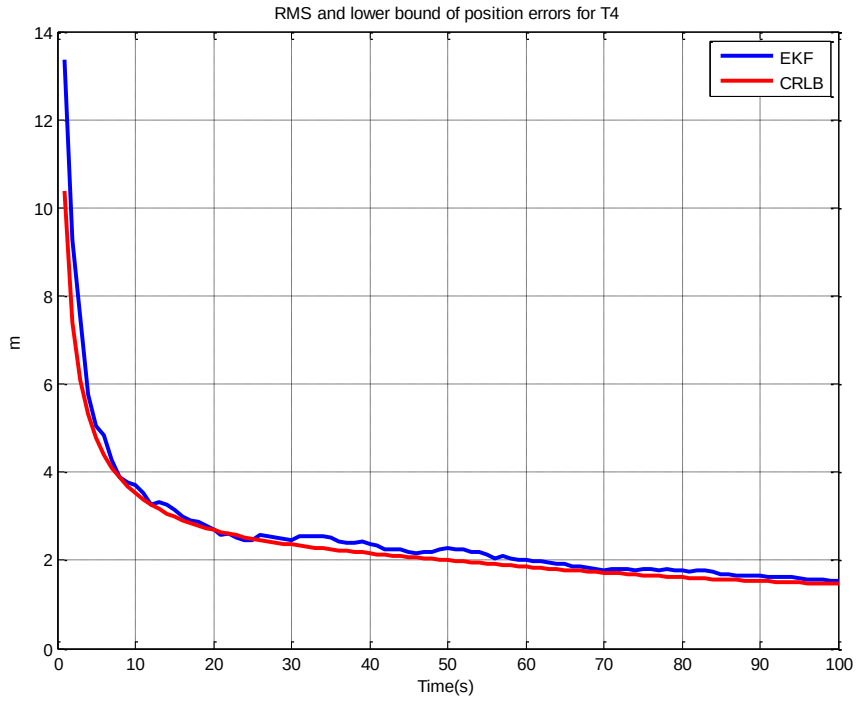

Figure 22 RMS and CRLB values for the position errors for T4.

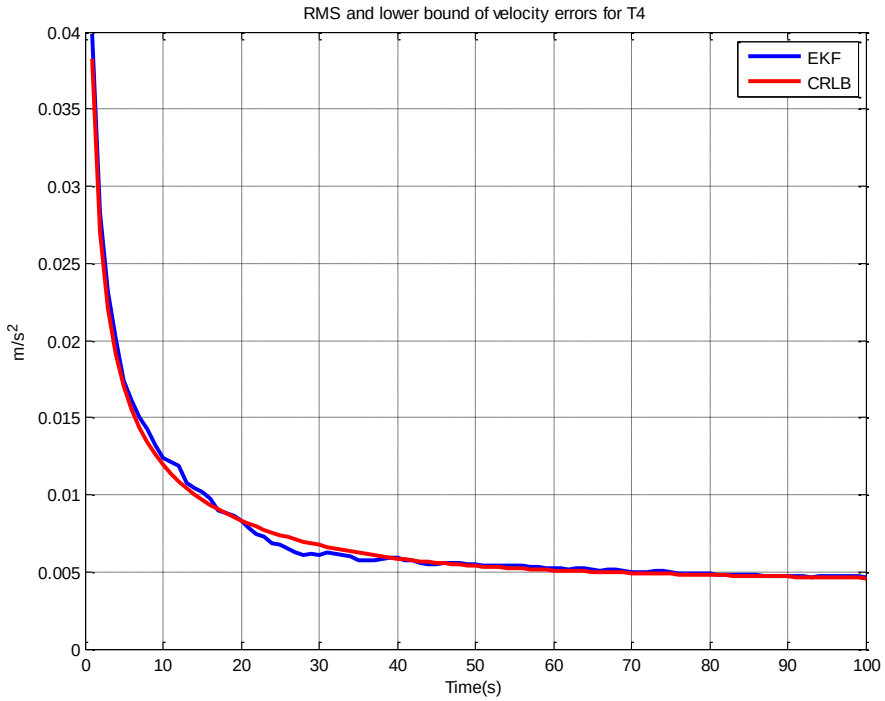

Figure 23 RMS and CRLB values for the velocity errors for T4.

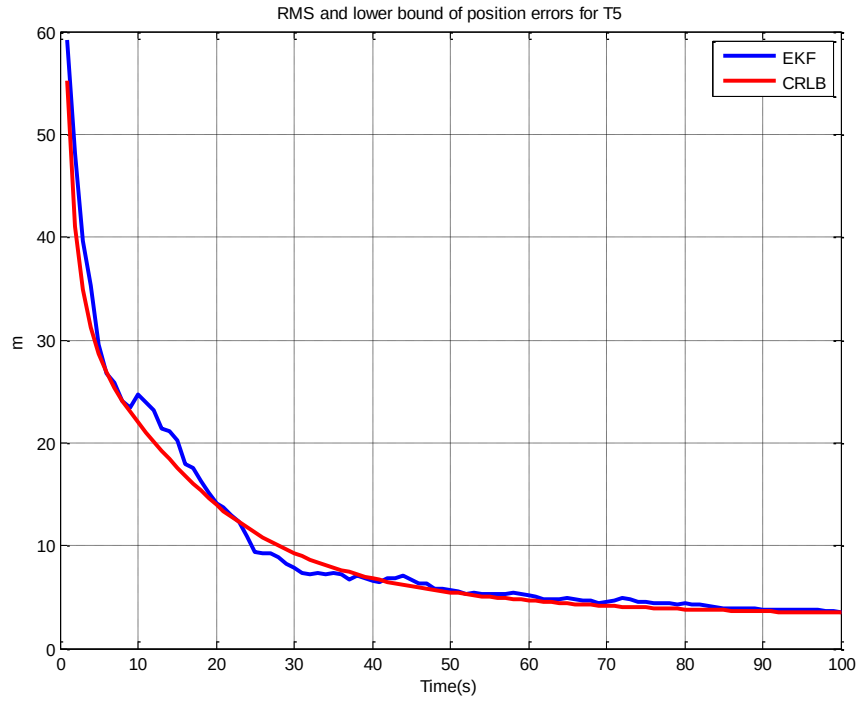

Figure 24 RMS and CRLB values for the position errors for T5.

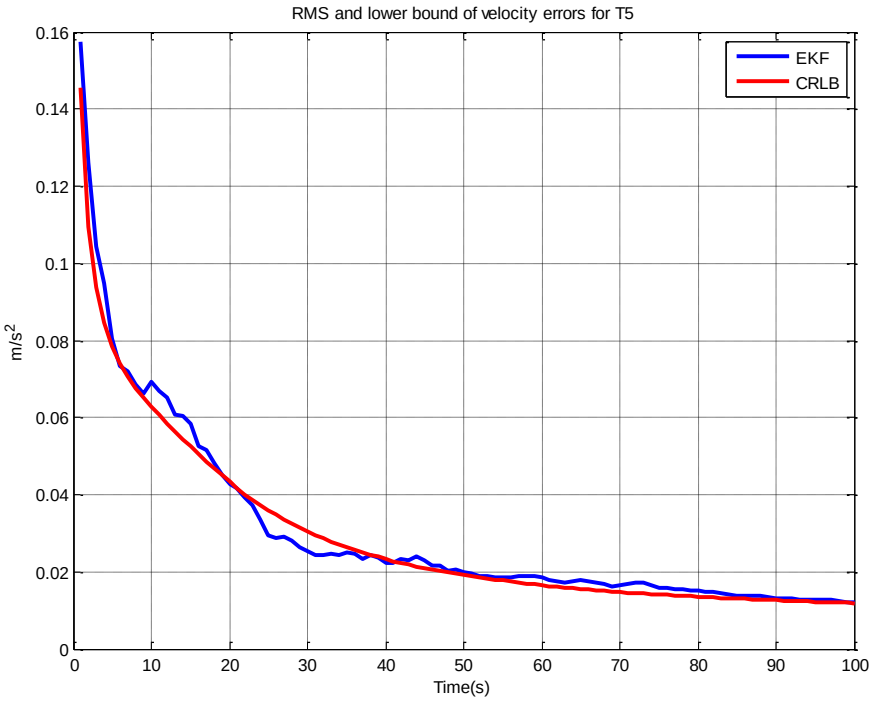

Figure 25 RMS and CRLB values for the velocity errors for T5.

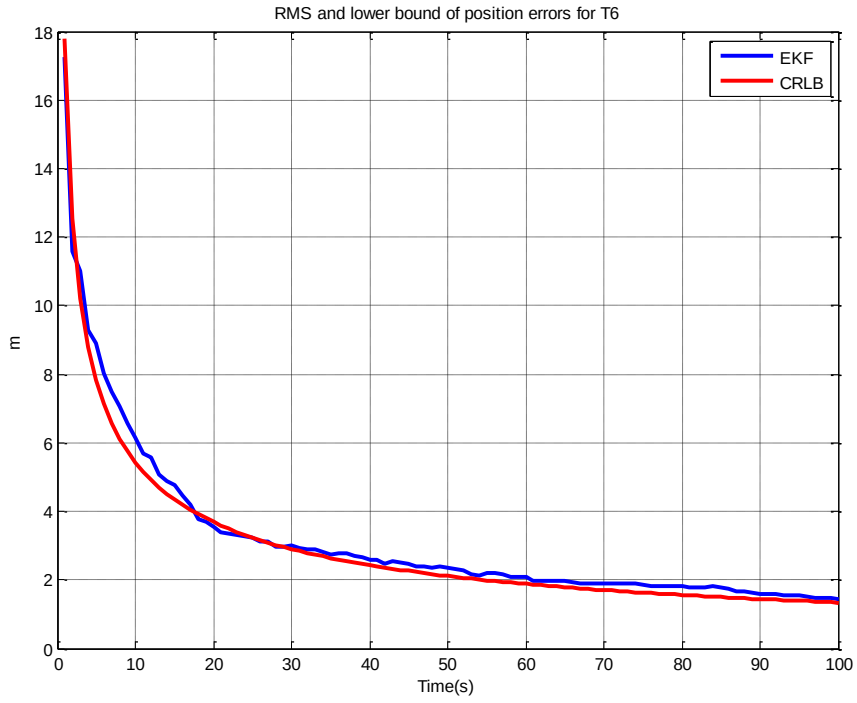

Figure 26 RMS and CRLB values for the position errors for T6.

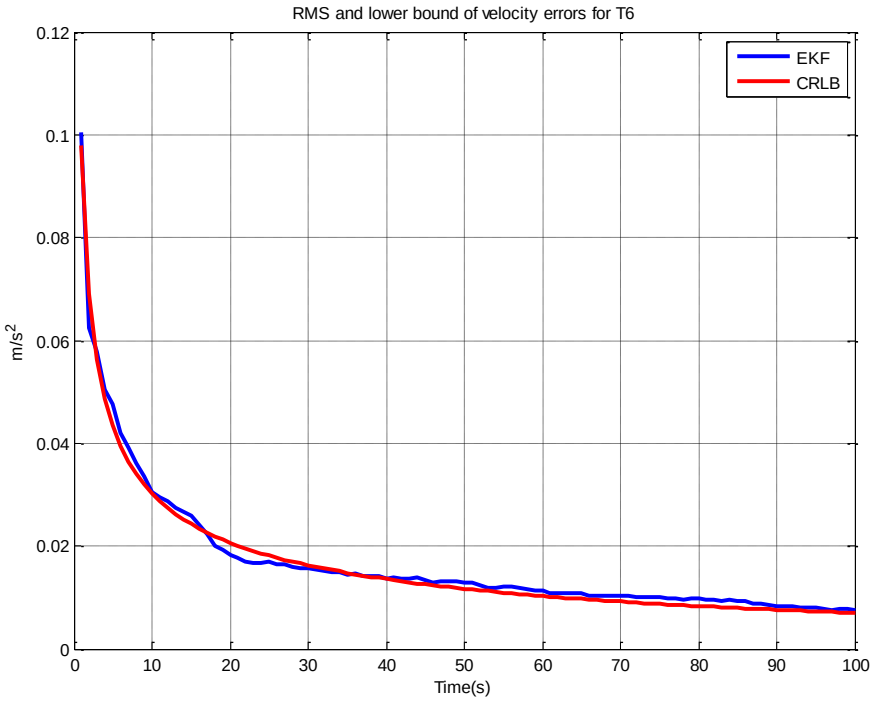

Figure 27 RMS and CRLB values for the velocity errors for T6.

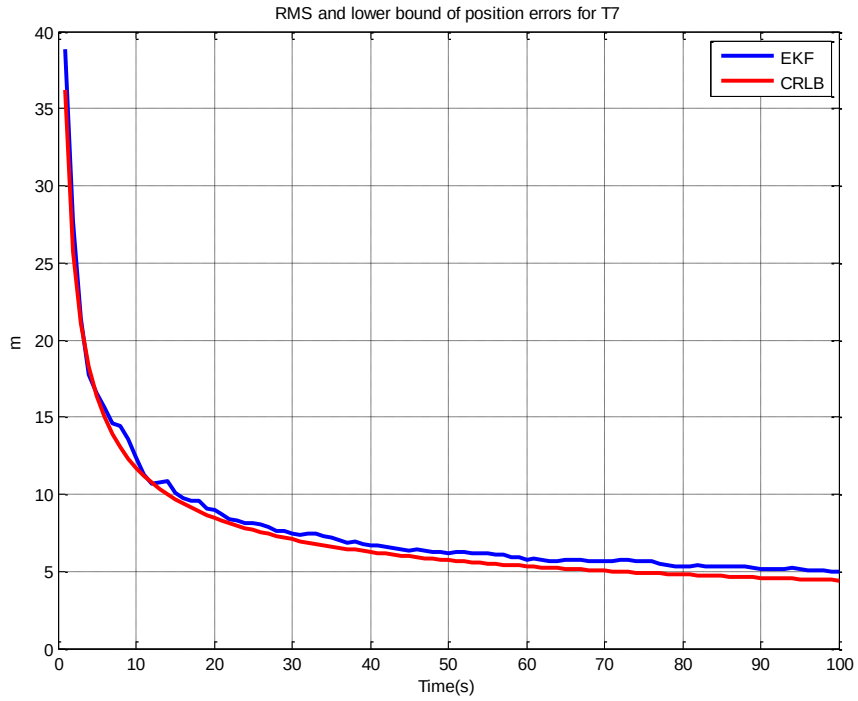

Figure 28 RMS and CRLB values for the position errors for T7.

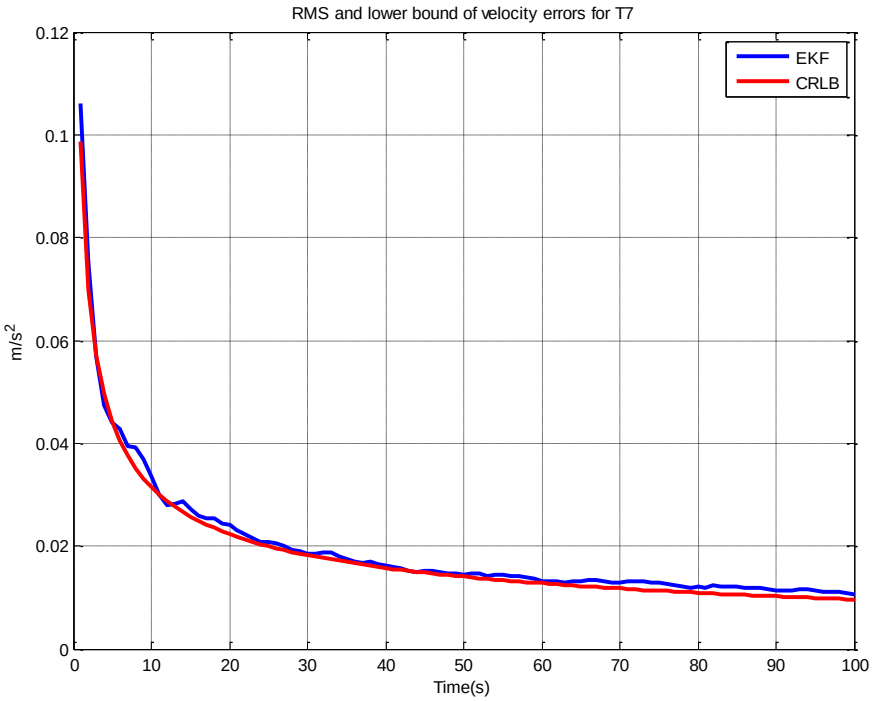

Figure 29 RMS and CRLB values for the velocity errors for T7.

As can be seen from the figures above, EKF has satisfactory performance near to CRLB when it is initialized with the initialization algorithm. Also with good initialization, the errors of the EKF can settle down in a short time. On the other hand, without using a good initial point, EKF may diverge from the true target trajectory or the track may continue with a large bias. In order to demonstrate the importance of initialization, the case of T4 above is repeated with faulty initial positions and velocities as shown in the Figure 30 and Figure 31. In Figure 30, the initial position and velocity are chosen as $x = -1000$ meters, $y = 500$ meters, $v_x = -20$ m/s, $v_y = 0$ m/s. In Figure 31 the initial position and velocity are chosen as $x = 1000$ meters, $y = 1000$ meters, $v_x = -20$ m/s, $v_y = 0$ m/s. EKF initial covariance matrix is selected to be diagonal with variances chosen as $\sigma_x^2 = \sigma_y^2 = 1e4\text{m}^2$ and $\sigma_{v_x}^2 = \sigma_{v_y}^2 = 225\ (\text{m/s})^2$.

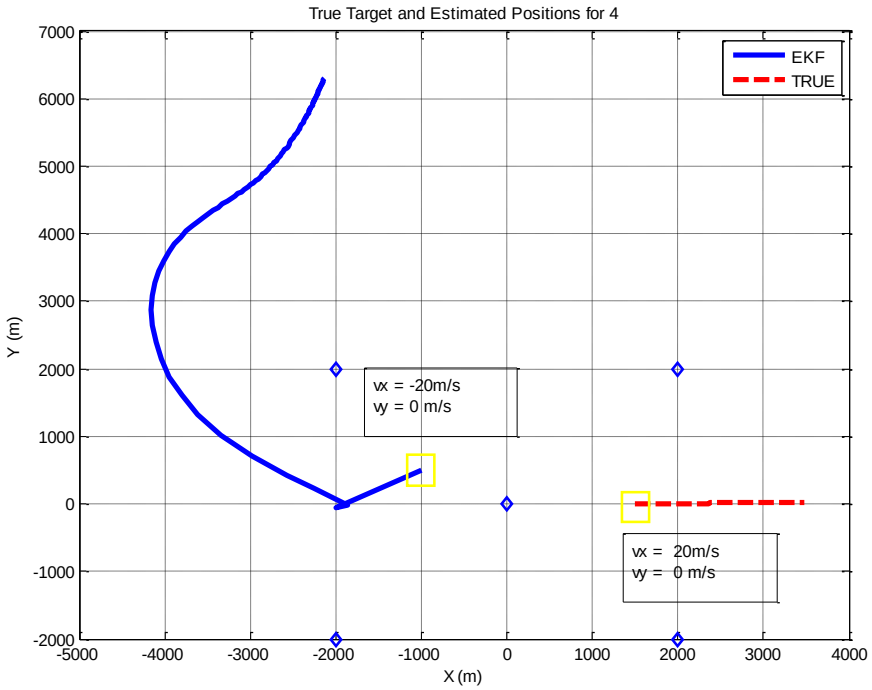

Figure 30 True and estimated trajectories for T4 with wrong initial position and velocity.

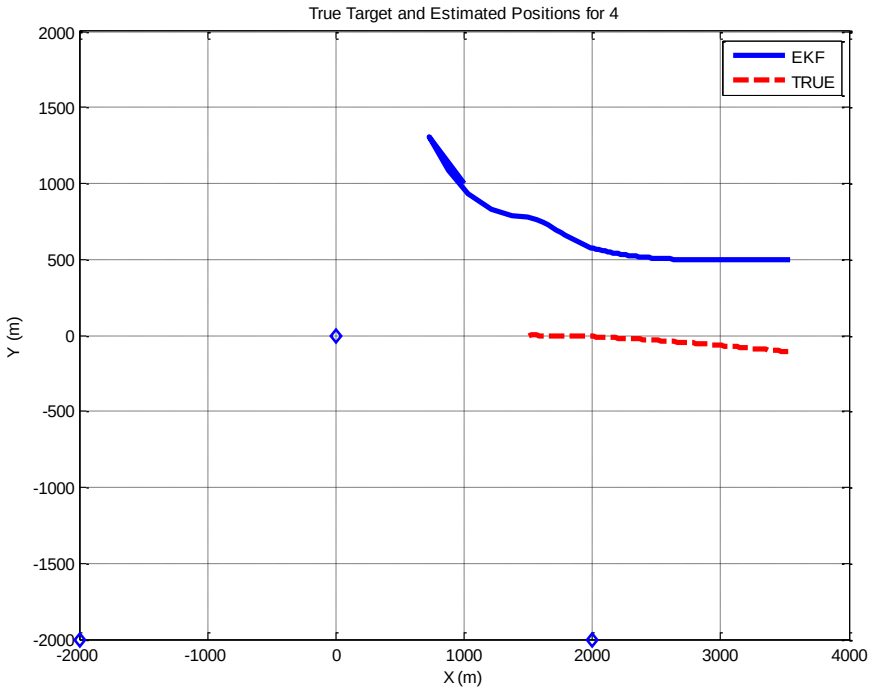

Figure 31 True and estimated trajectories for T4 with wrong initial position and velocity.

To observe the initialization algorithm error performance numerically, average (along time) RMS position and velocity errors are calculated using a Monte Carlo simulation with 50 runs for each initial position. CRLB values for the position and velocity errors are listed with Monte Carlo results in Table 2. Here, the grid spacing of 20 meters and the measurement noise variance of 6.25 Hz^2 are used.

Table 2 Average position and velocity CRLBs and corresponding average RMS errors with the initiator, grid spacing = 20 m, f = 9 GHz

Points	Average Square-root position CRLB (m)	Average RMS position error (m)	Average Square-root velocity CRLB (m/s)	Average RMS velocity error (m/s)
T1	7.1669	13.482	0.0391	0.0448
T2	18.1868	19.108	0.0498	0.0608
T3	12.9442	17.008	0.0535	0.0650
T4	10.4130	12.888	0.0383	0.0388
T5	19.7553	29.442	0.0962	0.1446
T6	17.8058	22.656	0.0979	0.1163
T7	36.384	39.313	0.099	0.107

As seen in Table 2, average velocity errors are very close to the lower bound and the position errors are rather satisfactory. Only T7 which is outside of the sensor region has large CRLB and RMS error values. To lower the initialization algorithm complexity, the grid spacing parameter can be chosen large, but with large grid spacing ghost targets can appear in the grid search. Average CRLB and RMS error results for the grid spacing of 100 meters are given in Table 3. Here, except T5 which has an initial velocity pointing towards the outside of the region of interest, nearly linear increase (around 5 times larger) is observed in the average RMS position errors with 100m grid spacing (which is 5 times the original grid spacing of 20m.).

Table 3 Average position and velocity CRLBs and corresponding average RMS errors with the initiator, grid spacing = 100 m, f = 9 GHz.

Points	Average Square-root position CRLB (m)	Average RMS position error (m)	Average Square-root velocity CRLB (m/s)	Average RMS velocity error (m/s)
T1	7.166	55.208	0.039	0.091
T2	18.186	57.233	0.049	0.206
T3	12.944	39.830	0.053	0.096
T4	10.413	56.849	0.038	0.069
T5	19.755	127.129	0.096	0.556
T6	17.805	52.323	0.097	0.294
T7	36.384	50.30	0.099	0.138

It should be noted that CRLB values and the average RMS errors are not the same for each initial position and velocity value (direction and speed). This is caused by the highly nonlinear measurement function characteristics. As noted in [17], CRLB is dependent on the wavelength, measurement noise variance, sensor placement, target position and target velocity. Sensor placement is another major issue for research in Doppler-only tracking and localization, and it is going to be discussed in one of the forthcoming chapters. Here, the effects of the wavelength are aimed to be shown. Therefore, the average CRLB and average RMS position and velocity errors are obtained for the lower frequency (higher wavelength) 0.9 GHz. The results are presented in Table 4 for grid spacing of 20 meters and in Table 5 for grid spacing of 100 meters.

Table 4 Average position and velocity CRLBs and corresponding average RMS errors with the initiator, grid spacing = 20 m, f = 0.9 GHz.

Points	Average Square-root position CRLB (m)	Average RMS position error (m)	Average Square-root velocity CRLB (m/s)	Average RMS velocity error (m/s)
T1	71.669	74.836	0.391	0.411
T2	181.868	183.624	0.498	0.509
T3	129.442	136.371	0.535	0.600

Tablo 4 Continued				
Points	Average Square-root position CRLB (m)	Average RMS position error (m)	Average Square-root velocity CRLB (m/s)	Average RMS velocity error (m/s)
T4	104.130	104.178	0.383	0.343
T5	197.553	213.568	0.962	1.039
T6	178.057	204.000	0.979	1.137
T7	363.845	445.974	0.990	1.060

Table 5 Average position and velocity CRLBs and corresponding average RMS errors with the initiator, grid spacing = 100 m, f = 0.9 GHz

Points	Average Square-root position CRLB (m)	Average RMS position error (m)	Average Square-root velocity CRLB (m/s)	Average RMS velocity error (m/s)
T1	71.669	83.533	0.391	0.3974
T2	181.868	234.378	0.498	0.500
T3	129.442	141.464	0.535	0.581
T4	104.130	110.585	0.383	0.404
T5	197.553	219.201	0.962	1.133
T6	178.057	189.838	0.979	1.075
T7	363.845	468.217	0.990	0.906

As seen in Table 4 and Table 5, increase in the wavelength (decrease in frequency) causes an almost linear increase in the CRLB. This is due to the fact that the SNR is decreased when the wavelength is increased as can be seen in the measurement expression (2.1-20). Average position and velocity errors are close to the CRLBs for both 20 m and 100 m grid spacing. The results with the grid spacing of 250 meters are given in Table 6which shows significant increase in the RMS position errors compared to the results with the grid spacing 100 meters.

Table 6 Average position and velocity CRLBs and corresponding average RMS errors with the initiator, grid spacing = 250 m, f = 0.9 GHz.

Points	Average Square-root position CRLB (m)	Average RMS position error (m)	Average Square-root velocity CRLB (m/s)	Average RMS velocity error (m/s)
T1	71.669	160.39	0.391	0.511
T2	181.868	253.60	0.498	0.663
T3	129.442	183.85	0.535	0.727
T4	104.130	145.12	0.383	0.374
T5	197.553	270.19	0.962	1.346
T6	178.057	224.11	0.979	1.183
T7	363.845	509.95	0.990	0.997

An important result from the comparisons above is that, with the higher wavelength, the grid spacing of 20 meters has nearly the same error performance with grid spacing of 100 meters. Hence in this case, 100 meters is preferable due to its lower computational complexity. On the other hand when the grid spacing is increased to 250 meters, a considerable increase is observed in the RMS errors. The reason which is thought to be behind these observations is that

- the grid spacing of 100 meters is already smaller or around the (square root) CRLB values obtained for the higher wavelength . Hence an increase of the grid spacing from 20 meters to 100 meters does not make much of a difference for the EKF.
- the grid spacing of 250 meters is much higher than the (square root) CRLB values obtained for the higher wavelength . Hence an increase of the grid spacing from 100 meters to 250 meters makes the performance of the EKF significantly worse.

As a result, a rule of thumb for selecting the grid spacing parameter might be to choose it to be similar to the CRLB for the problem to optimize the performance and the amount of computations.

Another important issue that should be pointed out is that initial positions outside the region circumscribed by the sensors can produce more RMS errors as seen in Table 3 when grid spacing is larger than the lower bound. This is caused by the ghost target positions produced by the grid search algorithm. This situation can be observed in Figure 32 which presents the cost function for the grid search for T5. In this case, the cost value of the real target position is actually lower than the ghost position, but the grid is too coarse to find the real target position and therefore the ghost position is chosen as the initial target position.

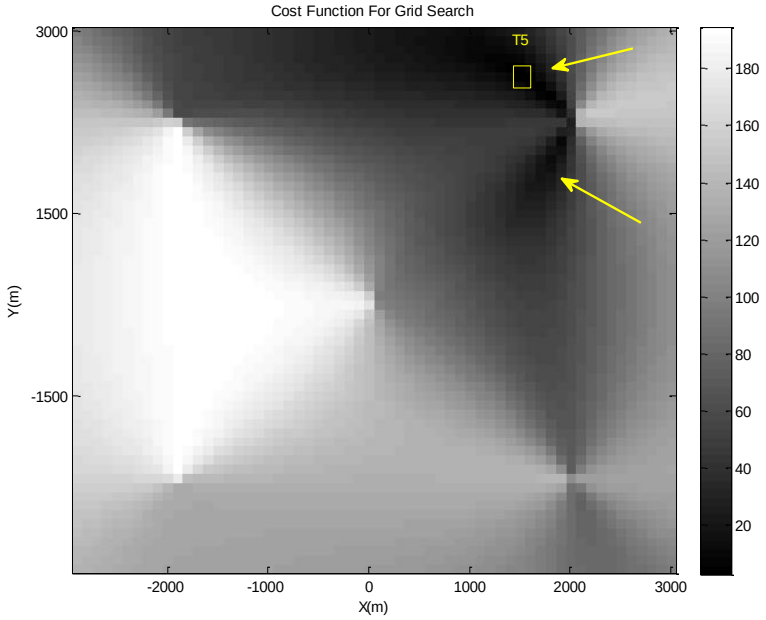

Figure 32 Cost function values over x-y plane.

From these results it can be said that CRLB can be thought of as a baseline for the grid spacing. The grid spacing can be increased within the tradeoff between the computational complexity and the initialization performance while keeping in mind that with large grid spacing, the performance will be decreased dramatically especially for a target located outside the region circumscribed by the sensors. CRLB depends on many parameters such as target position, velocity, sensor positions, wavelength and measurement noise variance. When the measurement noise variance, sensor placement and the wavelength are known a priori, for all possible initial target

position and velocity of interest, lower bounds can be calculated and the maximum or average values of these lower bounds can be considered. It should be stated that points outside of the region bounded by the sensors has larger lower bounds and they can produce large position errors compared to the inner points when the grid spacing is larger than the lower bound. In the lower bound, the linear effects of measurement noise variance and wavelength are clear. But the effects of the sensor placement are more ambiguous. To show this, circular sensor geometry is simulated in Figure 33. CRLB values for the same targets with this new sensor geometry are given in Table 7. As seen in Table 7, the changes in the CRLB values are different for different initial positions and velocities.

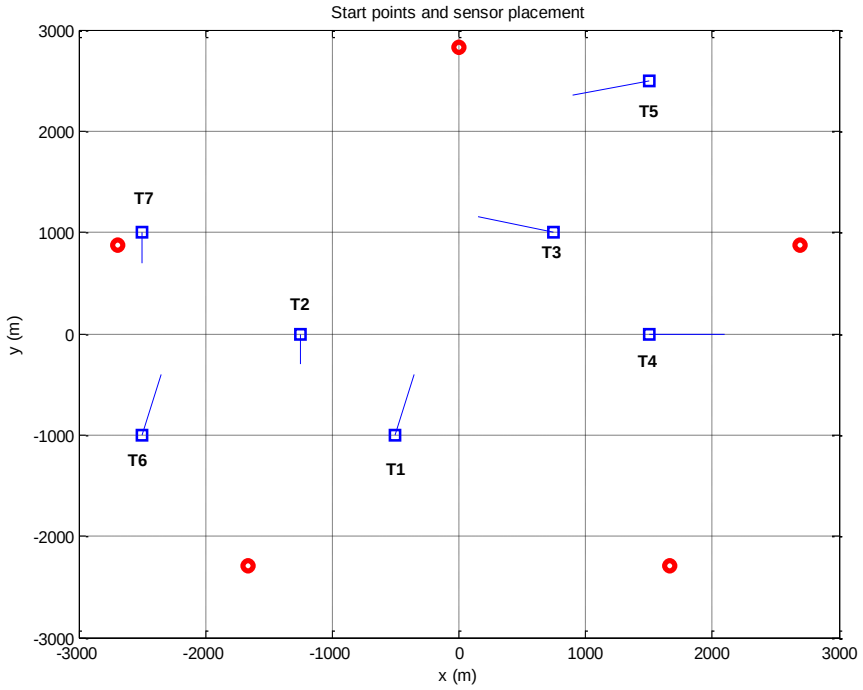

Figure 33 Circular sensor geometry and targets with 5 sensors.

Table 7 CRLB values for different sensor geometries.

	Square Root Position CRLB (m)	
Target	Square Sensor Geometry	Circular Sensor Geometry
T1	71.669	78.33
T2	181.868	246.54
T3	129.442	125.22
T4	104.130	74.09
T5	197.553	1743.4
T6	178.057	1110.5
T7	363.845	735.5

Finally, it can be said that separable least square estimation with a grid search can be used to initialize a nonlinear Doppler-only tracking filter such as EKF. For the choice of grid spacing, the position CRLB constitutes a baseline. There is a trade-off between the computational complexity and the performance. With large grid spacing, performance will be decreased dramatically, especially when the target is located outside the region circumscribed by the sensors. It is important to note that the CRLB values can be different for different target position/velocity values and sensor geometry.

CHAPTER 3

PARTICLE FILTERS FOR DOPPLER ONLY MEASUREMENTS

In this chapter, the use of particle filters for Doppler-only tracking is investigated. The organization of the chapter is given as follows. In Section 3.1, it is shown that for a simple Doppler-only tracking problem, the classic bootstrap particle filter (a sequential importance resampling (SIR) particle filter using state transition density $p(X_{k+1}|X_k^{(i)})$ as its proposal distribution) performs poorly compared to EKF. The reasons for this surprising behavior are discussed in Section 3.1. In the following sections, different types of particle filters are derived and implemented for the same problem with the aim of improving the bootstrap particle filter's performance. In Section 3.2, the Sequential Importance Resampling (SIR) particle filter using optimal proposal density is derived. The optimal proposal density is obtained by making EKF updates in the filter. In Section 3.3, a Rao-Blackwellized particle filter is given for Doppler-only tracking. In the Rao-Blackwellized particle filter, the linear velocity states are estimated using Kalman filters whereas a particle filter estimates the position states. The simulation results for these particle filters are presented in Section 3.4 along with a discussion on the results.

3.1. Bootstrap Particle Filter

In this section, the so-called bootstrap particle filter for Doppler-only tracking is discussed. Bootstrap particle filter is the first particle filter method to be proposed by Gordon et al., [34]. The bootstrap particle filter holds the target state particles and

weights shown as $X_{k|k}^{(i)}$, $\pi_{k|k}^{(i)}$ for $i = 1, \dots, N_p$ where N_p is the number of particles. The main difference of the bootstrap particle filter from the other particle filters is that, the bootstrap particle filter uses the state transition density as the proposal density in the prediction update as discussed below.

Firstly, the target and measurement model used in the derivation of the bootstrap particle filter are given as follows:

$$X_k = A_{k-1}X_{k-1} + B_{k-1}w_{k-1} \tag{3.1-1}$$

$$y_k = F(X_k) + e_k \tag{3.1-2}$$

where

$$A_k = \begin{bmatrix} 1 & 0 & T & 0 \\ 0 & 1 & 0 & T \\ 0 & 0 & 1 & 0 \\ 0 & 0 & 0 & 1 \end{bmatrix} \quad B_k = \begin{bmatrix} 0.5T^2 & 0 \\ 0 & 0.5T^2 \\ T & 0 \\ 0 & T \end{bmatrix} \tag{3.1-3}$$

Here, $X_k = \left[x_k, y_k, v_{x,k}, v_{y,k}\right]^T$ represents the target state, y_k represents the measurements and $F(.)$ is the measurement function given in (2.1-19). $w_k \sim N(w_k; 0, \sigma_{proc}^2 I_2)$ represents the target's unknown acceleration, i.e., the process noise, and $e_k \sim N(w_k; 0, \sigma_{meas}^2 I_2)$ represents the measurement error, i.e., the measurement noise. σ_{proc}^2 and σ_{meas}^2 are the variances of the process noise and measurement noise respectively. I_n denotes an identiy matrix of size n x n.

The matrix B_k is not dependent on time and the unknown acceleration term can be expressed as a single term as follows:

$$X_k = A_{k-1}X_{k-1} + l_{k-1} \tag{3.1-4}$$

where

$$l_k \sim N(l_k; 0, Q), \tag{3.1-5}$$

$$Q = \sigma_{proc}^2 B^T B. \tag{3.1-6}$$

By using the target and the measurement model given above, the steps of the bootstrap particle filter for Doppler-only tracking are given below. A single iteration of the Bootstrap particle filter for Doppler-only tracking has the following steps:

- **Prediction Update:** In this step, the particles $X_{k+1}^{(i)}, i = 1, \dots, N_p$ are propagated to obtain the predicted particles by using (3.1-4) as follows:

$$X_{k+1|k}^{(i)} = AX_{k|k}^{(i)} + l_k^{(i)} \tag{3.1-7}$$

where

$$l_k^{(i)} \sim N(l_k^{(i)}; 0, Q). \tag{3.1-8}$$

The weights remain the same at this step and they are shown as follows:

$$\pi_{k+1|k}^{(i)} = \pi_{k|k}^{(i)}. \tag{3.1-9}$$

Note that since 3.1-9 is used to obtain the new particles, the proposal density is implicitly set to the state transition density $p(X_{k+1}|X_k^{(i)})$, i.e., $X_{k+1|k}^{(i)} \sim p(X_{k+1}|X_k^{(i)})$.

- **Measurement Update:** In this step, the predicted particles are directly taken as the estimated particles as follows:

$$X_{k+1|k+1}^{(i)} = X_{k+1|k}^{(i)} \tag{3.1-10}$$

Particle weights are updated as follows:

$$\hat{\pi}_{k+1|k+1}^{(i)} = \pi_{k|k}^{(i)} \frac{p(y_{k+1}|X_{k+1}^{(i)}) p(X_{k+1}^{(i)}|X_k^{(i)})}{G(X_{k+1}^{(i)}|X_{0:k}^{(i)}, y_{0:k+1})}, \tag{3.1-11}$$

$$\pi_{k+1|k+1}^{(i)} = \frac{\hat{\pi}_{k+1|k+1}^{(i)}}{\sum_i^N \hat{\pi}_{k+1|k+1}^{(i)}}. \tag{3.1-12}$$

Here $G(X_{k+1}^{(i)}|X_{0:k}^{(i)}, y_{0:k+1})$ represents the proposal (or sometimes called the importance) distribution. In the bootstrap particle filter, as mentioned above,

the state transition density $p\left(X_{k+1}\middle|X_k^{(i)}\right)$ is used as the proposal and hence the weight update is simplified as follows:

$$G\left(X_{k+1}^{(i)}\middle|X_{0:k}^{(i)}, y_{0:k+1}\right) = p(X_{k+1}^{(i)}|X_k^{(i)}), \quad 3.1\text{-}13$$

$$\hat{\pi}_{k+1|k+1}^{(i)} = \pi_{k+1|k}^{(i)} p(y_k|X_{k+1|k+1}^{(i)}). \quad 3.1\text{-}14$$

As a result, the weight update in the bootstrap particle filter can be expressed as follows.

$$\pi_{k+1|k+1}^{(i)} = \frac{\hat{\pi}_{k+1|k+1}^{(i)}}{\sum_{i=1}^{N} \tilde{\pi}_{k+1|k+1}^{(i)}} \quad 3.1\text{-}15$$

where

$$\hat{\pi}_{k+1|k+1}^{(i)} = \pi_{k+1|k}^{(i)} p(y_k|X_{k+1|k+1}^{(i)}). \quad 3.1\text{-}16$$

At the final stage, the estimated state and its covariance are calculated as follows:

$$\hat{X}_{k+1|k+1} = \sum_{i=1}^{N} \pi_{k+1|k+1}^{(i)} X_{k+1|k+1}^{(i)}, \quad 3.1\text{-}17$$

$$P_{k|k} = \sum_{i=1}^{N} \pi_{k+1|k+1}^{(i)} (X_{k+1|k+1}^{(i)} - \hat{X}_{k+1|k+1}) (X_{k+1|k+1}^{(i)} - \hat{X}_{k+1|k+1})^T. \quad 3.1\text{-}18$$

Resampling is made at the end of the each iteration to avoid the sample impoverishment problem. In the resampling algorithm, the particles with high weights are replicated according to their weight value and the particles which have low weights are deleted.

To compare the performance of the Bootstrap particle filter with EKF for Doppler-only tracking, these filters are used for tracking a target with four Doppler sensors. Here, the sensors are active similar to the measurement model used in Chapter 2. The sensor positions and the target trajectory are shown in Figure 34.

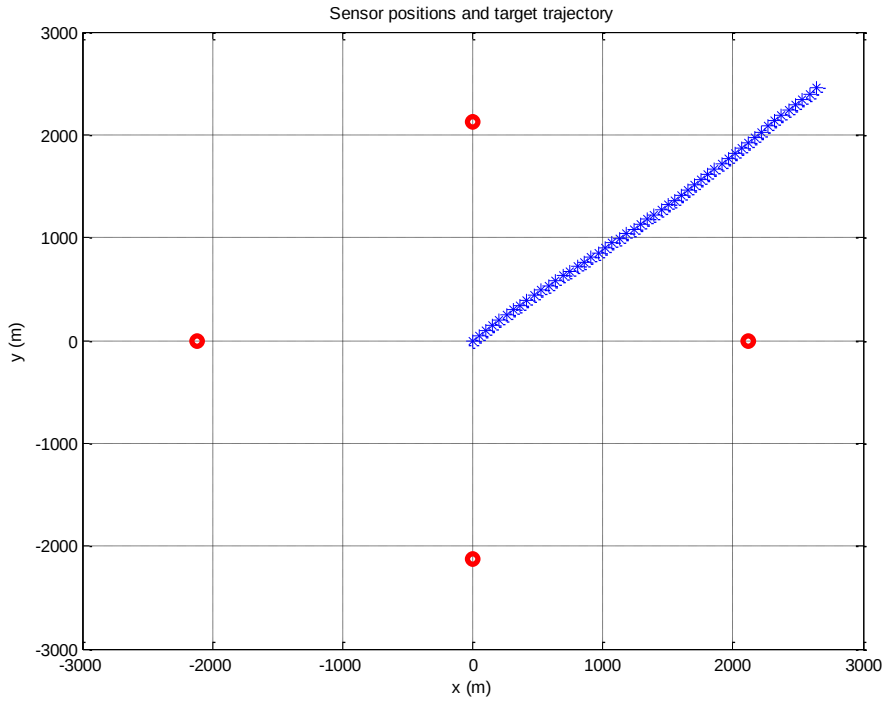

Figure 34 Sensor positions and target trajectory for Bootstrap PF-EKF comparison

Here, the constant velocity model is used while the unknown acceleration has unity variance, i.e., $\sigma_{proc}^2 = 1$. Measurements are taken with a wavelength value of $\lambda = 0.033$ m and the measurement noise variance of $\sigma_{meas} = 10\,Hz$ is used. For the bootstrap PF, 1000 particles are used. With this configuration the target motion is continued for 50 seconds. To compare the performance, RMS position and velocity errors are calculated over 100 Monte-Carlo runs for both filters. Bootstrap PF particle positions are shown in Figure 35 where it is seen clearly that the particle filter has a large bias. RMS errors are shown in Figure 36 and Figure 37.

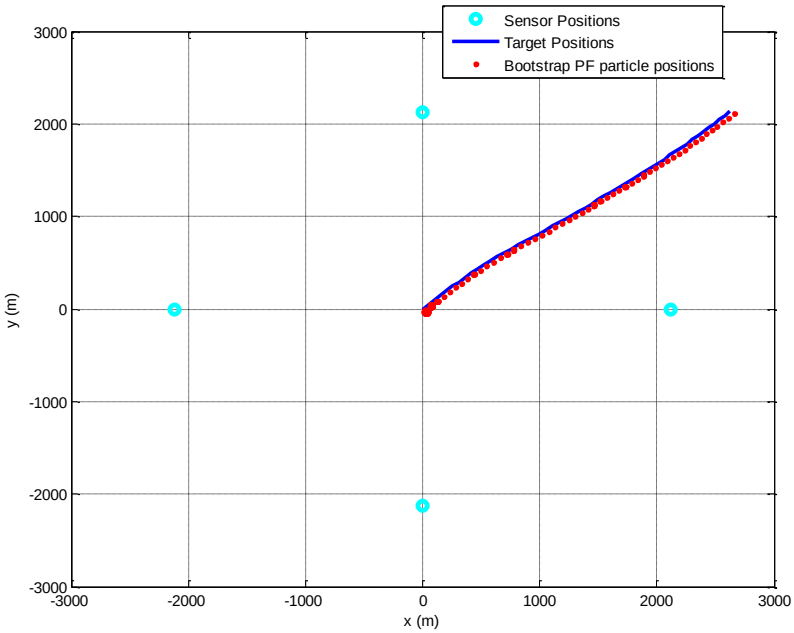

a)

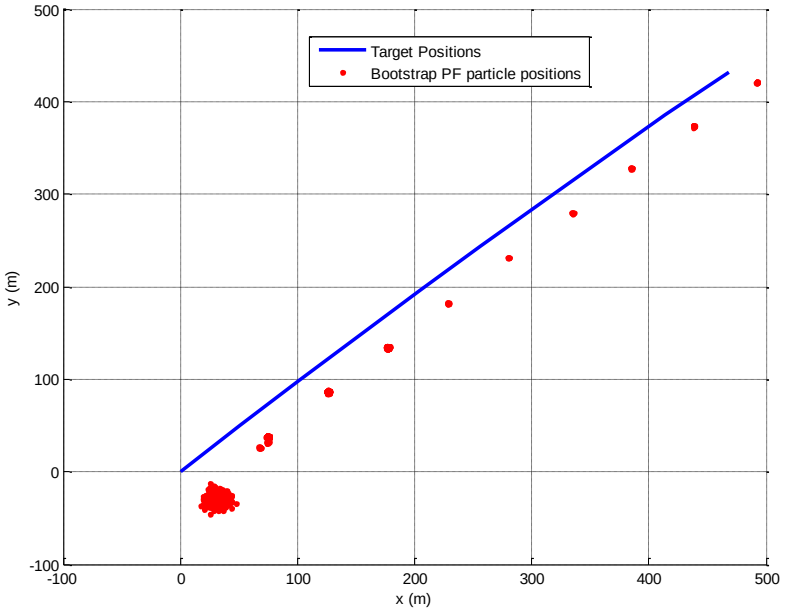

b)

Figure 35 True target and Bootstrap PF particle positions a) whole trajectory b) zoomed around initial position.

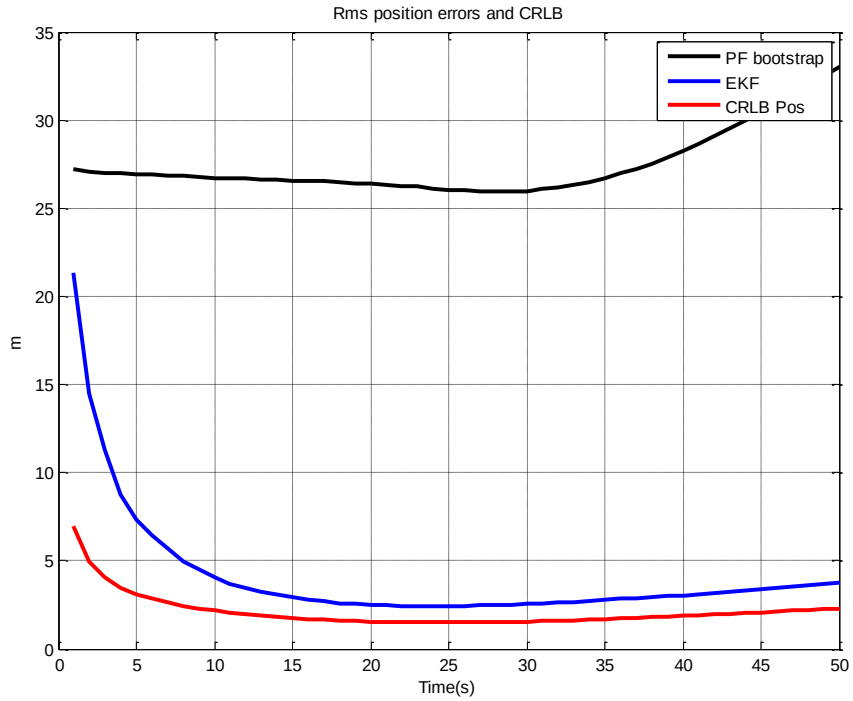

Figure 36 RMS position errors of EKF and Bootstrap PF for $\sigma_{meas} = 10\ Hz$.

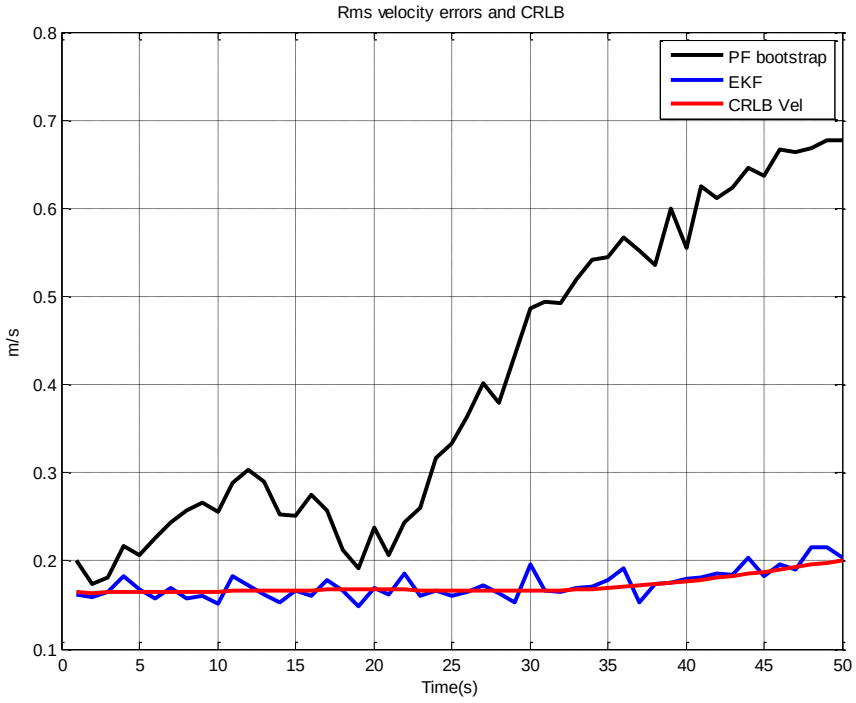

Figure 37 RMS velocity errors of EKF and Bootstrap PF for $\sigma_{meas} = 10\ Hz$.

As seen in the figures, even if the number of particles is as high as 1000, the Bootstrap particle filter has worse performance than EKF especially for position estimation. The main reason for this is that the measurements contain more information about the velocity rather than the position and therefore the position variables are very weakly observable. This can for example be observed from the sample Jacobian matrix of the measurement function with respect to the state elements given in the Table 8.

Table 8 Jacobian matrix of the measurement function at time instant of 34 seconds

Partial Derivative / Sensor	$\frac{\partial F_k^i}{\partial x}\left(\frac{Hz}{m}\right)$	$\frac{\partial F_k^i}{\partial y}\left(\frac{Hz}{m}\right)$	$\frac{\partial F_k^i}{\partial v_x}\left(\frac{Hz}{m/s}\right)$	$\frac{\partial F_k^i}{\partial v_y}\left(\frac{Hz}{m/s}\right)$
S1	0.1066	-0.2957	-57.0178	20.5443
S2	-2.4213	-0.5294	12.9461	59.2072
S3	-0.6499	-1.6717	-56.4870	21.9615
S4	-0.3660	0.1874	-27.6185	-53.9473

In the Jacobian matrix, the derivatives of the measurements with respect to velocity states are very high in comparison to the derivative of the measurements with respect to position states. The ratio of the derivatives observed in this scenario is about 50. By using the analytical Jacobian matrix, EKF can extract the very small amount of information from the measurements using the correlation information in the covariance matrix. On the other hand, this type of small correlations and small amount of information is very difficult for a particle filter to hold and propagate even with a high number of measurements. Therefore, although the particle filter can extract information about the velocity, the small amount of information about the position cannot be extracted from the measurements using random sampling. As a result, the information about the position is not handled properly using a reasonable number of the particles in the particle filter and the position estimates of the particle filter always has bias.

It would be interesting to see if the particle filter's estimation capability for the position states can be increased by using standard sequential Monte Carlo tools like optimal proposal distributions and Rao-Blackwellization. In the following sections, these ideas will be investigated to propose and implement two different particle filters for Doppler-only tracking.

3.2. SIR Particle Filter with Optimal Proposal Density

In this section, the SIR particle filter with optimal proposal density for Doppler-only tracking is derived. The SIR particle filter, similar to a bootstrap particle filter, holds the particles and their weights. The particles and the weights are denoted as $X_{k|k}^{(i)}$, $\pi_{k|k}^{(i)}$ for $i = 1, \dots, N_p$, where N_p is the number of particles. Contrary to the bootstrap particle filter, the optimal proposal density $p\left(X_{k+1}\middle|X_k^{(i)}, y_{k+1}\right)$ is used in the prediction step instead of the state transition density $p\left(X_{k+1}\middle|X_k^{(i)}\right)$.

In the derivation of the SIR particle filter with optimal proposal density, the target and the measurement model presented in Section 3.1 are used. A single iteration of the SIR particle filter with optimal proposal density for Doppler-only tracking has the following steps:

- **Prediction Update:** In this step, the particles $X_{k+1}^{(i)}, i = 1, \dots, N_p$ are first propagated to obtain the intermediate predicted particles by using (3.1-4) as follows:

$$\bar{X}_{k+1|k}^{(i)} = AX_{k|k}^{(i)}. \tag{3.2-1}$$

  The intermediate predicted particles need to be updated for obtaining optimal the proposal density $p\left(X_{k+1}\middle|X_k^{(i)}, y_{k+1}\right)$ to obtain the final predicted particles. To do this, EKF measurement update steps are used. Firstly, the predicted measurements are obtained for each particle as follows:

$$\hat{y}_{k+1}^{(i),ekf} = F(X_{k+1|k}^{(i)}) \tag{3.2-2}$$

where the measurement function $F(.)$ is given in (2.1-19).

Now, the intermediate predicted particles are updated by using the measurement as follows:

$$X_{k+1|k+1}^{(i),ekf} = X_{k+1|k}^{(i)} + K_{k+1}^{(i),ekf}(y_{k+1} - \hat{y}_{k+1}^{(i),ekf}) \quad 3.2\text{-}3$$

where

$$K_{k+1}^{(i),ekf} = Q(J_{k+1}^{(i),ekf})^T(S_{k+1}^{(i),ekf})^{-1}, \quad 3.2\text{-}4$$

$$S_{k+1}^{(i),ekf} = J_{k+1}^{(i),ekf} Q(J_{k+1}^{(i),ekf})^T + R. \quad 3.2\text{-}5$$

Here, $J_{ekf}^{(i)}$ represents the Jacobian of the measurement function $F(.)$ evaluated at the i[th] intermediate predicted particle. Q and R represent the covariance of the process noise and measurement noise respectively. The covariance of the updated particles can be obtained as follows:

$$P_{k+1}^{(i),ekf} = Q - K_{k+1}^{(i),ekf} S_{k+1}^{(i),ekf} (K_{k+1}^{(i),ekf})^T \quad 3.2\text{-}6$$

The final predicted particles are drawn from the optimal proposal distribution. The distribution is approximated by the normal distribution given below.

$$X_{k+1|k}^{(i)} \sim N(X_{k+1|k+1}^{(i)}; X_{k+1|k+1}^{(i),ekf}, P_{k+1}^{(i),ekf}). \quad 3.2\text{-}7$$

The weights remain the same at this step and they are shown as follows:

$$\pi_{k+1|k}^{(i)} = \pi_{k|k}^{(i)}. \quad 3.2\text{-}8$$

- **Measurement Update: :** In this step, the final predicted particles are directly taken as the estimated particles as follows.

$$X_{k+1|k+1}^{(i)} = X_{k+1|k}^{(i)}. \quad 3.2\text{-}2$$

Particle weights are updated as follows.

$$\hat{\pi}_{k+1|k+1}^{(i)} = \pi_{k|k}^{(i)} \frac{p(y_{k+1}|X_{k+1}^{(i)})p(X_{k+1}^{(i)}|X_k^{(i)})}{G(X_{k+1}^{(i)}|X_{0:k}^{(i)}, y_{0:k+1})}, \quad 3.2\text{-}3$$

$$\pi_{k+1|k+1}^{(i)} = \frac{\hat{\pi}_{k+1|k+1}^{(i)}}{\sum_i^N \hat{\pi}_{k+1|k+1}^{(i)}}. \quad 3.2\text{-}4$$

Here $G(X_{k+1}^{(i)}|X_{0:k}^{(i)}, y_{0:k+1})$, as before, represents the proposal density. The optimal proposal distribution $p\left(X_{k+1}\middle|X_k^{(i)}, y_{k+1}\right)$ is employed as the proposal density. By using the Bayes' rule, optimal proposal distribution can be expressed as follows.

$$p\left(X_{k+1}^{(i)}\middle|X_k^{(i)}, y_{k+1}\right) = \frac{p\left(y_{k+1}\middle|X_{k+1}^{(i)}\right)p\left(X_{k+1}^{(i)}\middle|X_k^{(i)}\right)}{p\left(y_{k+1}\middle|X_k^{(i)}\right)}. \quad 3.2\text{-}5$$

When the optimal proposal distribution is used in the weight update equation, it can be simplified as follows.

$$\hat{\pi}_{k+1|k+1}^{(i)} = \pi_{k|k}^{(i)} \frac{p(y_{k+1}|X_{k+1}^{(i)})p(X_{k+1}^{(i)}|X_k^{(i)})}{p\left(X_{k+1}^{(i)}\middle|X_k^{(i)}, y_{k+1}\right)}, \quad 3.2\text{-}6$$

$$= \pi_{k|k}^{(i)} p\left(y_{k+1}\middle|X_k^{(i)}\right). \quad 3.2\text{-}7$$

Finally, the weight update can be expressed as follows:

$$\pi_{k+1|k+1}^{(i)} = \frac{\hat{\pi}_{k+1|k+1}^{(i)}}{\sum_{i=1}^N \hat{\pi}_{k+1|k+1}^{(i)}} \quad 3.2\text{-}8$$

where

$$\hat{\pi}_{k+1|k+1}^{(i)} = \pi_{k|k}^{(i)} p(y_{k+1}|X_{k|k}^{(i)}). \quad 3.2\text{-}9$$

Here, $p(y_{k+1}|X_{k|k}^{(i)})$ is equal to the normal distribution with mean value $\mu = \hat{y}_{k+1}^{(i),ekf}$ and covariance matrix $C = S_{k+1}^{(i),ekf}$.

At the final stage, the estimated state and its covariance are calculated as follows.

$$\hat{X}_{k+1|k+1} = \sum_{i=1}^{N} \pi_{k+1|k+1}^{(i)} X_{k+1|k+1}^{(i)}, \quad 3.2\text{-}10$$

$$P_{k|k} = \sum_{i=1}^{N} \pi_{k+1|k+1}^{(i)} (X_{k+1|k+1}^{(i)} - \hat{X}_{k+1|k+1}) (X_{k+1|k+1}^{(i)} - \hat{X}_{k+1|k+1})^{T}. \quad 3.2\text{-}11$$

Resampling is made at the end of the each step to avoid the sample impoverishment problem as in the bootstrap particle filter.

3.3. Rao-Blackwellized Particle Filter for Doppler-only Tracking

In this section, the derivation of a Rao-Blackwellized particle filter for Doppler-only tracking is given. This filter is based on the fact that the nonlinear states and linear states in the target and the measurement model can be handled separately in a particle filter to increase the overall performance of the filter. The nonlinear states, in such a case, can be estimated using a reduced order particle filter. For the linear states, on the other hand, Kalman filters might be utilized to improve the estimation performance. The target motion model given in (2.1-23) is repeated here by giving the dynamics of the velocity and position states separately.

$$p_{k+1} = p_k + T v_k + \frac{T^2}{2} w_k \quad 3.3\text{-}1$$

$$v_{k+1} = v_k + T w_k \quad 3.3\text{-}2$$

$$y_k = C(p_k) v_k + e_k \quad 3.3\text{-}3$$

where the measurement model given in (2.1-2) is used.

Here, $p_k = [x_k, y_k]$ represents the target position in 2D, $v_k = [v_{x,k}, v_{y,k}]$ represents the target velocity in 2D, $w_k \sim N(w_k; 0, Q)$ represents the unknown accelerations of the target, i.e., the process noise, and $e_k \sim N(w_k; 0, R)$ represents the measurement errors, i.e., the measurement noise. $C(p_k) = \frac{2}{\lambda} H(p_t)$ represents the measurement matrix where $H(p_t)$ is given in (2.1-20).

Note that in the model given above, given the position states p_k, the model is linear with respect to the velocity states v_k. The dependence of the model on the position states is, on the other hand, highly nonlinear. The Rao-Blackwellized particle filter we consider here estimates the nonlinear states, i.e., the position variables, using a reduced-order particle filter and given the position state particles, estimates the velocity states using Kalman filters. Hence, the Rao-Blackwellized particle filter holds the nonlinear position particles and weights shown as $p_k^{(i)}$, $\pi_{k|k}^{(i)}$ and linear velocity estimates $\hat{v}_{k|k}^{(i)}$ and covariances $P_{k|k}^{(i)}$ for $i = 1, \dots, N_p$, where N_p is the number of particles. The particles $\left\{p_k^{(i)}\right\}_{i=1}^{N_p}$ are propagated using a reduced-order particle filter while the estimates $\hat{v}_{k|k}^{(i)}$ and covariances $P_{k|k}^{(i)}$ are propagated using Kalman filters. A single iteration of the Rao-Blackwellized particle filter has the following steps.

- **Particle Filter Prediction Update**: In this step, the particles $p_{k+1}^{(i)}, i = 1, \dots, N_p$ are obtained. These particles $p_k^{(i)}, i = 1, \dots, N_p$ are predicted using (3.3-1). In order to be able to use (3.3-1) for this purpose, $\hat{v}_{k|k}^{(i)}$ is substituted into v_k on the right hand side. When this is done, p_{k+1} can be expressed as follows:

$$p_{k+1} = p_k + T\hat{v}_{k|k}^{(i)} + \bar{w}_k + \frac{T^2}{2} w_k \qquad 3.3\text{-}4$$

$$= p_k + T\hat{v}_{k|k}^{(i)} + \tilde{w}_k \qquad 3.3\text{-}5$$

where $\tilde{w}_k \triangleq \bar{w}_k + \frac{T^2}{2} w_k$ and $\tilde{w}_k \sim N(\bar{w}_k, 0, T^2 P_{k|k}^{(i)})$ represents the error introduced into (3.3-1) by making the substitution. Using (3.3-1), $p_{k+1}^{(i)}$ can be predicted as follows:

$$p_{k+1}^{(i)} = p_k^{(i)} + T\hat{v}_{k|k}^{(i)} + \tilde{w}_k^{(i)} \qquad 3.3\text{-}6$$

where

$$\widetilde{w}_k^{(i)} \sim N\left(\widetilde{w}_k^{(i)}; 0, T^2 P_{k|k}^{(i)} + \frac{T^4}{4} Q\right). \quad \text{3.3-7}$$

- **Kalman Filter Pseudo-Measurement Update**: As soon as $p_{k+1}^{(i)}$ is known, this new information can be used to update the estimate $\hat{v}_{k|k}^{(i)}$ and the covariance $P_{k|k}^{(i)}$. The reason can be seen by substituting $p_{k+1}^{(i)}$ and $p_k^{(i)}$ into the original model given in (3.3-1) as follows:

$$p_{k+1}^{(i)} - p_k^{(i)} = T v_k + \frac{T^2}{2} w_k \quad \text{3.3-8}$$

which is written as

$$z_k^{(i)} = H \begin{bmatrix} v_k \\ w_k \end{bmatrix} \quad \text{3.3-9}$$

where

$$\mathrm{z}_{\mathrm{k}}^{(\mathrm{i})} \triangleq p_{k+1}^{(i)} - p_k^{(i)}, \quad \text{3.3-10}$$

$$H \triangleq \begin{bmatrix} T I_2 & \frac{T^2}{2} I_2 \end{bmatrix}. \quad \text{3.3-11}$$

Here, I_n denotes an identiy matrix of size n x n, where $n = 2$ in this case. As observed above, the quantity $z_k^{(i)}$ behaves as a pseudo-measurement for v_k and w_k. Note that if the dynamics of v_k did not involve w_k, $z_k^{(i)}$ would be considered as a pseudo-measurement of only v_k, and then w_k would be just a measurement noise term not to be estimated. However, since w_k appears in the dynamics of both p_k and v_k, the information coming from $z_k^{(i)}$ about w_k must be taken into account. The information about v_k and w_k can be summarized as below.

$$\begin{bmatrix} v_k \\ w_k \end{bmatrix} \sim N\left(\begin{bmatrix} v_k \\ w_k \end{bmatrix}; \begin{bmatrix} \hat{v}_{k|k}^{(i)} \\ 0 \end{bmatrix}, \begin{bmatrix} P_{k|k}^{(i)} & 0_2 \\ 0_2 & Q \end{bmatrix}\right). \quad \text{3.3-12}$$

Here 0_n denotes a zero-matrix of size n x n, where $n = 2$ in this case. Now, the information about v_k and w_k can be updated using a Kalman filter measurement update with the pseudo-measurement $z_k^{(i)}$.

First, the calculation of the innovation covariance $S_k^{z,(i)}$ for $z_k^{(i)}$ is given as follows.

$$S_k^{z,(i)} = H \begin{bmatrix} P_{k|k}^{(i)} & 0_2 \\ 0_2 & Q \end{bmatrix} H^T, \tag{3.3-13}$$

$$= \begin{bmatrix} TI_2 & \frac{T^2}{2} I_2 \end{bmatrix} \begin{bmatrix} P_{k|k}^{(i)} & 0_2 \\ 0_2 & Q \end{bmatrix} \begin{bmatrix} TI_2 \\ \frac{T^2}{2} I_2 \end{bmatrix}, \tag{3.3-14}$$

$$= T^2 P_{k|k}^{(i)} + \tfrac{T^4}{4} Q\,. \tag{3.3-15}$$

The Kalman gain is then given as follows.

$$K_k^{z,(i)} = \begin{bmatrix} P_{k|k}^{(i)} & 0_2 \\ 0_2 & Q \end{bmatrix} H^T \left(S_k^{z,(i)}\right)^{-1}, \tag{3.3-16}$$

$$= \begin{bmatrix} P_{k|k}^{(i)} & 0_2 \\ 0_2 & Q \end{bmatrix} \begin{bmatrix} TI_2 \\ \frac{T^2}{2} I_2 \end{bmatrix} \left(S_k^{z,(i)}\right)^{-1}, \tag{3.3-17}$$

$$= \begin{bmatrix} TP_{k|k}^{(i)} \left(S_k^{z,(i)}\right)^{-1} \\ \frac{T^2}{2} Q \left(S_k^{z,(i)}\right)^{-1} \end{bmatrix}. \tag{3.3-18}$$

The updated information about v_k and w_k are given as follows:

$$\begin{bmatrix} \hat{v}_{k|k}^{z,(i)} \\ \hat{w}_{k|k}^{z,(i)} \end{bmatrix} = \begin{bmatrix} \hat{v}_{k|k}^{(i)} \\ 0 \end{bmatrix} + K_k^{z,(i)} \left(z_k^{(i)} - H \begin{bmatrix} \hat{v}_{k|k}^{(i)} \\ 0 \end{bmatrix} \right), \tag{3.3-19}$$

$$= \begin{bmatrix} \hat{v}_{k|k}^{(i)} \\ 0 \end{bmatrix} + \begin{bmatrix} TP_{k|k}^{(i)} \left(S_k^{z,(i)}\right)^{-1} \\ \frac{T^2}{2} Q \left(S_k^{z,(i)}\right)^{-1} \end{bmatrix} \left(z_k^{(i)} - H \begin{bmatrix} \hat{v}_{k|k}^{(i)} \\ 0 \end{bmatrix} \right), \quad 3.3\text{-}20$$

$$= \begin{bmatrix} \hat{v}_{k|k}^{(i)} + TP_{k|k}^{(i)} \left(S_k^{z,(i)}\right)^{-1} \left(z_k^{(i)} - H \begin{bmatrix} \hat{v}_{k|k}^{(i)} \\ 0 \end{bmatrix} \right) \\ \frac{T^2}{2} Q \left(S_k^{z,(i)}\right)^{-1} \left(z_k^{(i)} - H \begin{bmatrix} \hat{v}_{k|k}^{(i)} \\ 0 \end{bmatrix} \right) \end{bmatrix}. \quad 3.3\text{-}21$$

Now, the pseudo-measurement updated information can be written as follows:

$$\hat{v}_{k|k}^{z,(i)} = \hat{v}_{k|k}^{(i)} + TP_{k|k}^{(i)} \left(S_k^{z,(i)}\right)^{-1} \left(z_k^{(i)} - T\hat{v}_{k|k}^{(i)} \right), \quad 3.3\text{-}22$$

$$\hat{w}_{k|k}^{z,(i)} = \frac{T^2}{2} Q \left(S_k^{z,(i)}\right)^{-1} \left(z_k^{(i)} - T\hat{v}_{k|k}^{(i)} \right). \quad 3.3\text{-}23$$

The updated covariance is given as:

$$\begin{bmatrix} P_{k|k}^{vv,(i)} & P_{k|k}^{vw,(i)} \\ P_{k|k}^{wv,(i)} & P_{k|k}^{ww,(i)} \end{bmatrix} = \begin{bmatrix} P_{k|k}^{(i)} & 0_2 \\ 0_2 & Q \end{bmatrix} - K_k^{z,(i)} S_k^{z,(i)} \left(K_k^{z,(i)}\right)^T, \quad 3.3\text{-}24$$

$$= \begin{bmatrix} P_{k|k}^{(i)} & 0_2 \\ 0_2 & Q \end{bmatrix} - \begin{bmatrix} TP_{k|k}^{(i)} \left(S_k^{z,(i)}\right)^{-1} \\ \frac{T^2}{2} Q \left(S_k^{z,(i)}\right)^{-1} \end{bmatrix} S_k^{z,(i)} \begin{bmatrix} T \left(S_k^{z,(i)}\right)^{-1} P_{k|k}^{(i)} & \frac{T^2}{2} \left(S_k^{z,(i)}\right)^{-1} Q \end{bmatrix}, \quad 3.3\text{-}25$$

$$= \begin{bmatrix} P_{k|k}^{(i)} & 0_2 \\ 0_2 & Q \end{bmatrix} - \begin{bmatrix} T^2 P_{k|k}^{(i)} \left(S_k^{z,(i)}\right)^{-1} P_{k|k}^{(i)} & \frac{T^3}{2} P_{k|k}^{(i)} \left(S_k^{z,(i)}\right)^{-1} Q \\ \frac{T^3}{2} Q \left(S_k^{z,(i)}\right)^{-1} P_{k|k}^{(i)} & \frac{T^4}{4} Q \left(S_k^{z,(i)}\right)^{-1} Q \end{bmatrix}, \quad 3.3\text{-}26$$

$$= \begin{bmatrix} P_{k|k}^{(i)} - T^2 P_{k|k}^{(i)} \left(S_k^{z,(i)}\right)^{-1} P_{k|k}^{(i)} & -\frac{T^3}{2} P_{k|k}^{(i)} \left(S_k^{z,(i)}\right)^{-1} Q \\ -\frac{T^3}{2} Q \left(S_k^{z,(i)}\right)^{-1} P_{k|k}^{(i)} & Q - \frac{T^4}{4} Q \left(S_k^{z,(i)}\right)^{-1} Q \end{bmatrix}, \quad 3.3\text{-}27$$

- **Kalman Filter Prediction Update:** After the information about v_k and w_k are updated with the pseudo measurement, the velocity dynamics given in (3.3-2) can be used to make the prediction for the Kalman filter estimate and covariance. It can be seen from (3.3-2) that

$$v_{k+1} = F \begin{bmatrix} v_k \\ w_k \end{bmatrix} \quad 3.3\text{-}28$$

where

$$F \triangleq [I_2 \quad TI_2]. \quad 3.3\text{-}29$$

Hence, $\hat{v}_{k+1|k}^{(i)}$ and its covariance $P_{k+1|k}^{(i)}$ are given as follows.

$$\hat{v}_{k+1|k}^{(i)} = \begin{bmatrix} \hat{v}_{k|k}^{z,(i)} \\ \hat{w}_{k|k}^{z,(i)} \end{bmatrix}, \quad 3.3\text{-}30$$

$$= [I_2 \quad TI_2] \begin{bmatrix} \hat{v}_{k|k}^{z,(i)} \\ \hat{w}_{k|k}^{z,(i)} \end{bmatrix}, \quad 3.3\text{-}31$$

$$= \hat{v}_{k|k}^{(i)} + T\hat{w}_{k|k}^{z,(i)}, \quad 3.3\text{-}32$$

$$= \hat{v}_{k|k}^{(i)} + TP_{k|k}^{(i)} \left(S_k^{z,(i)}\right)^{-1} \left(z_k^{(i)} - T\hat{v}_{k|k}^{(i)}\right) + \frac{T^3}{2} Q \left(S_k^{z,(i)}\right)^{-1} \left(z_k^{(i)} - T\hat{v}_{k|k}^{(i)}\right), \quad 3.3\text{-}33$$

$$= \hat{v}_{k|k}^{(i)} + T\left(P_{k|k}^{(i)} + \frac{T^2}{2} Q\right) \left(S_k^{z,(i)}\right)^{-1} \left(z_k^{(i)} - T\hat{v}_{k|k}^{(i)}\right). \quad 3.3\text{-}34$$

$$P_{k+1|k}^{(i)} = F \begin{bmatrix} P_{k|k}^{vv,(i)} & P_{k|k}^{vw,(i)} \\ P_{k|k}^{wv,(i)} & P_{k|k}^{ww,(i)} \end{bmatrix} F^T, \tag{3.3-35}$$

$$= [I_2 \quad TI_2] \begin{bmatrix} P_{k|k}^{vv,(i)} & P_{k|k}^{vw,(i)} \\ P_{k|k}^{wv,(i)} & P_{k|k}^{ww,(i)} \end{bmatrix} \begin{bmatrix} I_2 \\ TI_2 \end{bmatrix}, \tag{3.3-36}$$

$$= P_{k|k}^{vv,(i)} + TP_{k|k}^{vw,(i)} + TP_{k|k}^{wv,(i)} + T^2 P_{k|k}^{ww,(i)}, \tag{3.3-37}$$

$$\begin{aligned} = \; & P_{k|k}^{(i)} - T^2 P_{k|k}^{(i)} \left(S_k^{z,(i)}\right)^{-1} P_{k|k}^{(i)} - \frac{T^4}{2} P_{k|k}^{(i)} \left(S_k^{z,(i)}\right)^{-1} Q, \\ & - \frac{T^4}{2} Q \left(S_k^{z,(i)}\right)^{-1} P_{k|k}^{(i)} + T^2 \left(Q - \frac{T^4}{4} Q \left(S_k^{z,(i)}\right)^{-1} Q\right). \end{aligned} \tag{3.3-38}$$

Now, predicted velocity and its covariance are obtained as follows.

$$\hat{v}_{k+1|k}^{(i)} = \hat{v}_{k|k}^{(i)} + T \left(P_{k|k}^{(i)} + \frac{T^2}{2} Q\right) \left(S_k^{z,(i)}\right)^{-1} \left(z_k^{(i)} - T\hat{v}_{k|k}^{(i)}\right), \tag{3.3-39}$$

$$\begin{aligned} P_{k+1|k}^{(i)} = \; & P_{k|k}^{(i)} - T^2 P_{k|k}^{(i)} \left(S_k^{z,(i)}\right)^{-1} P_{k|k}^{(i)} - \frac{T^4}{2} P_{k|k}^{(i)} \left(S_k^{z,(i)}\right)^{-1} Q \\ & - \frac{T^4}{2} Q \left(S_k^{z,(i)}\right)^{-1} P_{k|k}^{(i)} + T^2 \left(Q - \frac{T^4}{4} Q \left(S_k^{z,(i)}\right)^{-1} Q\right), \end{aligned} \tag{3.3-40}$$

where

$$z_k^{(i)} = p_{k+1}^{(i)} - p_k^{(i)}, \tag{3.3-41}$$

$$S_k^{z,(i)} = T^2 P_{k|k}^{(i)} + \frac{T^4}{4} Q. \tag{3.3-42}$$

- **Particle Filter Measurement Update**: The particle weights $\pi_{k|k}^{(i)}$ should be updated with the measurement y_{k+1} using (3.3-3). In order to do this, $\hat{v}_{k+1|k}^{(i)}$ is substituted for v_{k+1} into (3.3-3) to obtain the following equations.

$$y_{k+1} = C(p_{k+1}) \hat{v}_{k+1|k}^{(i)} + \bar{e}_{k+1} + e_{k+1} \tag{3.3-43}$$

$$= C(p_{k+1})\hat{v}_{k+1|k}^{(i)} + \tilde{e}_{k+1} \quad \text{3.3-44}$$

where $\tilde{e}_{k+1} \triangleq \bar{e}_{k+1} + e_{k+1}$ and $\bar{e}_{k+1} \sim N(\bar{e}_{k+1}; 0, C(p_{k+1})P_{k+1|k}^{(i)}C^T(p_{k+1}))$ represents the error introduced into (3.3-3) by making the substitution. Notice that the new measurement noise term $\tilde{e}_{k+1}$ has distribution $\tilde{e}_{k+1} \sim N(\bar{e}_{k+1}; 0, C(p_{k+1})P_{k+1|k}^{(i)}C^T(p_{k+1}))$. This gives the weight update as follows:

$$\begin{aligned}\pi_{k+1|k+1}^{(i)} &\propto p\left(y_k \middle| p_{k+1}^{(i)}\right)\pi_{k|k}^{(i)} \\ &= N(y_k; C\left(p_{k+1}^{(i)}\right)\hat{v}_{k+1|k}^{(i)}, C\left(p_{k+1}^{(i)}\right)P_{k+1|k}^{(i)}C^T\left(p_{k+1}^{(i)}\right) + R)\pi_{k|k}^{(i)}.\end{aligned} \quad \text{3.3-45}$$

- **Kalman Filter Measurement Update:** The final step in the Rao-Blackwellized particle filter iteration is the update of the predicted estimates $\hat{v}_{k+1|k}^{(i)}$ and covariances $P_{k+1|k}^{(i)}$ with the measurement y_{k+1}. This is carried out once again using (3.3-3). Given the position particle $p_{k+1}^{(i)}$, (3.3-3) can be written as follows.

$$y_{k+1} = C\left(p_{k+1}^{(i)}\right)v_{k+1} + e_{k+1} \quad \text{3.3-46}$$

which is linear in v_{k+1}. Hence a standard Kalman filter measurement update can be used to update $\hat{v}_{k+1|k}^{(i)}$ and $P_{k+1|k}^{(i)}$ with y_{k+1} as follows:

$$\hat{v}_{k+1|k+1}^{(i)} = \hat{v}_{k+1|k}^{(i)} + K_{k+1}^{y,(i)}\left(y_{k+1} - C\left(p_{k+1}^{(i)}\right)\hat{v}_{k+1|k}^{(i)}\right) \quad \text{3.3-47}$$

$$P_{k+1|k+1}^{(i)} = P_{k+1|k}^{(i)} - K_{k+1}^{y,(i)}S_{k+1}^{y,(i)}\left(K_{k+1}^{y,(i)}\right)^T \quad \text{3.3-48}$$

where

$$S_{k+1}^{y,(i)} = C\left(p_{k+1}^{(i)}\right)P_{k+1|k}^{(i)}C^T\left(p_{k+1}^{(i)}\right) + R, \quad \text{3.3-49}$$

$$K_{k+1}^{y,(i)} = P_{k+1|k}^{(i)}C^T\left(p_{k+1}^{(i)}\right)\left(S_{k+1}^{y,(i)}\right)^{-1}. \quad \text{3.3-50}$$

3.4. Simulation Results of Particle Filters for Doppler-only Tracking

In this section, the simulation results of the particle filters for Doppler-only tracking are presented. Moreover, some remarks and comments for these simulation results are made. Three different particle filters were derived in Section 3.1, 3.2 and 3.3. Also, the details of EKF are given in Chapter 2. These filters are compared by using them to track a target with multiple Doppler-only sensors. Here, the multiple active Doppler sensors measurement model and the constant velocity target motion model are used. The details of these models are given in Section 2.1. The sensor positions and target trajectory are shown in Figure 38. In all of the filters, the track initialization algorithm of Chapter 2 is utilized.

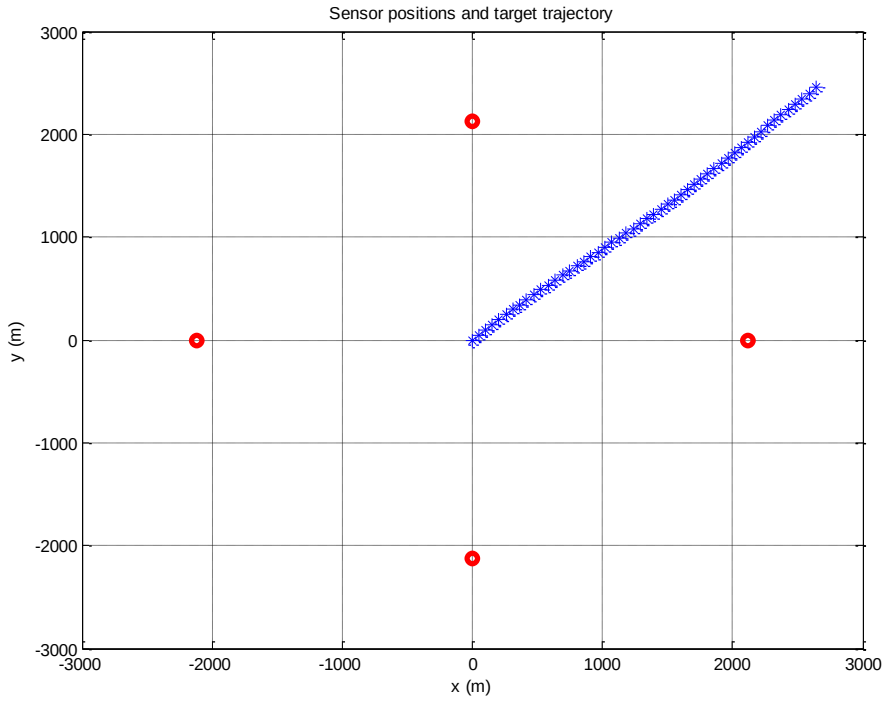

Figure 38 Sensor positions and target trajectory for tracking filters comparison.

In the simulations, RMS position errors and velocity errors are obtained for each tracking filter by repeating the target tracking simulation over 100 Monte-Carlo runs. At each run, target tracking is continued for 50 seconds and the measurements are

taken with a period of 1 second. In these simulations, the unknown target acceleration (process noise) has a variance value of $\sigma_{proc}^2 = 1\ (m/s^2)^2$. We evaluate the RMS position and velocity errors with different measurement noise variances. For this purpose, Monte Carlo simulations which include 100 runs are repeated for seven different measurement noise standard deviation values $\sigma_{meas} = 10, 50, 100, 150, 200, 250, 300\ Hz$. The RMS position and velocity errors of four tracking filters with different measurement noise variance values are given in Figure 39 to Figure 52.

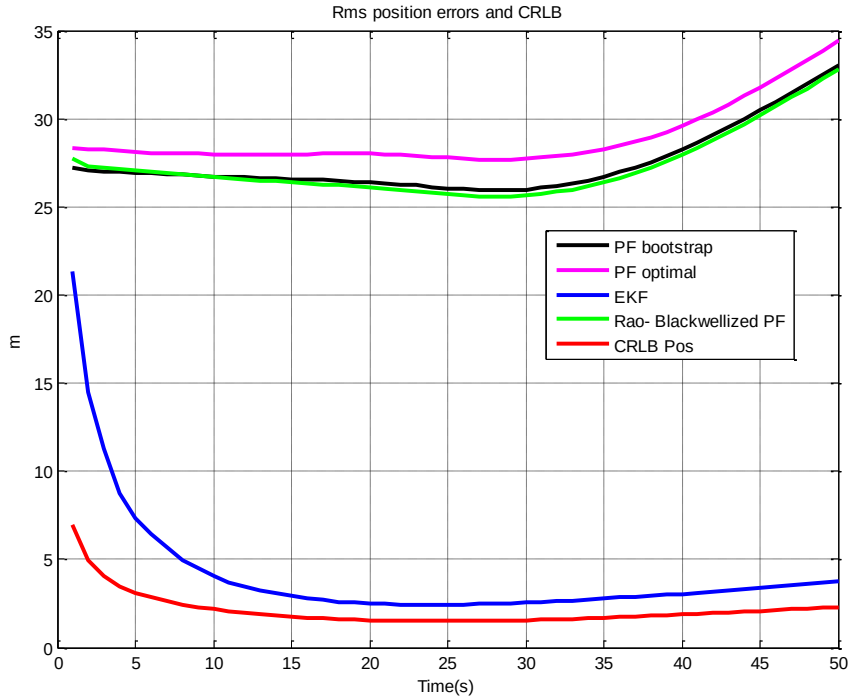

Figure 39 RMS position errors for $\sigma_{meas} = 10\ Hz$.

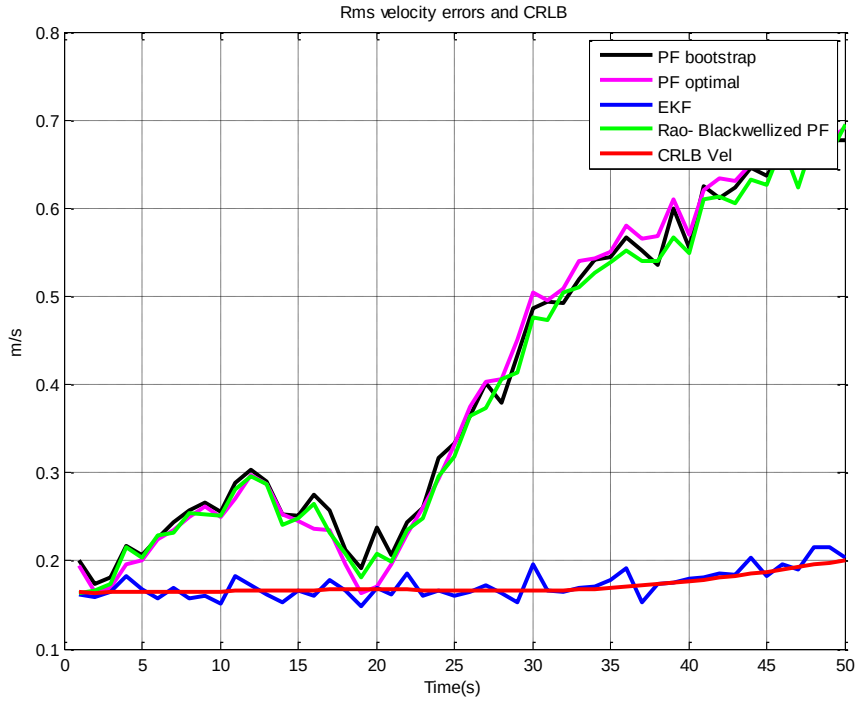

Figure 40 RMS velocity errors for $\sigma_{meas} = 10\ Hz$.

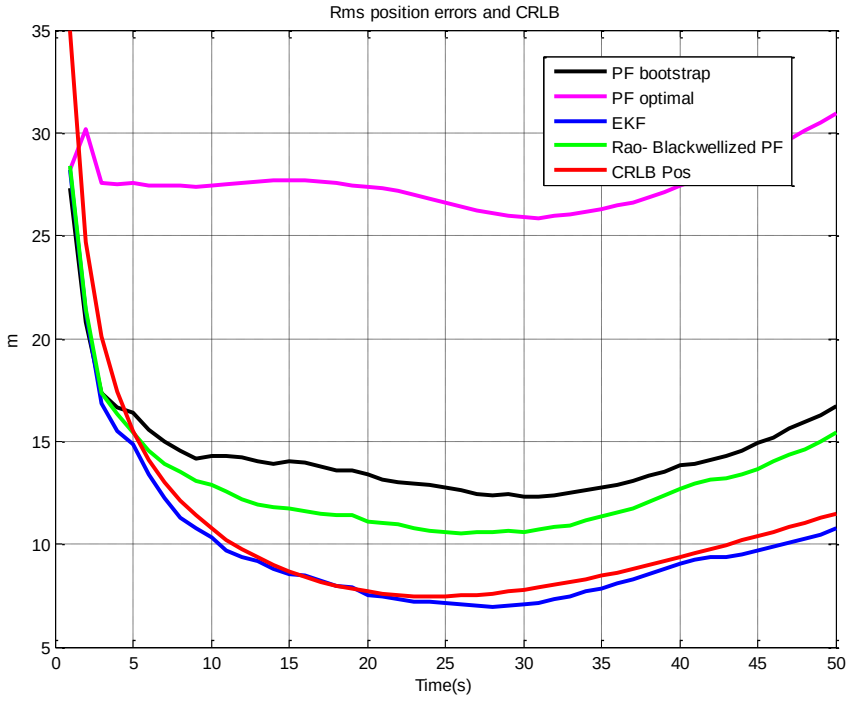

Figure 41 RMS position errors for $\sigma_{meas} = 50\ Hz$.

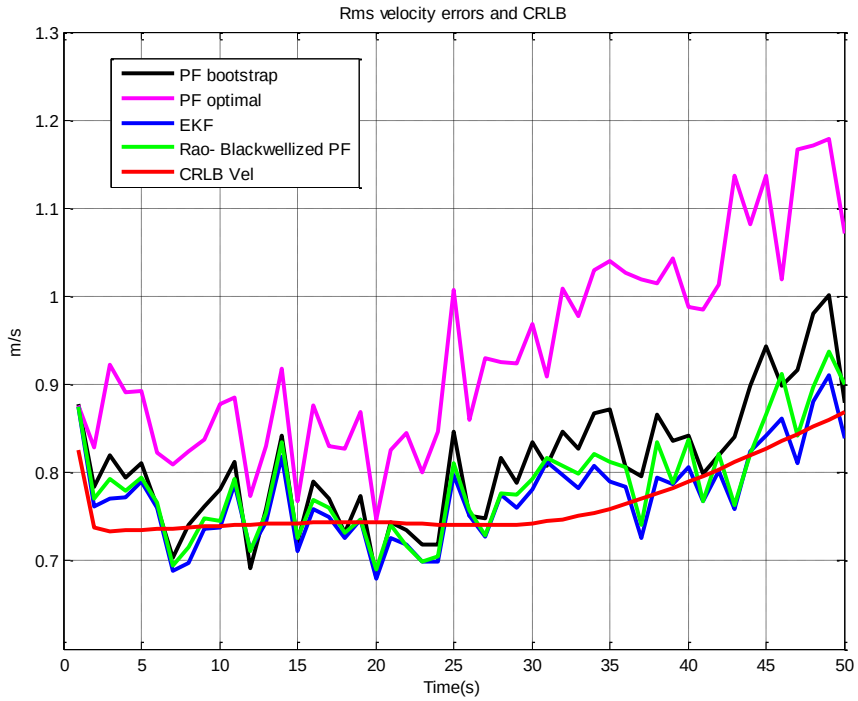

Figure 42 RMS velocity errors for $\sigma_{meas} = 50\ Hz$.

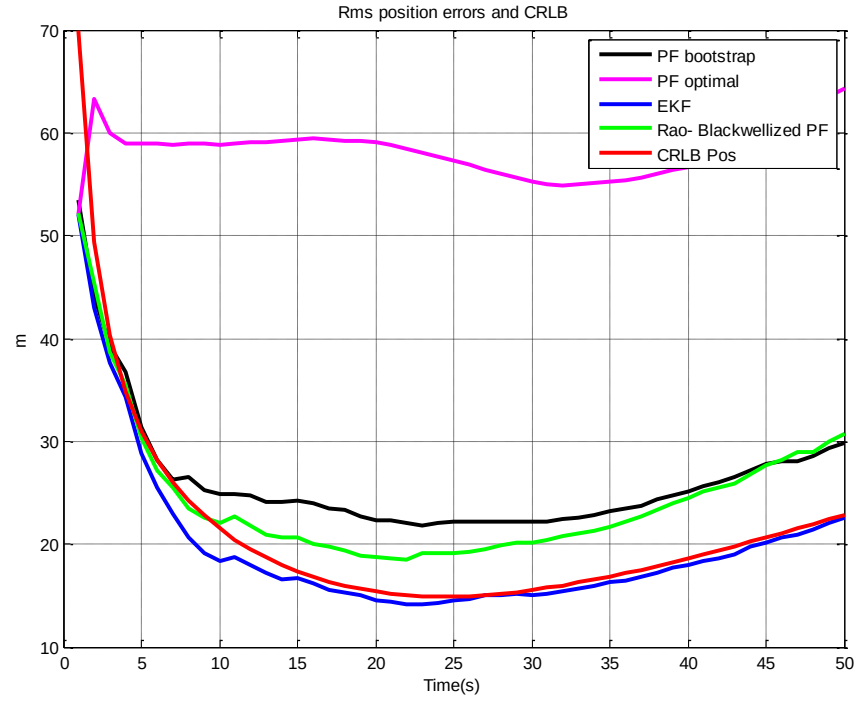

Figure 43 RMS position errors for $\sigma_{meas} = 100\ Hz$.

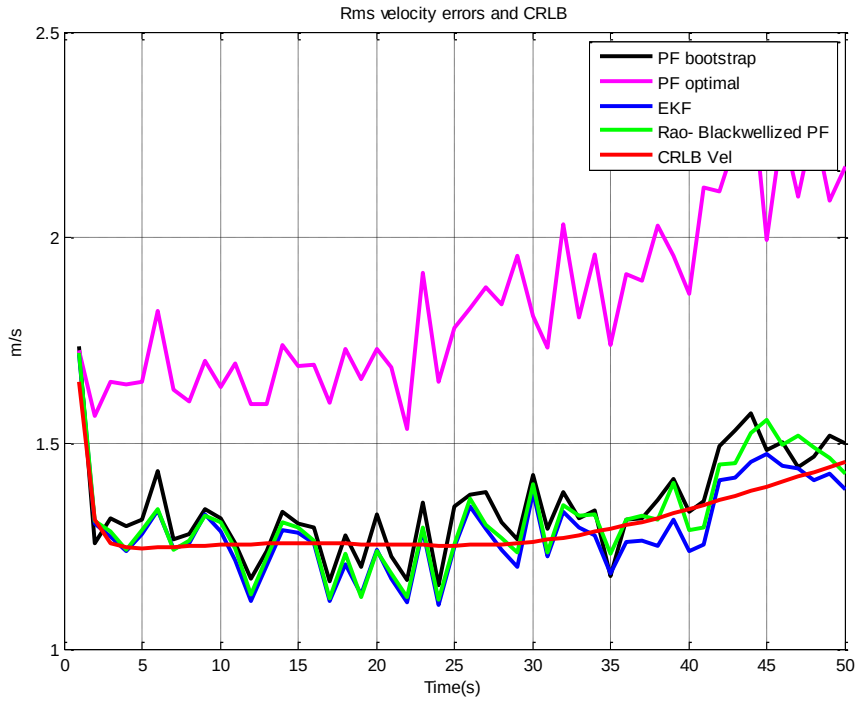

Figure 44 RMS velocity errors for $\sigma_{meas} = 100\ Hz$.

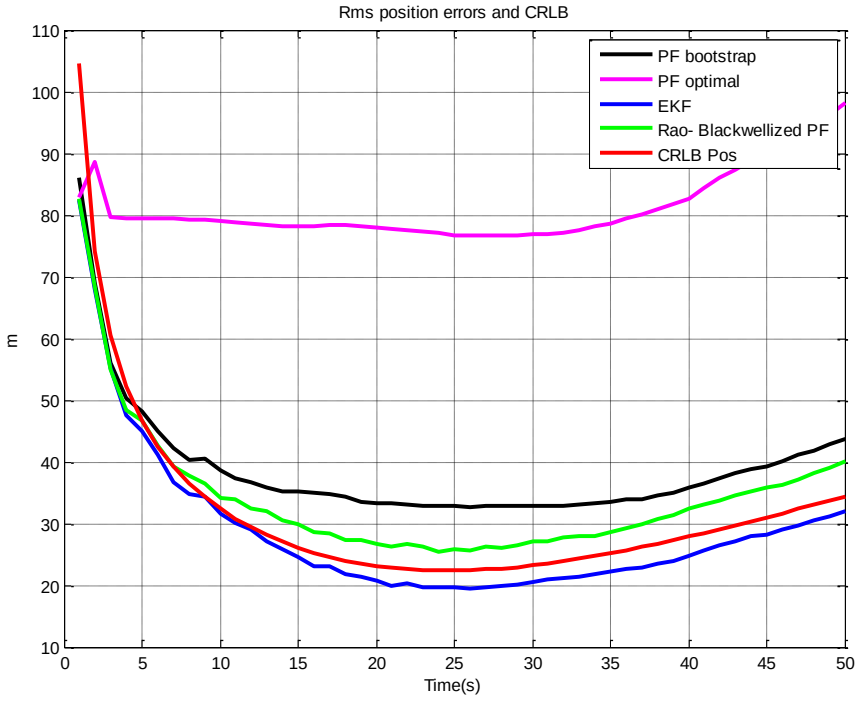

Figure 45 RMS position errors for $\sigma_{meas} = 150\ Hz$.

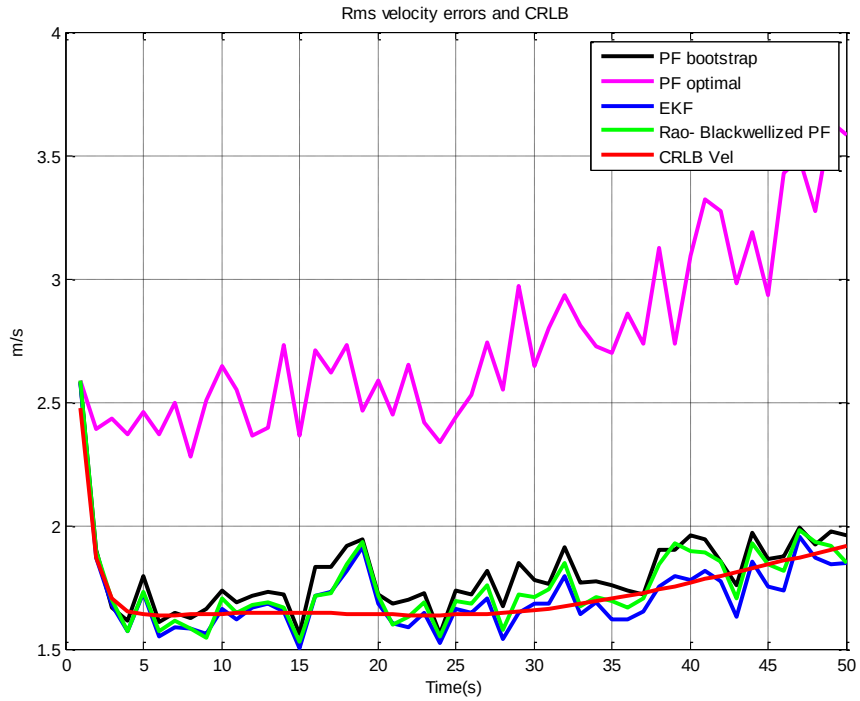

Figure 46 RMS velocity errors for $\sigma_{meas} = 150\ Hz$.

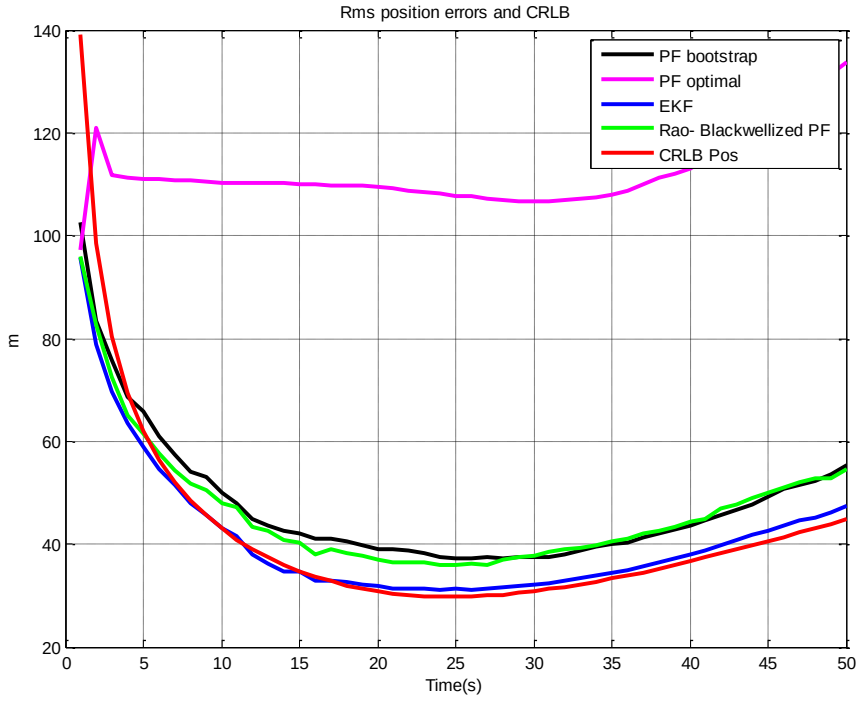

Figure 47 RMS position errors for $\sigma_{meas} = 200\ Hz$.

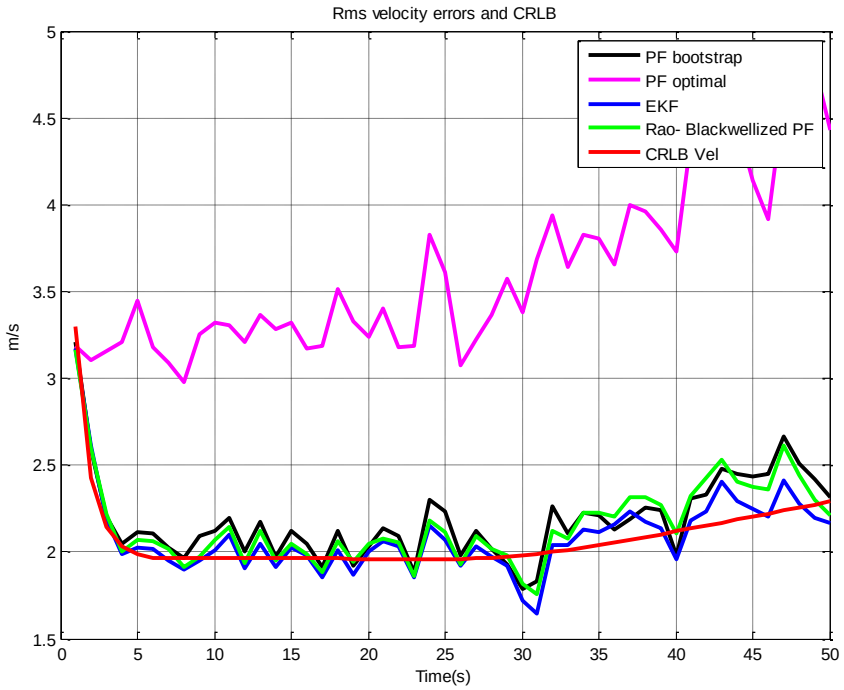

Figure 48 RMS velocity errors for $\sigma_{meas} = 200\ Hz$.

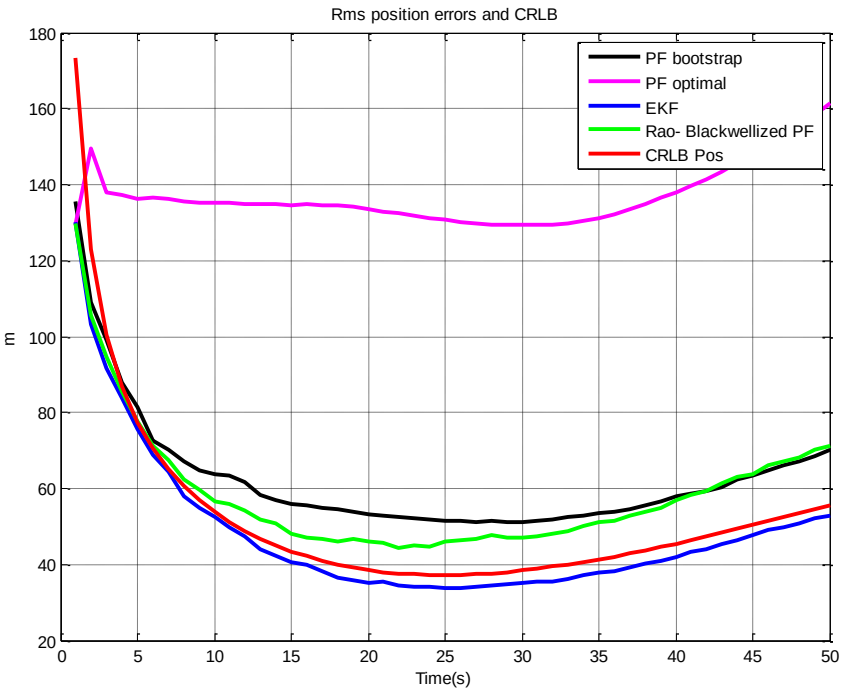

Figure 49 RMS position errors for $\sigma_{meas} = 250\ Hz$.

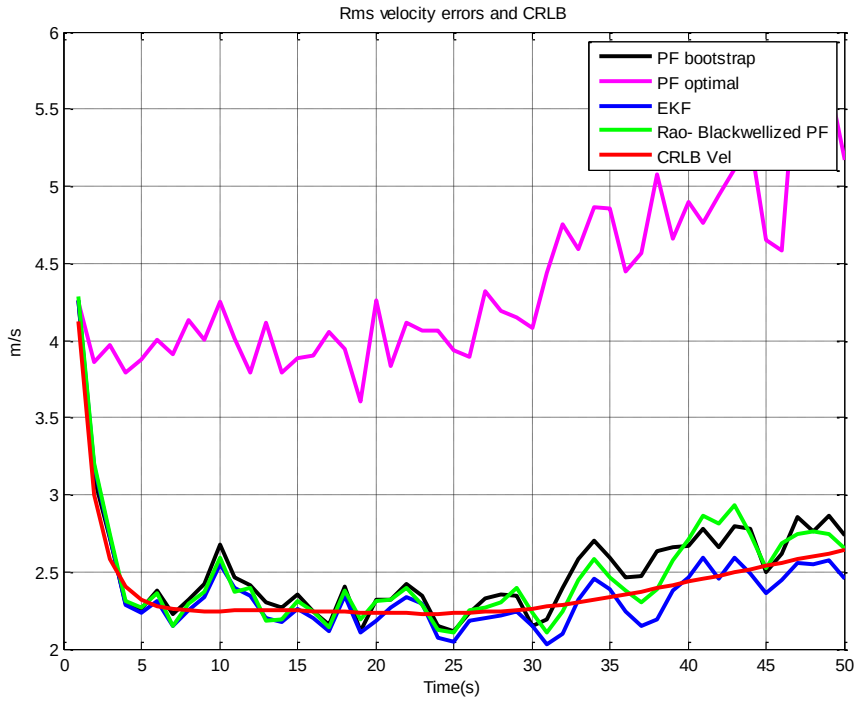

Figure 50 RMS velocity errors for $\sigma_{meas} = 250\ Hz$.

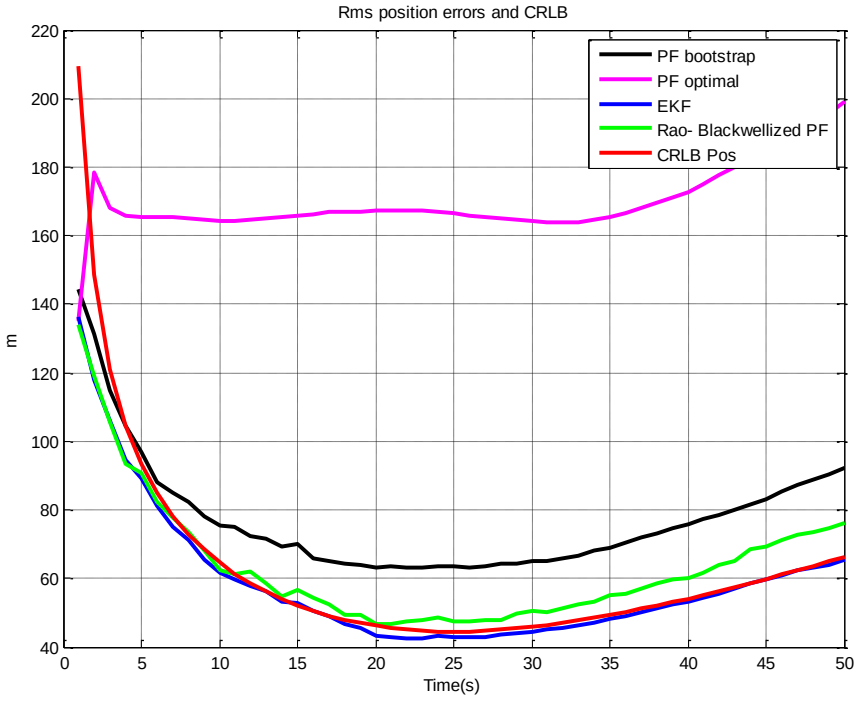

Figure 51 RMS position errors for $\sigma_{meas} = 300\ Hz$.

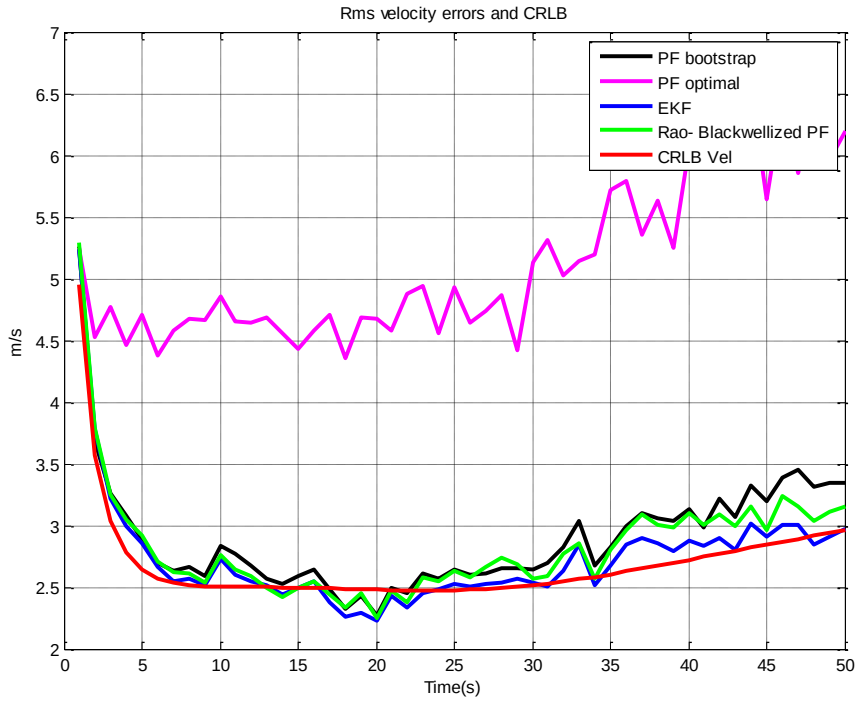

Figure 52 RMS velocity errors for $\sigma_{meas} = 300\ Hz$.

As seen from the figures, EKF still has the lowest RMS position and velocity errors amongst the four different tracking filters. For lower measurement noise variances, the particle filters have much poorer performance in comparison to EKF, especially in terms of position estimates.

In some individual runs for low measurement noise standard deviation values, it has been seen that the particle filter with optimal proposal can many times beat the EKF in terms of velocity estimation errors. However, since the EKF with optimal proposal can sometimes diverge, the effect of these individual runs is not seen in the aggregate RMS error results.

When high measurement noise standard deviation is used, even if the performance of the particle filters is more comparable with that of EKF, they still cannot reach the EKF performance. For high measurement error standard deviation, the performance of the particle filter with optimal proposal becomes worse than the bootstrap filter since the prediction update step uses very noisy measurements, and therefore the

proposal density dependent on these noisy measurements makes things worse. For high measurement noise standard deviation case, Rao-Blackwellized particle filter has the lowest RMS errors among other particle filters.

In this chapter, although it has been seen that the performance of the particle filters used for Doppler only tracking might be improved a little for some specific scenarios, the overall performance of the improved filters could still not beat EKF. Therefore, it has been understood that more intelligent improvement techniques has to be utilized for this purpose. In the literature, the failure of the bootstrap particle filter for this problem is usually attributed to the initialization of the filters. On the other hand, in this chapter, a successful track initialization algorithm was utilized in all simulations and the bad performance was still observed. Therefore, it should be clear that the problem of the particle filters with Doppler-only tracking problem is not about initialization; rather it is about very low observability of the position variables compared to the velocity variables.

CHAPTER 4

OPTIMUM SENSOR PLACEMENT FOR DOPPLER-ONLY TRACKING

In multi-static applications, it is well known that sensor placement and/or the directions of the sensors with respect to the target play a crucial role on the performance. Effective sensor placement strategies are very important to gain as much information about the target as possible out of the sensors. This fact is confirmed by the vast number of theoretical studies on the subject in the tracking and localization applications. In the literature, many researchers have investigated the sensor placement problem for different sensor and measurement types, such as time of arrival and angle of arrival, [21, 24, 28, 29 and 30]. For Doppler-only measurements, the solution to the optimal sensor placement problem is available only for a localization application (i.e., a static parameter estimation problem), [32]. For tracking applications, the relationship between the number of the sensors and error performance is analyzed in [17]. But, in this study, sensors are located on the vertices of the regular polygon and the optimality of this placement is not discussed. With this motivation, in this chapter an optimum sensor placement strategy for tracking with Doppler-only measurements is also studied in this thesis.

The organization of this chapter is given as follows. The sensor placement problem definition is given in Section 4.1. Here the sensor placement problem in the case of Doppler only tracking is defined after a discussion about the optimality criteria used in the general sensor placement problem. To gain insight for the sensor placement

problem in the Doppler only case, only 1D target motion is considered. The objective function for the sensor placement is selected to be the integral of the position CRLB over a road segment of a specified length and the optimum sensor placement for this criterion is found by using the optimization routines in MATLAB. Inspired by the numerical results which are presented in Section 4.2, in Section 4.3, a suboptimum sensor placement strategy is proposed which

- is much simpler compared to the optimum placement (which requires numerical optimization) with explicit expressions for the sensor positions;
- has very close performance to the optimum sensor placement strategy.

4.1. Sensor Placement Problem Definition for Doppler Only Measurement

In the optimum sensor placement problem, the aim is to increase the information about the target contained in the measurements as much as possible. For this purpose, generally lower bounds, specifically CRLBs, for the corresponding estimation problem are minimized. From this perspective, an optimization based approach is proposed based on the CRLB matrices. There are two problems associated with the CRLB based sensor placement approaches. The first problem is that CRLB is a matrix valued quantity and therefore a single scalar value should be extracted from this matrix to be used in the optimization routine. The second problem is that CRLB is dependent on many parameters other than the sensor positions such as the target position, target velocity, wavelength, variance of the measurement noise etc.

In the literature, sensor placement approaches use three different objective functions extracted from the CRLB matrix as optimization criteria and each has a different physical meaning. These criteria are listed as follows.

- **A-Optimality:** The trace of the CRLB matrix is minimized. Hence, an approach based on this criterion aims to minimize the total variance of the estimated quantities.
- **D-Optimality:** The determinant of the FIM is maximized which is equivalent to the minimization of the determinant of the CRLB matrix. An approach

based on this criterion aims to minimize the area of the uncertainty ellipse around the estimate.

- **E-Optimality:** The largest eigenvalue of the CRLB matrix is minimized. An approach based on this criterion aims to keep the largest axis of the uncertainty ellipsoid as small as possible.

These criteria can also have the following drawbacks. A-optimality, by considering only the trace of the CRLB matrix, hence only the diagonal elements of the CRLB matrix, does not take the correlations between the estimated quantities into account. Hence, an uncorrelated but large uncertainty case might be preferred to a correlated but small uncertainty case. In D-optimality, there is a risk of obtaining a very thin uncertainty ellipsoid which may result in significantly large errors on the major axis of the uncertainty ellipsoid.

CRLB matrix is dependent on the target position and velocity as well as the sensor positions for the Doppler-only measurement case. Therefore different sensor placement solutions can be obtained for different target positions and velocities. In tracking applications, a track can start from and pass through any point with any velocity in a region of interest. These facts make the sensor placement for the specific aim of target tracking (using Doppler only measurements) quite a difficult problem to solve. Considering this issue, in this chapter, we constrain the target movements to 1D so that the optimization problem is simplified and meaningful and insightful results are obtained. The target we consider can move on a straight path/road with any velocity value. By taking into account the fact that the velocity errors are small compared to position errors with Doppler measurements, we aim to optimize only the position error CRLB in 1D. Since the target can be on any point on the straight path/road at any time instant during tracking, we consider the integral of the CRLBs for position as the cost function for the sensor placement.

The visualization of the 1D target scenario is given in Figure 53. Here, the target can move in both directions on the path/road of length L with any velocity. Optimal sensor placement is to be made in the 2D area excluding the path itself.

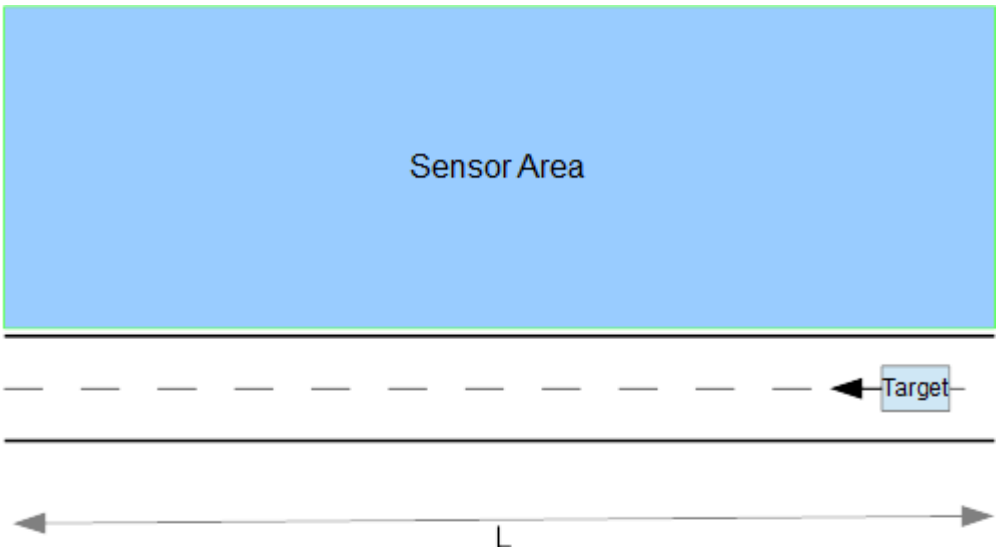

Figure 53 Sensor placement scenario considered in the thesis.

Without loss of generality, the road is chosen on the x-axis for simplicity and therefore, the target motion is constrained to the x-axis. The leftmost tip of the road segment is assumed to be the origin. Hence, only the target position on the x-axis in the interval $[0, L]$ is of interest. The target state is chosen to consist of the target position and target velocity on the x-axis as follows.

$$X = [x, v_x]^T \tag{4.1-1}$$

The calculation of the CRLB matrix for the target state is described as follows.

$$CRLB = (J^T(X)R^{-1}J(X))^{-1} \tag{4.1-2}$$

$$= \sigma_{meas}^2 (J^T(X)J(X))^{-1} \tag{4.1-3}$$

where $R = \sigma_{meas}^2 I_N$ represents the measurement noise covariance and I_N denotes an identity matrix of size N x N where N is the number of the Doppler sensors. Note that with this form of the measurement noise covariance, we assume that all Doppler sensors collect independent and identically distributed Doppler information. The Jacobian matrix $J(X)$ is given as

$$J(X) = \begin{bmatrix} j^1(X) \\ \vdots \\ j^N(X) \end{bmatrix} \tag{4.1-4}$$

where the rows $j^i(X)$ are given as

$$j^i(X) = \left[\frac{\partial F^i}{\partial x}(X) \;\; \frac{\partial F^i}{\partial v_x}(X)\right] \tag{4.1-5}$$

for $i = 1, \dots, N$. The functions F^i for the Doppler measurements are given as

$$F^i(X) = \frac{2}{\lambda}\frac{(x - x^i)v_x}{d^i} \tag{4.1-6}$$

where

$$d^i = \sqrt{(x - x^i)^2 + (y^i)^2}. \tag{4.1-7}$$

Here, x^i and y^i represents i^{th} sensor position in x axis and y axis, respectively. The partial derivatives $\frac{\partial F^i}{\partial x}$ and $\frac{\partial F^i}{\partial v_x}$ can be calculated as follows.

$$\frac{\partial F^i}{\partial x} = -\frac{2}{\lambda}\left(\frac{v_x . d^i - (x - x^i).\dot{d}^i}{(d^i)^2}\right), \tag{4.1-8}$$

$$= -\frac{2}{\lambda}\frac{v_x - v_x p_x^i p_x^i}{d^i}, \tag{4.1-9}$$

$$= -\frac{2}{\lambda}\frac{v_x\left(1 - \left(p_x^i\right)^2\right)}{d^i}. \tag{4.1-10}$$

$$\frac{\partial F^i}{\partial v_x} = -\frac{2}{\lambda}\frac{(x - x^i)}{d^i}, \tag{4.1-11}$$

$$= -\frac{2}{\lambda}p_x^i. \tag{4.1-12}$$

where

$$p_x^i = \frac{(x - x^i)}{d^i}, \tag{4.1-13}$$

$$\dot{d}^i = \frac{v_x(x - x^i)}{d^i} = v_x p_x^i. \tag{4.1-14}$$

When Jacobian matrix J is substituted into (4.1-3), the CRLB matrix can be expressed as follows.

$$CRLB = \sigma_{meas}^2 (J^T J)^{-1} \tag{4.1-15}$$

$$= \sigma_{meas}^2 \frac{\lambda^2}{4} \begin{bmatrix} {v_x}^2 \sum_{i=1}^{N} \left(\frac{(1-(p_x^i)^2)}{d_k^i} \right)^2 & v_x \sum_{i=1}^{N} p_x^i \frac{(1-(p_x^i)^2)}{d_k^i} \\ v_x \sum_{i=1}^{N} p_x^i \frac{(1-(p_x^i)^2)}{d_k^i} & \sum_{\mathrm{i}=1}^{N} (p_x^i)^2 \end{bmatrix}^{-1}. \quad \text{4.1-16}$$

When the inverse is calculated, $CRLB(1,1)$, i.e., the first column, first row element of the CRLB matrix which corresponds to the CRLB of the target position, can be expressed as follows.

$$CRLB(1,1)$$
$$= \sigma_{meas}^2 \frac{\lambda^2}{4{v_x}^2} \frac{\sum_{\mathrm{i}=1}^{N} (p_x^i)^2}{\sum_{\mathrm{i}=1}^{N} (p_x^i)^2 * \sum_{i=1}^{N} \left(\frac{(1-(p_x^i)^2)}{d_k^i} \right)^2 - \left(\sum_{i=1}^{N} p_x^i \frac{(1-(p_x^i)^2)}{d_k^i} \right)^2}. \quad \text{4.1-17}$$

The quantity $CRLB(1,1)$ represents the uncertainty in the position estimation. As seen in the expression above, it is dependent on the target position, velocity, signal wavelength and measurement noise covariance as well as the sensor positions. Note that the dependences on the target velocity v_x, wavelength λ and measurement noise variance σ_{meas}^2 are all in the form of a positive scaling constant. Therefore, the result of an optimization of $CRLB(1,1)$ with respect to sensor positions will not be affected by these parameters. On the other hand, the dependence on the target position cannot be neglected. In this study, we select to get rid of the effect of this dependence on the target position by integrating out the target position from $CRLB(1,1)$. Hence, the cost function used in this study for sensor placement is given as follows.

$$Cost = \int_{x=0}^{x=L} CRLB(1,1)dx \quad \text{4.1-18}$$

which is given in explicit form as below.

$$Cost$$
$$= \frac{\sigma_{meas}^2 \lambda^2}{4\,{v_x}^2} \int_{x=0}^{L} \frac{\sum_{\mathrm{i}=1}^{N} (p_x^i)^2}{\sum_{\mathrm{i}=1}^{N} (p_x^i)^2 * \sum_{i=1}^{N} \left(\frac{(1-(p_x^i)^2)}{d_k^i} \right)^2 - \left(\sum_{i=1}^{N} p_x^i \frac{(1-(p_x^i)^2)}{d_k^i} \right)^2} dx. \quad \text{4.1-19}$$

The cost function given above represents the total position uncertainty over the road segment considered in the sensor placement problem. The aim is to minimize this total uncertainty by considering a predefined number of Doppler sensors with respect to sensor positions. The minimization of the overall uncertainty over the whole road can be thought of as the tracking aspect of the cost considered here and it ensures that the tracks of a tracker would be in good quality over the whole road segment.

4.2. Simulation Results

The cost function to be optimized for the optimum sensor placement was given in the previous section. It is difficult to evaluate the cost function because the integral in (4.1-19) is impossible to take analytically. Therefore, the integral is taken numerically on a uniform grid over the x-axis with grid spacing of 0.04 m. The road length is taken to be 100 meters. The minimization task is achieved using the Matlab function *fmincon(.)* for different numbers of sensors. The optimum sensor placements obtained for different numbers of sensors, N, are shown in Figure 54 to Figure 57.

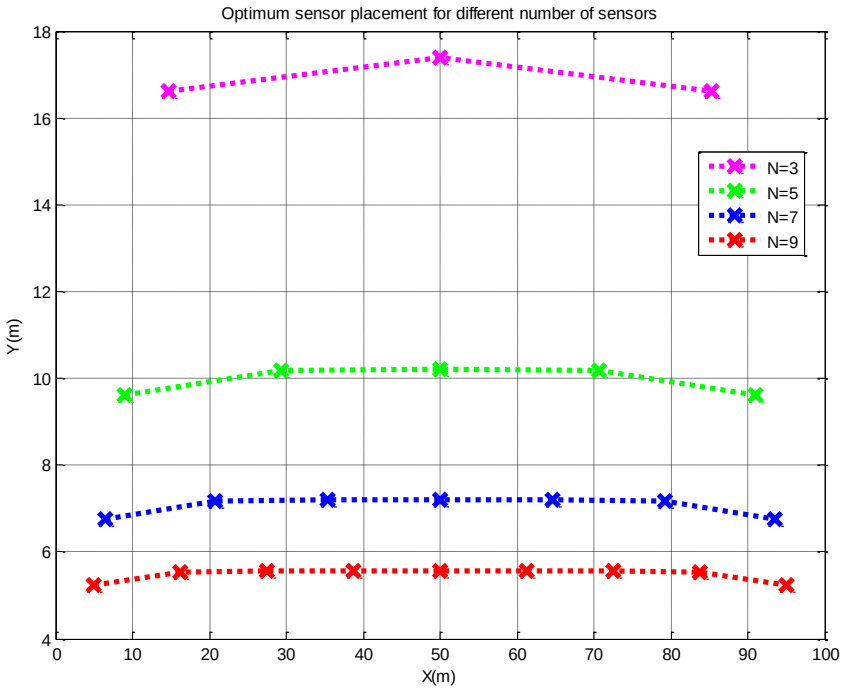

Figure 54 Optimum sensor placement for *N*=3, 5, 7, 9.

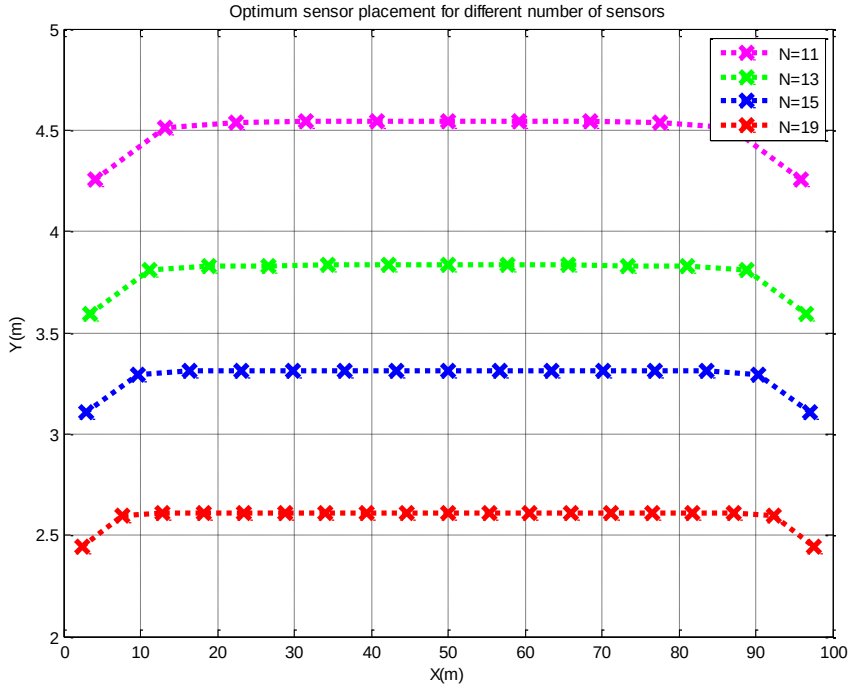

Figure 55 Optimum sensor placement for *N*=11, 13, 15, 19.

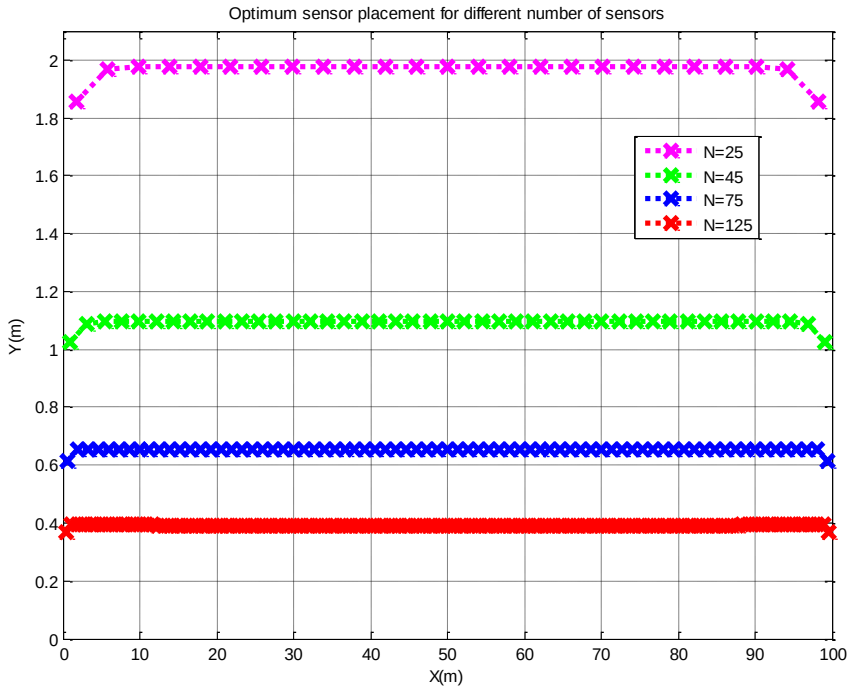

Figure 56 Optimum sensor placement for N =25, 45, 75, 125.

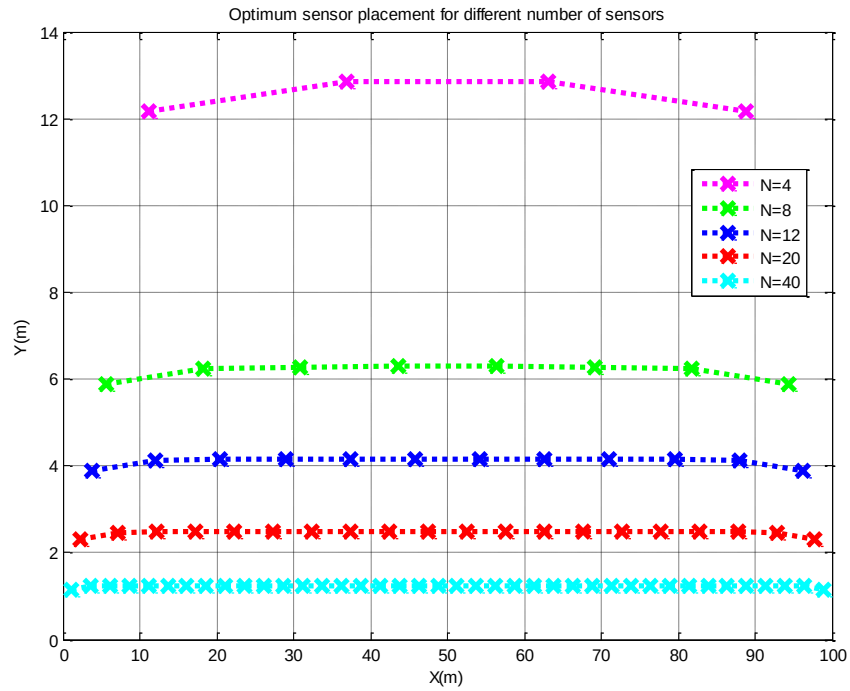

Figure 57 Optimum sensor placement for N=4, 8, 12, 20, 40.

It is seen in the figures that the y-values of the optimally placed sensors are close to each other. As the number of sensors increases, the optimally placed sensors get closer to the road segment considered and vice versa. For both even and odd numbers of sensors, the optimal sensor placement is symmetric with respect to the line $x = 50$, i.e., with respect to the orthogonal bisector of the road segment.

4.3. An Explicit Simple-Form Suboptimal Sensor Placement Strategy

In this thesis, by observing the figures of the previous section, it has been discovered that the optimally placed sensors have some characteristic features which can be summarized as follows.

- y-positions are concentrated around a single y-value which is equal to the division of the road length by two times the number of sensors. For example, for the 5 sensor case, y positions of the sensors are around 10 meters. For the 25 sensor case, y-positions of the sensors are around 2 meters. These examples can be extended to all of the cases shown in the figures. As seen in the figures above, as the sensors get closer to the beginning and the end of the road segment, they deviate slightly from the characteristics described above. Especially the left-most and the right-most sensors have slightly lower y-positions than the other sensors.
- x-positions are located along the road in a symmetrical manner. The x-axis distance between all adjacent sensors is approximately equal to the division of the road length by the number of sensors. The x-position of the left-most sensor is approximately half of the distance between the adjacent sensors. For example, in the case when there are 5 sensors, the sensors are located such that the distances between adjacent sensors are approximately 20 meters and the x-position of the left-most sensor is approximately 10 meters. For the 25 sensor case, the distance between the adjacent sensors is around 4 meters and the x-position of the left-most sensor is around 2 meters. Again these examples can be extended for all other cases presented in the figures.

In view of the observations described above, in this section, we present a suboptimal sensor placement strategy. The proposed suboptimal sensor placement strategy is described below.

Explicit Sensor Positions for the Proposed Sub-Optimal Strategy: Suppose that we would like to place N Doppler sensors optimally with respect to the cost function given in (4.1-19).

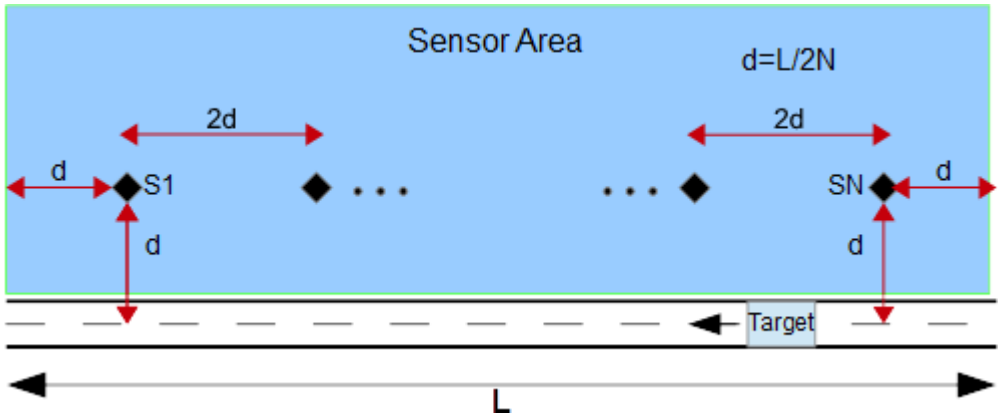

Figure 58 The proposed simple sensor placement strategy.

We first define the critical parameter

$$d = \frac{L}{2N} \tag{4.3-1}$$

where L is the length of the road segment considered.

The proposed sub-optimal sensor positions are then given as

$$x^i = d + (i-1)2d$$
$$y^i = d \tag{4.3-2}$$

for $i = 1, 2, \dots, N$.

The proposed suboptimal sensor placement strategy is illustrated in Figure 58. As seen in the figure, y-positions of all sensors are selected to be equal to d. The x-distance between the adjacent sensors is selected to be $2d$ and the x-position of the first sensor is equal to d. With the proposed sensor placement strategy, when the number of sensors is odd, the x-position of the $(N+1)/2$'th sensor is in the middle of the road segment as in the optimal sensor placement strategy. This gives us the opportunity to compare the y-positions of the sensors in the middle for the

suboptimal and optimal sensor placement strategies. Figure 59 illustrates the y-values of the sensor in the middle for the optimal and sub-optimal sensor placement strategies when the number of sensors is odd. In Figure 60, in a similar way, x-positions of the left-most sensor are shown for the optimal and sub-optimal sensor placement strategies. As seen in these figures, the position values for the proposed suboptimal sensor placement strategy are very close to those of the optimal strategy.

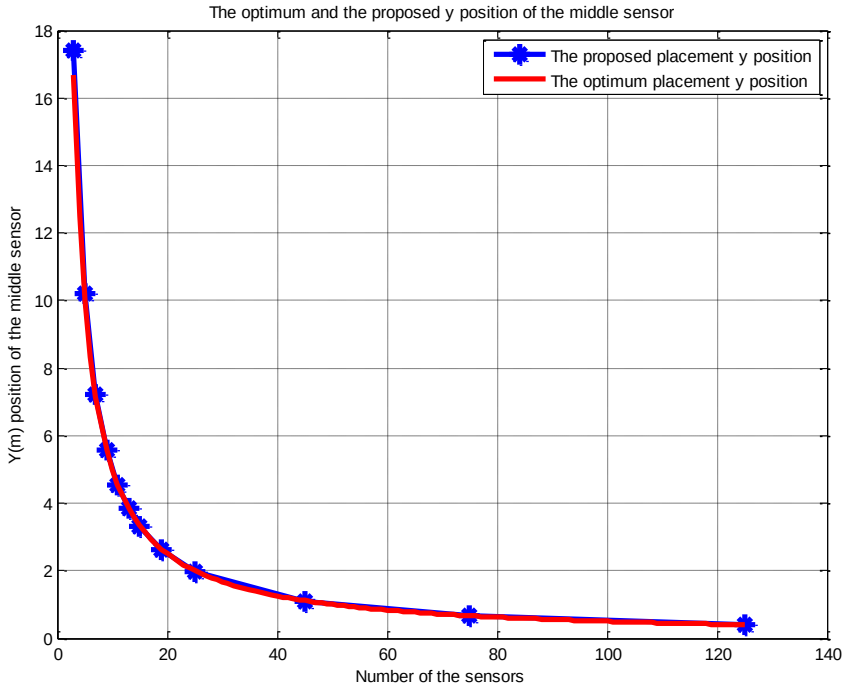

Figure 59 y-axis position of the sensor in the middle of the array.

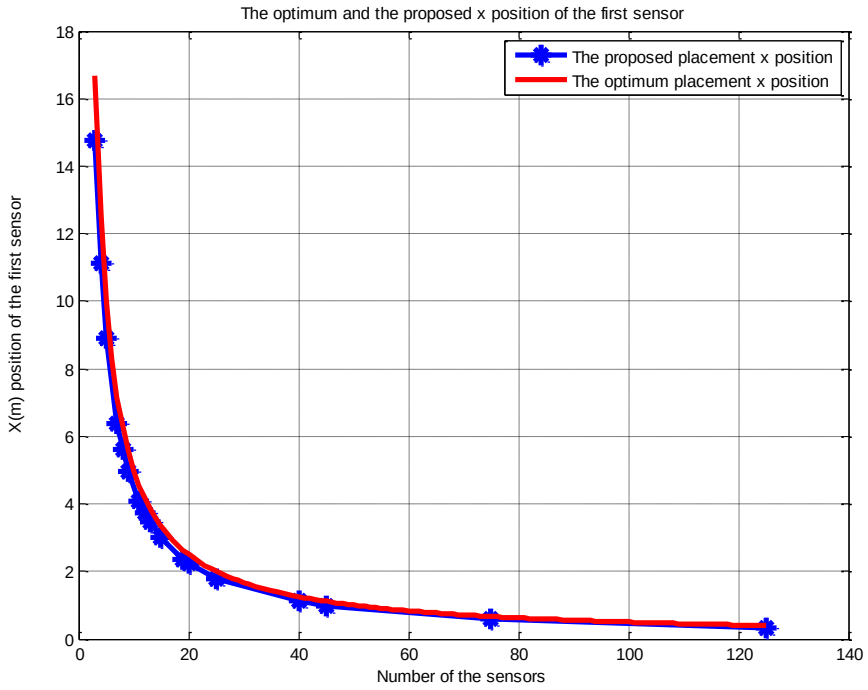

Figure 60 x-axis position of the left-most sensor of the array.

In order to describe the performance of the proposed strategy in a more physically meaningful manner, average position CRLB of the proposed strategy and optimum placement are compared. Average position CRLB is obtained by taking square-root of the total cost (which is the total position CRLB) divided by the road length as in (4.3-3). Here the term $Cost$ is given in (4.1-19) and L is the length of the road segment.

$$Average\ Position\ CRLB = \sqrt{\frac{Cost}{L}} \qquad 4.3\text{-}3$$

Average position CRLB that would be obtained for the optimal and the proposed strategies for different numbers of sensors are shown in Figure 61. Also the ratios of the average position CRLB obtained by the proposed strategy to that obtained by the

optimal strategy for different numbers of sensors are shown in Figure 62. The parameter values used for obtaining these figures are given as follows.

- Wavelength is $\lambda = 0.33$ meters.
- Target speed is v_x = 5 m/s
- Measurement noise variance is σ^2_{meas}= 1 Hz^2.

It should also be noted that these parameters do not affect the argument of the optimization but they just scale the average position CRLB. As seen in the figures, the average position CRLB difference is very small or even negligible for the sub-optimal strategy compared to the optimal one. Moreover, as the number of sensors gets larger, the difference becomes more and more negligible.

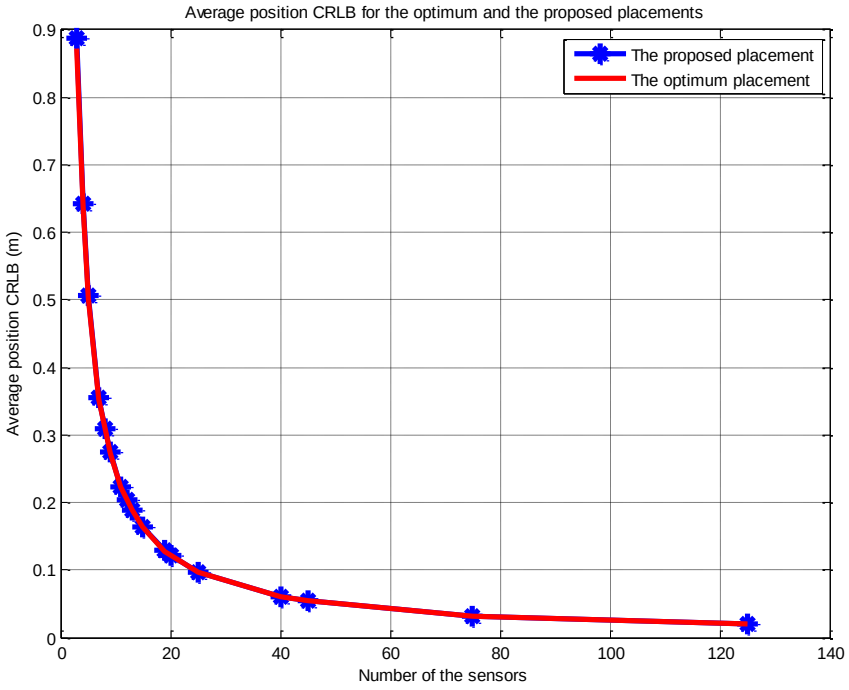

Figure 61 The average position CRLB for the optimum and the proposed sensor placement strategies for different number of sensors.

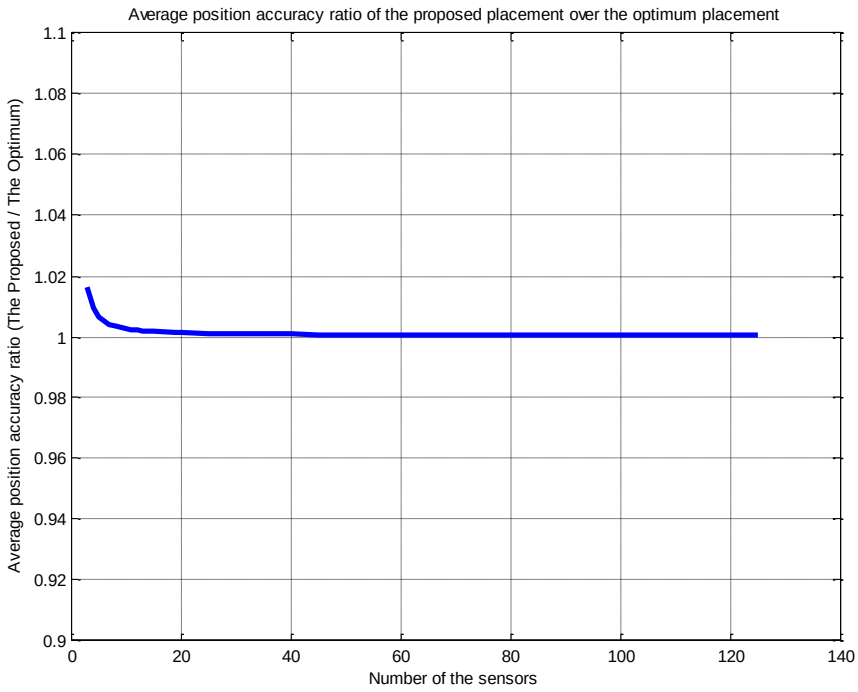

Figure 62 The ratio of the average position CRLB that are obtained by the optimum and proposed suboptimal sensor placement strategy for different number of sensors.

The x-positions of the sensors in the proposed sensor placement strategy could have been obtained using just intuition without any cost function minimization by arguing that sensors should be distributed almost uniformly along the road segment for good performance. On the other hand, it would be difficult to discover the y-position of the sensors in the proposed strategy intuitively. To evaluate the effect of the y-position of the sensors in the proposed strategy, a simulation study is performed. On a target tracking example with EKF, average RMS x-position errors are obtained for different sensor y-positions.

Average RMS values are calculated using 1000 Monte Carlo runs. In this simulation, five sensors are used. x-positions of the sensors are chosen as in the proposed strategy. y-positions of the sensors are changed between 4 meters and 20 meters with 2 meters steps. In this simulation the selected parameters for the true target trajectory and measurements are given as follows.

- Measurement noise variance is $\sigma_{meas}^2 = 1\ Hz^2$.
- Process noise variance $\sigma_{meas}^2 = \ 0\ (m/s^2)^2$.

- EKF initial covariance matrix is selected to be diagonal with variances chosen as $\sigma_x^2 = 1e2\text{m}^2$ and $\sigma_{v_x}^2 = 225\ (\text{m/s})^2$.
- The target trajectory is constrained on the road segment. The trajectory starts at $x = 0\ m$ and ends at $x = 100\ m$ .The constant target speed is $v_x = 5\ m/s$.
- True initial state of target is used as the initial state of EKF.

Average RMS x-position errors obtained for different sensor y-positions are shown in Figure 63. As seen in the figure, as expected, the minimum average RMS error occurs at y position of 10 meters which is y-position of the sensors in the proposed sensor placement strategy. The RMS errors increase rather sharply if the sensors are placed closer to the road segment than the proposed y-position. The error increase is milder if the sensors are placed further to the road segment than the proposed y-position.

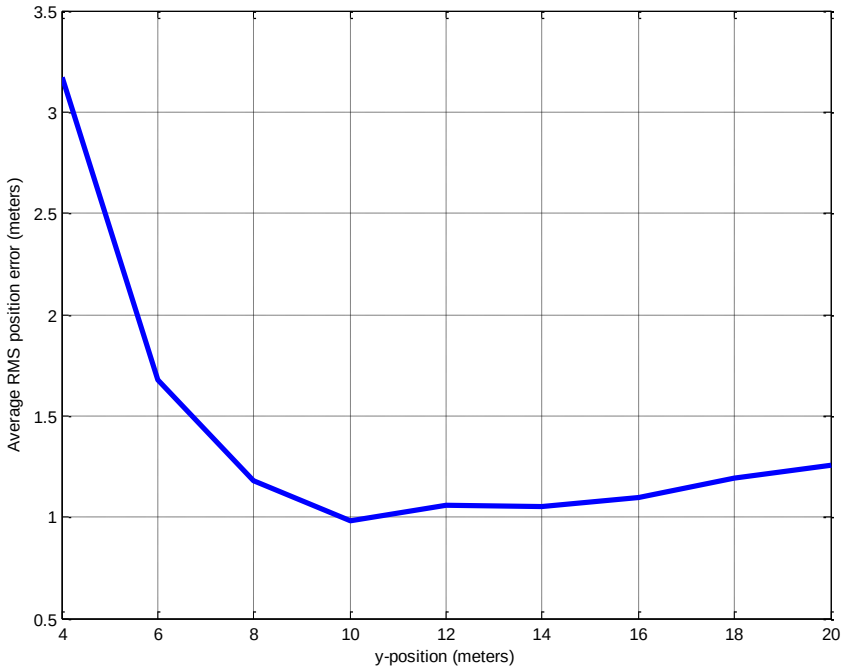

Figure 63 Average RMS x-position errors for different y-position of the sensors.

CHAPTER 5

CONCLUSION

In this thesis, we have considered three important problems in Doppler-only target tracking. First, we have adapted a localization algorithm for Doppler-only measurements proposed in the literature to a single point track initialization algorithm for Doppler-only tracking. This method was based on the separable least squares method. The implemented track initialization algorithm has been shown to work successfully with EKF. It has been seen that EKF obtains very close results to CRLB when it is initialized with the track initialization procedure proposed and it, most of the time, diverges without such a procedure. The most important parameter for the track initialization algorithm considered is the grid spacing parameter. Using various simulation results it has been seen that, for selecting grid spacing parameter, CRLB values for the problem of interest can serve as a baseline as also observed in the literature before. It was shown that for grid spacing values lower than or equal to the CRLB of the problem, the performance difference for EKF is minor. On the other hand, for grid spacing much larger than the CRLB, there is significant performance degradation for EKF. Therefore, as was done in the literature, it is suggested to check the CRLB for a problem before designing a tracking filter and to select the grid spacing around this value to optimize both the amount of computations and the initialization performance.

Secondly, in the thesis, we have shown that the bootstrap particle, which can easily beat EKF in many nonlinear state estimation problems, fails to do so for Doppler-only tracking. We have discussed the reasons for this behavior and concluded that

the cause is the weaker observability of the position variables compared to the velocity variables. In order to see whether standard sequential Monte Carlo tools can improve the behavior of the bootstrap filter for this problem, we have derived a SIR particle filter with optimal proposal distribution and a Rao-Blackwellized particle filter for Doppler-only tracking. The evaluation of the performances of these filters has shown that these improved filters still fail to beat EKF although there are occasional improvements over the bootstrap particle filter for some specific parameter selections. As a final remark, it is said that more clever and problem specific improvement strategies has to be devised in order to increase the performance of particle filters for Doppler-only tracking.

The final contribution of this thesis is in the area of sensor placement. Although there are many sensor placement studies in the literature for e.g., range or bearing measurements, the case of Doppler-only measurements seem to lack detailed research. In this thesis, for the 1D target motion case, sensor placement problem has been solved for minimizing the total position CRLB/uncertainty over a line/road segment. Based on the numerical results, an explicit and simple sensor placement strategy has been proposed. The resulting strategy has been shown to have quite close results to the optimal sensor placement strategy.

The invention of the new ways to improve the particle filter performance for Doppler-only tracking would be a fruitful research in the future. The generalization of the sensor placement methodology proposed in the thesis to 2D target motion and the investigation of different criteria for sensor placement for Doppler-only measurements are also left as future research topics.

REFERENCES

1. PETERSON, A. M. Radio and radar tracking of the Russian Earth satellite. Proc. IRE, 1957, 45.11: 1553-1554.
2. SALINGER, Sheldon N.; BRANDSTATTER, Julius J. Application of recursive estimation and Kalman filtering to Doppler tracking. Aerospace and Electronic Systems, IEEE Transactions on, 1970, 4: 585-592.
3. SCHULTHEISS, Peter M.; WEINSTEIN, Ehud. Estimation of differential Doppler shifts. The Journal of the Acoustical Society of America, 1979, 66.5: 1412-1419.
4. WEBSTER, Robert J. An exact trajectory solution from Doppler shift measurements. IEEE Transactions on Aerospace Electronic Systems, 1982, 18: 249-252.
5. CHAN, Yiu-Tong; JARDINE, Frederick L. Target localization and tracking from Doppler-shift measurements. Oceanic Engineering, IEEE Journal of, 1990, 15.3: 251-257.
6. CHAN, Y. T.; TOWERS, J. J. Passive localization from Doppler-shifted frequency measurements. Signal Processing, IEEE Transactions on, 1992, 40.10: 2594-2598.
7. KALKAN, Yilmaz; BAYKAL, Buyurman. MIMO radar target localization by using Doppler shift measurement. In: Radar Conference, 2009. EuRAD 2009. European. IEEE, 2009. p. 489-492.
8. CHAN, Y. T.; TOWERS, Jeff J. Sequential localization of a radiating source by Doppler-shifted frequency measurements. Aerospace and Electronic Systems, IEEE Transactions on, 1992, 28.4: 1084-1090.
9. CHAN, Y. T. A 1-D search solution for localization from frequency measurements. Oceanic Engineering, IEEE Journal of, 1994, 19.3: 431-437.

10. FUCHENG, Guo; ZHONGKANG, Sun; KAN, Huangfu. A modified covariance extended Kalman filtering algorithm in passive location. In: Robotics, Intelligent Systems and Signal Processing, 2003. Proceedings. 2003 IEEE International Conference on. IEEE, 2003. p. 307-311.
11. KUSY, Branislav; LEDECZI, Akos; KOUTSOUKOS, Xenofon. Tracking mobile nodes using RF Doppler shifts. In: Proceedings of the 5th international conference on Embedded networked sensor systems. ACM, 2007. p. 29-42.
12. RISTIC, Branko; FARINA, Alfonso. Recursive Bayesian state estimation from Doppler-shift measurements. In: Intelligent Sensors, Sensor Networks and Information Processing (ISSNIP), 2011 Seventh International Conference on. IEEE, 2011. p. 538-543.
13. BATTISTELLI, G., CHISCI, L., FANTACCI, C., FARINA, A., & GRAZIANO, A. (2013, July). A new approach for Doppler-only target tracking. In Information Fusion (FUSION), 2013 16th International Conference on (pp. 1616-1623). IEEE.
14. RISTIC, Branko; FARINA, Alfonso. Joint detection and tracking using multi-static Doppler-shift measurements. In: Acoustics, Speech and Signal Processing (ICASSP), 2012 IEEE International Conference on. IEEE, 2012. p. 3881-3884.
15. MAHLER, Ronald PS. Statistical multisource-multitarget information fusion. Artech House, Inc., 2007.
16. RISTIC, Branko; FARINA, Alfonso. Target tracking via multi-static Doppler shifts. Radar, Sonar & Navigation, IET, 2013, 7.5: 508-516.
17. XIAO, Yang-Can; WEI, Ping; YUAN, Ting. Observability and performance analysis of bi/multi-static Doppler-only radar. Aerospace and Electronic Systems, IEEE Transactions on, 2010, 46.4: 1654-1667.
18. LIANG, Ma; KIM, Du Yong; KAI, Xue. Multi-Bernoulli filter for target tracking with multi-static Doppler only measurement. Signal Processing, 2015, 108: 102-110.
19. LINDGREN, D., GULDOGAN, M. B., GUSTAFSSON, F., HABBERSTAD, H., & HENDEBY, G. (2013, July). Acoustic source localization in a network of Doppler shift sensors. In Information Fusion (FUSION), 2013 16th International Conference on (pp. 1281-1288). IEEE.

20. GULDOGAN, M. B., LINDGREN, D., GUSTAFSSON, F., HABBERSTAD, H., & ORGUNER, U. Multiple target tracking with Gaussian mixture PHD filter using passive acoustic Doppler-only measurements. In Information Fusion (FUSION), 2012 15th International Conference on (pp. 2600-2607). IEEE.
21. GULDOGAN, M. B., LINDGREN, D., GUSTAFSSON, F., HABBERSTAD, H., & ORGUNER, U. (2014). Multi-target tracking with PHD filter using Doppler-only measurements. Digital Signal Processing, 27, 1-11.
22. MORENO-SALINAS, David; PASCOAL, Antonio; ARANDA, Joaquin. Sensor networks for optimal target localization with bearings-only measurements in constrained three-dimensional scenarios. Sensors, 2013, 13.8: 10386-10417.
23. SIM, Robert; ROY, Nicholas. Global a-optimal robot exploration in slam. In: Robotics and Automation, 2005. ICRA 2005. Proceedings of the 2005 IEEE International Conference on. IEEE, 2005. p. 661-666.
24. ABEL, Jonathan. Optimal sensor placement for passive source localization. In: Acoustics, Speech, and Signal Processing, 1990. ICASSP-90., 1990 International Conference on. IEEE, 1990. p. 2927-2930.
25. CARTER, G. Clifford. Variance bounds for passively locating an acoustic source with a symmetric line array. The Journal of the Acoustical Society of America, 1977, 62.4: 922-926.
26. ZHANG, Hong. Two-dimensional optimal sensor placement. Systems, Man and Cybernetics, IEEE Transactions on, 1995, 25.5: 781-792.
27. LEVANON, Nadav. Lowest GDPO in 2D Scenarios. 2000.
28. MARTÍNEZ, Sonia; BULLO, Francesco. Optimal sensor placement and motion coordination for target tracking. Automatica, 2006, 42.4: 661-668.
29. BISHOP, A. N., FIDAN, B., ANDERSON, B. D., PATHIRANA, P. N., & DOGANÇAY, K. (2007, December). Optimality analysis of sensor-target geometries in passive localization: Part 1 - Bearing-only localization. In Proceedings of the 3rd International Conference on Intelligent Sensors, Sensor Networks and Information Processing (ISSNIP).
30. BISHOP, A. N., FIDAN, B., ANDERSON, B. D., PATHIRANA, P. N., & DOGANÇAY, K. (2007, December). Optimality analysis of sensor-target geometries in passive localization: Part 2-Time-of-arrival based localization. In

Proceedings of the 3rd International Conference on Intelligent Sensors, Sensor Networks and Information Processing (ISSNIP).

31. SOYSAL, Gokhan; BOZDOGAN, Ali Onder; EFE, Murat. Information analysis in passive radar networks for target tracking. In: Information Fusion, 2009. FUSION'09. 12th International Conference on. IEEE, 2009. p. 1115-1122.
32. NGUYEN, Ngoc Hung; DOGANCAY, Kutluyil. Optimal sensor placement for Doppler shift target localization. In: Radar Conference (RadarCon), 2015 IEEE. IEEE, 2015. p. 1677-1682.
33. KAY Steve M.; Fundamentals of Statistical Signal Processing, Vol. I - Estimation Theory
34. GORDON, Neil J., SALMOND, David J., and SMITH, Adrian FM. Novel approach to nonlinear/non-Gaussian Bayesian state estimation. In IEE Proceedings F (Radar and Signal Processing), vol. 140, no. 2, pp. 107-113. IET Digital Library, 1993.